

**Dissertation zur Erlangung des Doktorgrades  
der Fakultät für Chemie und Pharmazie  
der Ludwig-Maximilians-Universität München**

**Structural and Functional Studies on Myosin Type V  
Dependent Transport in Vertebrates**



Hana Velvarská

aus Brandeis a.d. Elbe, Tschechische Republik

2012

### **Erklärung**

Diese Dissertation wurde im Sinne von § 7 der Promotionsordnung vom 28. November 2011 von Herrn Prof. Dr. Klaus Förstemann betreut.

### **Eidesstattliche Versicherung**

Diese Dissertation wurde eigenständig, ohne unerlaubte Hilfe erarbeitet.

München,

.....

Hana Velvarská

Dissertation eingereicht am 24. September 2012

1. Gutachter: Prof. Dr. Klaus Förstemann

2. Gutachter: Prof. Dr. Mario Halic

Mündliche Prüfung am 19. November 2012

# TABLE OF CONTENTS

SUMMARY.....	1
1. INTRODUCTION .....	3
1.1 Intracellular transport.....	3
1.2 Microtubules .....	4
1.3 Dynein and kinesin proteins .....	4
1.4 EB1 .....	5
1.5 Actin.....	6
1.6 Unconventional myosins .....	6
1.7 Type V Myosin.....	7
1.8 Type V myosin in human .....	8
1.8.1 Myo5a .....	9
1.8.2 Myo5b .....	10
1.8.3 Myo5c.....	11
1.8.4 Autoinhibition .....	12
1.8.5 Regulation by $\text{Ca}^{2+}$ .....	14
1.8.6 Regulation by cargo attachment.....	16
1.8.7 Phosphorylation.....	16
1.8.8 Griscelli syndrome .....	17
1.9 Melanophilin .....	18
1.10 Rab GTPases.....	20
1.10.1 Rab27a.....	21
1.10.2 Rab11a.....	22
1.11 Type V myosin in yeast and plants .....	22
1.11.1 Myo2p .....	23
1.11.2 Myo4p .....	24
1.11.3 Myosins in plant.....	25
1.12 Myo6 .....	25
1.13 Objectives .....	27
2. RESULTS.....	28
2.1 Structural studies on Melanophilin.....	28
2.1.1 Melanophilin-Rab27a complex.....	28
2.1.2 Melanophilin-Myo5a complex.....	29
2.1.3 Melanophilin-EB1 complex .....	32
2.2 Structural studies on Myo6 CBD .....	34
2.2.1 Myo6 CBD crystallization .....	35
2.2.2 Myo6 interaction with Miranda.....	37
2.2.3 Myo6 Initial NMR experiments.....	38
2.3 Structural studies on Myo5a.....	40
2.3.1 Defining the limits of Myo5a GD and crystallization attempts .....	40
2.3.2 Shape analysis by Small Angle X-ray Scattering.....	41

2.3.3	Shape analysis by SAXS of Myo5a, Myo5b, and Myo5c GDs .....	42
2.3.4	Crystallization of the Myo5a GD .....	44
2.3.5	Structure determination of the Myo5a GD .....	46
2.3.6	Structure determination of the Myo5b GD .....	48
2.3.7	Model of Myo5c GD .....	50
2.3.8	Myo5a GD-mutations found to cause Griscelli-syndrome .....	51
2.3.9	Comparison of the human MyoV GD with the yeast type V Myosins .....	53
2.3.10	Comparison of surface properties of the Myo5a, Myo5b, and Myo5c GD.....	54
2.3.11	Investigation of structurally similar proteins.....	57
2.3.12	Residues required for Myo5a autoinhibition are conserved in Myo5b and Myo5c.....	58
2.3.13	Not only Myo5a, but also Myo5b and Myo5c GD mediates autoinhibition.....	59
2.3.14	Binding of Rab11a does not relieve the autoinhibition.....	60
2.3.15	Docking of Myo5a GD crystal structure into EM density of autoinhibited Myo5a .....	62
2.3.16	The loop I and II of the GD are required for autoinhibition .....	64
2.3.17	A phospho-mimicking mutation in Myo5a loop I abolishes autoinhibition .....	66
3.	DISCUSSION .....	67
3.1	Myo5 regulation by autoinhibition .....	68
3.2	Myo5 regulation by cargo binding and phosphorylation .....	69
3.3	Regulation by Ca <sup>2+</sup> concentration .....	71
3.4	The Myo5a autoinhibition model.....	72
4.	MATERIALS AND METHODS .....	75
4.1	Chemicals .....	75
4.2	DNA Oligonucleotides for cloning.....	75
4.3	Plasmids.....	78
4.4	Competent bacterial strains.....	80
4.5	Insect cells lines.....	80
4.6	Antibodies .....	80
4.7	Solutions and buffers .....	80
4.8	Peptides used for co-crystallization .....	81
4.9	Software.....	81
4.10	Molecular biology.....	82
4.11	Protein Expression .....	83
4.11.1	Recombinant protein expression in <i>E.coli</i> .....	83
4.11.2	Recombinant protein expression in insect cells (Myo5a HMM).....	83
4.12	Protein purification.....	84
4.12.1	Protein fragments purification with 6xHis tag.....	84
4.12.2	Purification of fragments with GST-tag.....	84
4.12.3	Purification of fragments with MBP-tag.....	85
4.12.4	Purification and crystallization of the protein complexes .....	85
4.12.5	Purification of Myo5a HMM.....	85
4.12.6	Selenomethionine-substituted Myo5a GD expression and purification .....	86
4.12.7	Purification of calmodulin.....	86
4.12.8	Purification of actin.....	86
4.12.9	Protein analysis .....	87
4.13	Biochemistry .....	88



4.13.1	Pull down assay Myo6 and Miranda .....	88
4.13.2	Pull down assay Myo5a, Myo5b, Myo5c, and Rab11a .....	88
4.13.3	Crystallization of Myo5a GD .....	88
4.13.4	Crystallization of Myo5b GD .....	89
4.13.5	Myo5a GD structure determination .....	89
4.13.6	Myo5b GD structure determination .....	89
4.13.7	Homology model of Myo5c GD .....	90
4.13.8	ATPase assay .....	90
4.13.9	Small-angle X-ray scattering (SAXS) .....	90
5.	ABBREVIATIONS .....	92
6.	REFERENCES .....	94
	CURRICULUM VITAE .....	i
	ACKNOWLEDGMENT .....	ii

## SUMMARY

In human, three type V myosins (Myo5a, 5b, and 5c) mediate transport of several different cargoes. These molecular motors are involved in a wide range of cellular processes, such as endo- and exocytotic pathways, transport of cell signaling components and their segregation as well as docking of organelles. Myo5a was shown to exist in an active cargo-transporting state and in an inactive autoinhibited state, where its C-terminal globular cargo-binding domain (GD) inhibits the N-terminal motor domain. Autoinhibition is a good strategy to avoid unnecessary ATP consumption in absence of cargo. However this regulation is not common to all myosins. Prior to my thesis work it was even not clear if autoinhibition is limited to Myo5a or whether it is also exerted by its closest human paralogs Myo5b and Myo5c. Moreover the mechanism of regulation is still poorly understood. Since no direct structural information was available for any vertebrate GD, a main aim of this study was to understand how the GD is structurally organized and how the interaction with the motor domain is achieved.

I solved crystal structures of both human Myo5a and Myo5b GDs at 2.2Å and 3.1Å resolution. Based on these structures a homology model of Myo5c GD was generated. Previously published low-resolution electron microscopy density of full length Myo5a suggested an atomic model of the autoinhibited dimer. However a major uncertainty in this interpretation was the lack of structural information for the Myo5a GD. I therefore docked the Myo5a GD structure into this low-resolution density and assembled a complete atomic model of the motor-GD interaction. I not only confirmed the importance of three previously reported residues (D136 in motor domain; K1708 and K1781 in the GD) for this interaction, but also predicted two other surface regions on the GD to be important for autoinhibition. When these two conserved loop regions were mutated or deleted autoinhibition was abolished. My ATPase experiments with the Myo5a motor also revealed that all human type V myosins undergo autoinhibition and that the presence of the adaptor protein Rab11a is unable to relieve autoinhibition. Together with previously published results, a new model emerges from the experiments. According to this model, the motor domain is

locked in the inhibited state by large conserved regions of the GD that fixes the motor in an inactive, post-powerstroke conformation. This kind of mechanism shows strong similarities to the inhibition of conventional kinesins.

# 1. Introduction

## 1.1 Intracellular transport

Each eukaryotic cell contains a dense meshwork of cytoskeleton fibers. Small particles can freely diffuse under such conditions, but larger particles are immobile. However, normal cellular function requires that macromolecules or organelles be positioned in specific locations. Distribution of these cellular components is organized with the help of several molecular motors. Highly ordered, motor protein-containing complexes transport their cargo along cytoskeletal tracks. Transport complexes that contain kinesin- and dynein-motor proteins move their cargo along microtubule fibers, whereas myosin-dependent transport complexes translocate along actin filaments (Figure 1.1). The list of transported cargoes includes large membrane organelles, smaller vesicles, RNAs, and proteins involved in signaling and establishing cell polarity (Vale 2003).

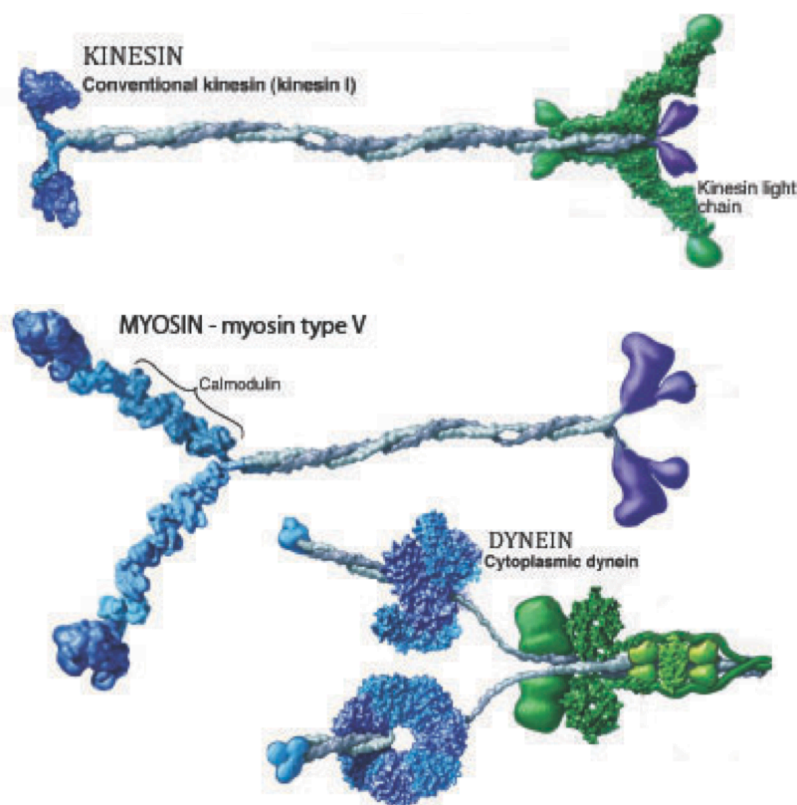


**Figure 1.1 Schematic drawings of one of kinesin, myosin, and dynein representant.** Conventional kinesin kinesin-1. Myosin - Myosin V from higher eukaryots. Dynein – cytoplasmic dynein. The color coding is as follows: the motor domain and calmodulins in blue, coil-coiled or unstructured parts in white and tail or cargo binding domains in purple. In green are other light chains. The picture is adapted from (Vale 2003).

## **1.2 Microtubules**

Tracks similar to microtubules were discovered in bacteria. Also AAA+ ATPases that are found in eukaryotic dynein motors were found in bacteria. However, so far no molecular motor was discovered that is able to move along these cables (Vale 2003). Similar to actin filaments, eukaryotic microtubules are important for intracellular transport, but also for the assembly of mitotic spindles, chromosome segregation or spatial organization of cells. Microtubules are highly dynamic oriented polymers, built of 13 cylindrical protopolymers that undergo growing and shrinking with the help of microtubule binding proteins (for instance EB1, see section 1.4) (Slep, Rogers et al. 2005). Microtubule assembly starts with the minus end at specific locations within the cell and grows in one direction, for instance towards the cell cortex or towards chromosomes during mitosis. The filament orientation is based on asymmetric head-tail polymerization of heterodimeric  $\alpha$ - $\beta$  tubulin units (Lansbergen and Akhmanova 2006).

## **1.3 Dynein and kinesin proteins**

Dyneins and kinesin are highly conserved microtubule-based motors. Kinesins are composed of N-terminal head, neck linker, coiled-coil stalk and a C-terminal cargo-binding domain. For processive movement towards the plus ends of microtubules, kinesins have to be dimerized and the heads hydrolyze ATP. Kinesins are divided into several types of which the conventional kinesin-1 is amongst the most prominent examples. Kinesin-1 is a processive motor that transports cargo for long distances without detaching from the microtubules (Mori, Vale et al. 2007). Moreover, Kinesin-1 also undergoes autoinhibition to prevent squandering of ATP (Wong, Dietrich et al. 2009). The crystal structure of a short tail fragment bound to both head domains revealed how the tail inhibits the motor by preventing the ADP release from both motor domains (Kaan, Hackney et al. 2011).

Dyneins are responsible for the majority of minus-end directed cargo transport events of microtubules. Since a large fraction of organelles appear to move both

to minus and plus ends of microtubules, many organelles are likely to be associated with dynein receptor. The cytoplasmic dynein is a processive dimer with complex composition (Akhmanova and Hammer 2010). It is bound to microtubule via a small region followed by a hexameric AAA+ domain containing head. The head domain is linked to the cargo binding tail by coiled-coil stalk. Dimeric motors create a huge complex with twelve AAA+ domains (Figure 1.1)(Veigel and Schmidt 2011; Ishikawa 2012).

#### **1.4 EB1**

End binding proteins are small proteins localized to the growing tip of microtubules. They recruit other proteins to the microtubule cytoskeleton that are required for cell polarity and signaling events. Furthermore end-binding proteins stimulate microtubule growth. Protein binding to the growing microtubule plus end can also serve to „push“ cargoes through the cell and thus contribute to intracellular transport. The best-described member of this class is the End Binding protein 1 (EB1). It is conserved from yeast to human, where three ubiquitously expressed paralogs were found (EB1, EB2, and EB3) (Su and Qi 2001). The overexpression of EB1 and EB3 in mammalian cells leads to microtubule bundling (Bu and Su 2001). EB1 consists of N-terminal microtubule-interacting domain (residues 12-133) and C-terminal region that binds to cargo (residues 185-255). Crystal structures of later revealed a coil-coiled domain that has a four-helix bundle on its end (Slep, Rogers et al. 2005; Huls, Storchova et al. 2012). In humans, this so-called EB1-like domain is sufficient to bind the adenomatous polyposis coli (APC) tumor suppressor protein and microtubule actin cross-linking factor (MACF). Its overexpression disrupts polarity signaling (Slep, Rogers et al. 2005). Both APC and spektraplaklin MACF are large proteins of 1000-5000 amino acids and have a microtubule binding motif by themselves (Sun, Leung et al. 2001). The proposed mechanism of microtubule growth stimulation is still not well understood. The plus end binding proteins have been suggested to bind tubulin dimers or multimers, raising its affinity for other tubulin molecules and acting as chaperones (Slep and Vale 2007).

A yeast homologue Bim1p shares 35% sequence identity with EB1 (Bienz 2001). Bim1p interacts with the polarity determinant Kar9p and both connect

microtubules to the cell cortex (Korinek, Copeland et al. 2000; Huls, Storchova et al. 2012). Kar9p is a functional homolog of APC, but its structure is unknown and the domain architecture different (Slep, Rogers et al. 2005).

## **1.5 Actin**

Actin is one of the most conserved proteins in nature. It is important for subcellular organization, maintenance of cell shape, motility, and the creation of contractile forces. In bacteria, the evolutionary related proteins MreB and ParM also form linear or helical filaments and are responsible for cell-shape and cell division organization (Kudryashov, Sawaya et al. 2005)

For its cellular function, actin assembles into ordered polymeric filaments. Actin monomer, the basic element of the filament, is called G-actin, which stands for globular-actin. The filamentous actin is called F-actin. The protein structure is well known, as the first crystal structure of G-actin was determined already in 1990 in a complex with DNase I that served as a polymerization inhibitor (Kabsch, Mannherz et al. 1990).

The filaments possess polarity that allows a directed transport by motors. Conventional myosins move from the pointed or minus end the filament towards the barbed or plus end mostly in the cellular periphery (Oda, Iwasa et al. 2009).

## **1.6 Unconventional myosins**

Myosins are large motor proteins that use energy from ATP hydrolysis to move along actin filaments. They are involved in wide spectrum of intracellular transport events and cellular functions like cytokinesis, cell adhesion, endocytosis, exocytosis, and movement of cargoes along actin filament. Some myosins have adapted to transport cargoes such as organelles, vesicles, mRNAs, or proteins, whereas others are rather load-bearing tension sensors (Hammer and Sellers 2012).

Based on the gene sequence and phylogenetic alignment, the large myosin family is divided into approximately 20 classes (Richards and Cavalier-Smith 2005). In human, over 40 myosin genes were found, divided into 17 classes (Berg, Powell

et al. 2001; Krendel and Mooseker 2005). The accepted nomenclature uses Arabic and roman numbers in abbreviations of classes. Myosin 5a (Myo5a) refers to a protein that belongs to the type V myosin class. There are few exceptions as Myo4p and Myo2p both belong to yeast MyoV class. MyoA and MyoJ are class I and V myosins resp. from *Dyctiostellium* etc (Krendel and Mooseker 2005).

Myosins are not only specialized in binding to diverse cargoes, but also by motor adaptation. The motors are characterized by for instance processivity, velocity, the amount of force produced during a single ATPase cycle, directionality of the movement and duty ratio. These properties that vary among all myosin classes and subclasses enable each molecule to be specialized for different cellular functions. For example, rapid contraction of actomyosins is induced by Myo2a, which is a low-duty-ratio motor (Krendel and Mooseker 2005).

Myosins are mostly cytoplasmic, located to the actin rich areas that are often tissue or cell specific. There are only few reports on myosin localization inside the nucleus. Myosin type I, II, VI and Myo5b are involved in RNA polymerase movement or interaction and thus in transcription (Pestic-Dragovich, Stojiljkovic et al. 2000; Vreugde, Ferrai et al. 2006; Li and Sarna 2009; Lindsay and McCaffrey 2009). This process is however poorly understood. In Myosin type I, the nuclear localization sequence is located within the second IQ motif at the neck domain and elevated concentrations of calmodulin (CaM) interfere with its nuclear localization (Dzijak, Yildirim et al. 2012).

## **1.7 Type V Myosin**

According to phylogenetic trees type V myosin is one of the oldest classes of this motor family (Richards and Cavalier-Smith 2005). This class of myosins is defined by its special C-terminal globular domain (GD). The MyoV motors play a role in the regulation of short distance intracellular transport, as well as in anchoring, positioning, segregation and docking of organelles or hitchhiking kinesins for long-distance cargo transport. In cargo protein complexes they move organelles, vesicles, and mRNA along actin cables (Sellers and Veigel 2006).



Myosins show similarity in their domain organization to kinesins (see chapter 1.3).

### **1.8 Type V myosin in human**

Myo5a, Myo5b, and Myo5c share an almost identical domain organization. However, each Myo5 show cargo specific differences and the expression patterns and local enrichments are also different (Lapierre, Kumar et al. 2001; Rodriguez and Cheney 2002).

Human type V myosins are composed of actin binding N-terminal motor domain called head, lever arm, rod and a globular tail at the C-terminus. The head consists of two 50 kDa motor domains connected by a loop. This organization is common to all types of myosins. The ATP-dependent motor domain transfers conformation changes from the active site to the stretch of 6 IQ motifs on the lever arm helix. The lever arm is decorated by calmodulins. Each IQ motif consists of the consensus sequence IQXXRGXXR, which is a highly conserved binding site for CaM. It has been suggested that perhaps also an Essential or Regulatory Light Chain binds to the first IQ motif (Syamaladevi, Spudich et al. 2012).

In contrast to other myosins, the MyoVs lever arm is very long and enables thus not only simultaneous binding of both motors to actin, but also very long steps (Purcell, Morris et al. 2002). The lever arm is followed by a coiled-coil rod of about 500 amino acids, which mediates dimerization of the motor protein. Few flexible loop regions, called exons are tissue-specifically spliced and interrupt the coil-coiled helix. In case of Myo5a, exons B, D and F are were found. For instance, in human melanocytes only the Myo5a isoform consisting of exons A, C, D, E and F is expressed, while the isoform containing exons A, B, C and E is prevalent in neuronal cells (Seperack, Mercer et al. 1995). The globular domains as well as regions encoded by differentially spliced exons bind to cargo or adapter proteins. In contrast to protozoan and invertebrates, mammals have three MyoV paralogs, whose gene products are termed myosin 5a (Myo5a), myosin 5b (Myo5b), and myosin 5c (Myo5c) (Vale 2003).

### 1.8.1 Myo5a

Around 20 different proteins are known to bind to the Myo5a GD, providing specificity for molecular transport (Vale 2003). Myo5a is most abundant in neuronal, skin, and testicular cells (Rodriguez and Cheney 2002; Desnos, Huet et al. 2007). Attention was particularly paid to the Myo5a-dependent transport in melanosomes and neuronal cells (Sellers and Veigel 2006). Dysfunction of the Myo5a gene has been linked to Griscelli syndrome (GS) type 3. Patients with this syndrome display partial albinism and immunodeficiencies (Menasche, Ho et al. 2003). Less understood is similar transport in retinal-pigmented epithelial cells in eye. In both cell types, Myo5a was shown to drive the short-range transport in the cell periphery. Many *in vivo* studies have demonstrated that Myo5a colocalizes also with centrosomes (Espreafico, Coling et al. 1998), Golgi, mitochondria, melanosome organelles, and endoplasmatic reticulum (Nascimento, Amaral et al. 1997; Sahlender, Roberts et al. 2005).

Melanosomes are lysosome-related organelles inside the melanocytes, where pigment (melanine) is produced. Melanosomes are transported from the Golgi region around nucleus along microtubules to the dendrites. This long-distance transport is mediated by kinesin motors. Then, melanocytes are captured by Myo5a and transported to the dendrite tips and further to keratinocytes, where the pigment is stored. Here melanin protects DNA against UV damage (Kukimoto-Niino, Sakamoto et al. 2008). For melanosome transport, Myo5a binds to the adapter melanophilin (Mlph), which itself associates with the small Rab GTPase Rab27a. The latter binds directly to the melanosome membrane (Fukuda, Kuroda et al. 2002). This complex was shown to move processively along actin filaments even *in vitro* (Wu, Sakamoto et al. 2006).

In the last years, evidence for a role of Myo5a in neuronal synaptic plasticity increased. Myo5a has been detected in presynaptic terminals (Schlamp and Williams 1996), axon terminals, and dendritic spines (Prekeris and Terrian 1997). A stoichiometry of 100 Myo5a molecules per brain vesicle has been reported (Miller and Sheetz 2000). The synaptic plasticity is supported by Myo5a transport of smooth endoplasmic reticulum tubules into the dendritic spines of cerebellar Purkinje neurons (Wagner, Brenowitz et al. 2011).

It has been speculated for a long time, whether type V myosins localize exclusively to the cytoplasm. However, in 2008, it was reported that Myo5a phosphorylated on serine 1650 localizes to nuclear speckles (Pranchevicius, Baqui et al. 2008). Later, this finding was confirmed and Myo5a as well as Myo5b were found in the nuclear fraction. While Myo5a was localized in the nucleoplasm, Myo5b was detected even in nucleoli (Lindsay and McCaffrey 2009). Indeed it has been claimed that a Myo5b region of the second IQ motif displays sequence homology to Nop25, which localizes to nucleus (Fujiwara, Suzuki et al. 2006; Lindsay and McCaffrey 2009). Since a truncation mutant of Myo5a (residues 710-1258) also localizes to the nucleus, a model has been postulated where Myo5a upon activation by  $\text{Ca}^{2+}$  loses CaM from the second IQ motif and exposes thus the nucleolar localization motif (Trybus, Gushchin et al. 2007). The nucleolus is a site where RNA Pol I as well as actin are located and surprisingly, both were shown to be associated with Myo5b (Lindsay and McCaffrey 2009).

### **1.8.2 Myo5b**

Mutations in the *myo5b* gene of patients are associated with microvillus inclusion disease (Muller, Hess et al. 2008; Szperl, Golachowska et al. 2011). Myo5b is found in almost all cell types and has been particularly studied in neuronal cells (Roland, Bryant et al. 2011) and enterocytes (Muller, Hess et al. 2008; Szperl, Golachowska et al. 2011). Myo5b colocalizes with IgA receptor, part of glutamate receptor GluR1 (Lapierre, Kumar et al. 2001). The transferrin receptor transport has been shown to be Myo5b dependent (Lapierre, Kumar et al. 2001; Wendt, Taylor et al. 2001). Also transport of the  $\text{M}_4$  muscarinic acetylcholine receptor might be directed by Myo5b (Volpicelli, Lah et al. 2002), as well as transport of the chemokine receptor CXCR2 (Fan, Lapierre et al. 2004; Roland, Kenworthy et al. 2007).

Recent publications also support the hypothesis that Myo5b is involved in remodeling of dendritic spines in the mammalian hippocampus. This spine membrane remodeling is thought to be important for learning and memory. The dendritic spine is a micron-sized protrusion, which stores recycling endosomes in its base. When the neuron is stimulated and the  $\text{Ca}^{2+}$  level increases the

vesicles move close to the spine surface. During stimulation or so called long-term potentiation of dendritic spines, the size of membrane surface increases as well as the number of AMPA (alfa-amino-3-hydroxy-5-methyl-4-isoxazol propionic acid) receptor upon NMDA (N-methyl-D-aspartate) receptor activation. The transient increase of  $\text{Ca}^{2+}$  levels is linked to Myo5b activation, which is then able to recruit a complex consisting of Rab11a and Rab11-FIP2. This complex is bound to recycling endosomes that serve as a storage places for AMPA receptors (Wang, Edwards et al. 2008; Hammer and Sellers 2012).

The same Rab11-FIP2 adaptor complex was found on vesicles rising from the endocytic-recycling compartment that are decorated by Rab11a. Rab11a binds to an adaptor protein Rab11-FIP2 (Rab11-Family of Interacting Proteins) and both bind to Myo5b (Hales, Vaerman et al. 2002; Lindsay and McCaffrey 2009). This complex has been linked to many types of cargoes, especially receptors and proteins that are internalized and recycled via clathrin-mediated endocytosis. Myo5b is also involved in clathrin-independent protein transport. Here, Myo5b is bound to Rab8a but not to Rab11a (Roland, Kenworthy et al. 2007).

### **1.8.3 Myo5c**

Myo5c appears to be mostly expressed in glandular tissues and in the apical domain of epithelial cells, such as exocrine pancreas, prostate and mammary gland (Rodriguez and Cheney 2002). Its localization is clearly distinct from Myo5a or Myo5b (Jacobs, Weigert et al. 2009). Together with Myo5b, Myo5c localize to transferrin receptor vesicles where it was found to bind Rab8 GTPase. Expression of the dominant negative Myo5c tail disrupts the production of Rab8 coated vesicles, which accumulate in large tubular structures and thus inhibits transferrin recycling. Expression of the dominant negative tail does not perturb the Golgi compartment, lysosomes, late endosomes, endogenous Myo5a or the Rab11a-associated recycling compartment (Rodriguez and Cheney 2002).

In the eye, Myo5c together with Rab3d is responsible for transport of vesicles that contain tear film proteins for the protection, provision of nutrition and growth factors for the eye surface (Marchelletta, Jacobs et al. 2008). In a large proteomics study of pancreatic zymogen granule membranes, Myo5c was found on the surface of secretory granules (Chen, Walker et al. 2006). Myo5c is still

poorly understood and so far, no heritable syndrome has been linked to a genetical mutation in Myo5c.

#### **1.8.4 Autoinhibition**

Already in 1982, a conformational change that inhibits ATPase activity was shown for myosin II (Trybus, Huiatt et al. 1982). In studies assessing hydrodynamic radii, myosin II was shown to exist in two distinct conformations. The molecule was elongated or open at 10S and more compact or closed at 6S (Trybus, Huiatt et al. 1982; Ikebe, Hinkins et al. 1983). The mechanism was revealed some years later, when it was shown that dimerization is important and the open 10S form possesses ATPase activity, whereas the closed is inactive. The closed conformation is asymmetric, because a converter domain of one head interacts with the actin-binding region of the other head and prevents it from binding to actin (Wendt, Taylor et al. 2001).

Another known case of autoinhibition comes from the distantly related kinesin family. Both inactive closed and active open conformations were shown for kinesin-1. In contrast to myosin II, the motor activity is inhibited by its cargo-binding domain in the absence of cargo (Verhey and Rapoport 2001).

A similar model of inhibition was suggested for myosin V. Myo5a constitutes 0.2% of the total protein in the brain (Cheney, O'Shea et al. 1993). It is therefore necessary to regulate the ATP consumption while the motor is not bound to cargo. Otherwise such unregulated motor activity would waste huge amounts of ATP.

In ultracentrifugation experiments similar to experiments with myosin II, Myo5a was as well shown to exist in two conformations with different sedimentation coefficients. The elongated form sediment at 14S and the closed autoinhibited conformation at 11S (Li, Mabuchi et al. 2004).

Biochemical studies with Myo5a confirmed that in the closed conformation is indeed the GD mediating autoinhibition of the motor domain (Li, Jung et al. 2006; Thirumurugan, Sakamoto et al. 2006). Another new approach to confirm the three-dimensional structure in autoinhibited state was a cryoelectron tomography of 2D-layer crystals of full-length Myo5a (Figure 1.2) (Liu, Taylor et al. 2006).

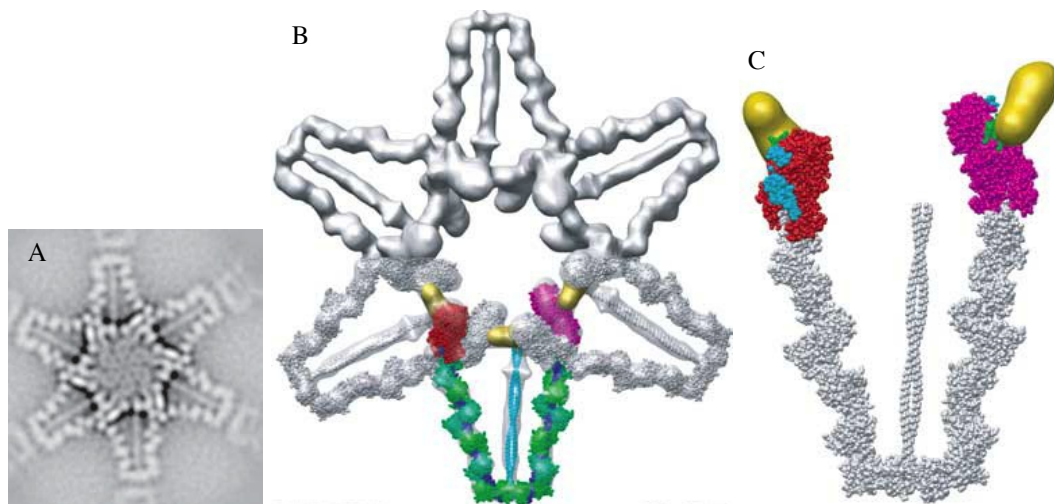


**Figure 1.2 Electron micrographs, molecular arrangement within the 'coneflower' motif and placement of the cargo-binding domain.** (A) Negatively stained Myo5a full-length 2D arrays highlighting the 'coneflower' motif. (B) The upper three molecules depicted in opaque surface rendering viewed from the solvent phase. The lower three molecules a translucent surface view, with the space filling atomic model of Myo5a rendered in colors in the middle. The color scheme is as follows: motor domains in red and magenta, light chains in green, the lever arm in dark blue, the coil-coiled in cyan, the cargo binding domain density envelope as yellow blob; adjacent molecules in grey. (C) Both cargo-binding domains were poorly resolved. The color scheme is as follows: motor domains in red and magenta, light chains and lever arm, the coil-coiled in grey, the cargo binding domain density envelope as yellow blob, the actin binding surface in cyan, the loop 1 in green. View from the same direction as (B). Picture taken from (Liu, Taylor et al. 2006)

In a subsequent mutational study, two basic amino acids K1706 and K1779 in the GD of mouse Myo5a and residue D136 in the motor domain were identified as required for autoinhibition (Li, Jung et al. 2008). Because residue D136 of the motor domain is somewhat distant from the ATP-binding pocket, an allosteric inhibition had been proposed.

Electron microscopy has shown both the extended and auto-inhibited forms, however the precise position and structure of the GD could not be determined (Liu et al., 2006). Consistently, single particle reconstruction by electron microscopy revealed that in this closed conformation the motor domain is placed in close vicinity to the GD, most likely forming the inactivated complex (Thirumurugan, Sakamoto et al. 2006). Also the tree-dimensional structure obtained by cryoelectron tomography revealed structural information on MyoV molecules in their autoinhibited state (Liu, Taylor et al. 2006). Here, six dimers are folded into a 'coneflower' motif; the motor domains are clearly folded back in direction of the Myo5a C-terminus (Figure 1.2 A). However both cargo-binding domains were poorly resolved and a direct interaction of motor domain with GD

could not be proved (Figure 1.2 B). The GD was solely modeled as a blob (Figure 1.2 C, in yellow).

Also autoinhibition of yeast myosins Vs remain elusive. The group of Lois Weisman tested whether the yeast two-hybrid assay would yield an interaction between the Myo2p tail and motor domain. However although several regions were tested, none revealed an interaction. They authors suggested that also the neck could be necessary for the interaction or some additional proteins, phosphorylation or more intact dimerization might be required (Pashkova, Jin et al. 2006).

### **1.8.5 Regulation by $\text{Ca}^{2+}$**

Folding of Myo5a into the inhibited state can be induced by defined calcium concentration. However the mechanism is still unclear. Furthermore, experimental data for full-length myosin purified from tissues are inconsistent with experiments on recombinant or truncated molecules (Cheney, O'Shea et al. 1993; Li, Mabuchi et al. 2004; Wang, Thirumurugan et al. 2004). Li and colleagues expressed recombinant full-length mouse Myo5a and showed that it forms a compact conformation in the presence of low  $\text{Ca}^{2+}$  (EGTA conditions) and an elongated conformation at high  $\text{Ca}^{2+}$  levels as revealed by analytical centrifugation. The apparent sedimentation coefficient  $S_{20,w}$  (the suffix 20,w indicates that the parameter has been corrected to 20.0°C and the density of water) from ultracentrifugation experiments decreased from 13.9S in EGTA to 11.3S in high  $\text{Ca}^{2+}$  levels (Figure 1.3). Another conformational change was observed in high ionic strength. In the presence of 600 mM KCl, the  $S_{20,w}$  of the full length molecule increased from 9.4S in EGTA to 9.7S in  $\text{Ca}^{2+}$  conditions. Electron micrographs shed light on the third type of the 9.7S conformation as depicted in Figure 1.3 (Li, Mabuchi et al. 2004).

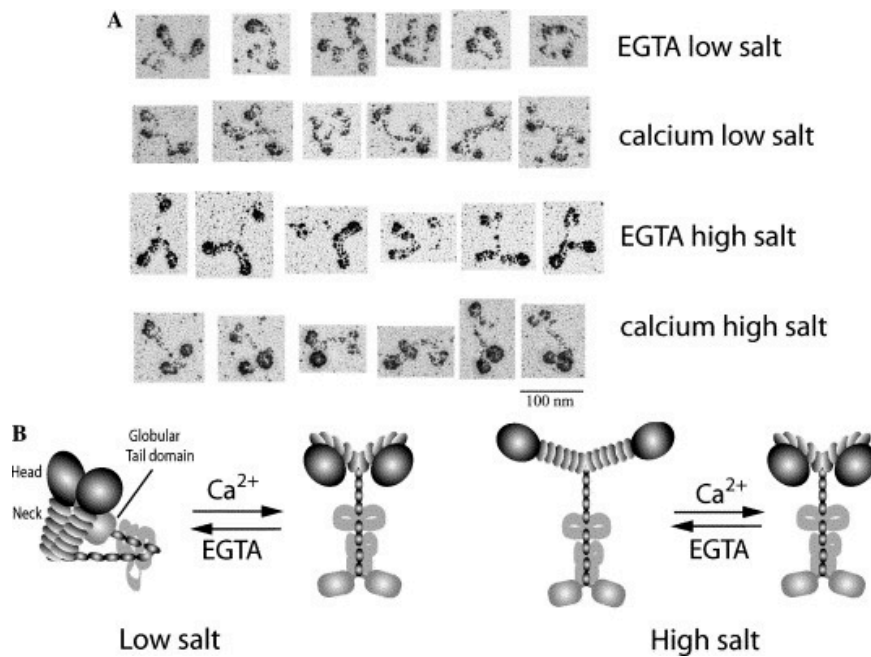


**Figure 1.3 Electron micrographs of full length Myo5a and model for the regulation of motor domains.** (A) Electron microscopic images of full length Myo5a in various conditions. (B) In low salt conditions, the globular tail domains are folded back and bind to the motor domains (13.9S). At high  $\text{Ca}^{2+}$  levels, the molecule unfolds, except of the motor domains (11.3S). The autoinhibition is abolished in high salt conditions (9.4S) and addition of  $\text{Ca}^{2+}$  folds the motor domains back (9.7S). Picture is taken from (Li, Mabuchi et al. 2004)

Later, Sellers and colleagues observed calcium-dependent actin-activated MgATPase activity in ATPase assays, but suggested that calcium is probably not the physiological mechanism of regulation (Sellers, Thirumurugan et al. 2008). Calmodulins bound to the Myo5a neck may as well behave as a supporting scaffold. At high levels of  $\text{Ca}^{2+}$  one or more CaMs could dissociate from the Myo5a lever arm. With missing CaMs, the lever arm becomes flexible and the molecule is unable to “walk” along actin filaments. Indeed, shortening of the run length was shown in single molecule motility studies in presence of EGTA and could be rescued by adding calmodulin (Li, Jung et al. 2006; Lu, Krementsova et al. 2006; Sellers, Thirumurugan et al. 2008). All unconventional myosins bind calmodulins or other types of light chains, but such regulation is likely not common to all of them. In case of the retrograde Myo6 calmodulins do not dissociate in the presence of calcium from the motor, but rather modulate its enzymatic activity (Morris, Wells et al. 2003).



### 1.8.6 Regulation by cargo attachment

The most straightforward mechanism of release from autoinhibited state could be the binding of cargo. Indeed it has been shown that melanophilin binding to the GD of Myo5a abrogates autoinhibition and activates the actin-activated ATPase. The experiment was carried out in 200 mM KCl, in the presence of GD in trans and Myo5a fragment lacking the GD, but including exon F. In the presence of melanophilin, the actin-dependent ATPase hydrolysis was activated by 4-fold (Li, Ikebe et al. 2005).

Wang et al. described unfolding of Myo5b in the presence of high  $\text{Ca}^{2+}$  levels in neuronal dendritic spines. This activation stimulates binding of Rab11 and Rab11-FIP2 and recruiting recycling endosomes (Wang, Edwards et al. 2008).

### 1.8.7 Phosphorylation

For a long time it has been speculated, whether Myo5a is at some point regulated by posttranslational modifications, such as phosphorylation. While searching for the motor responsible for pigment granule distribution in frog melanophores, Rogers and colleagues found that both Myo5a and kinesin are involved (Karcher, Roland et al. 2001). They also found that washing these purified granules with metaphase-arrested cell extracts caused dissociation of Myo5a. This dissociation was driven by phosphorylation of Myo5a serine 1650 (Rogers, Karcher et al. 1999; Karcher, Roland et al. 2001). Moreover, *in vitro* studies indicated that calmodulin dependent protein kinase II interacts with Myo5a tail, which activates its kinase activity (Costa, Mani et al. 1999). The effect of S1650E mutation on melanophilin-induced activation of the ATPase activity of Myo5a was tested in an *in vitro* assay in the presence of 200m mM KCl. At this relatively high salt concentration, phosphorylated Myo5a was not activated by melanophilin (Ikebe, Li et al. 2005). In a subsequent study, it was reported that Myo5a phosphorylated on serine 1650 localizes the motor to nuclear speckles (Pranchevicius, Baqui et al. 2008).

### 1.8.8 Griscelli syndrome

For some myosin classes, genetic and phenotypic characterization of mutants in mice or human myosins is available. Disease-causing mutations in the head domain are often situated in the actin binding site or ATPase pocket. However some mutations lead to reduced protein levels and thus it is difficult to predict the molecular reason for observed phenotypes. (Huang, Cope et al. 1998; Huang, Mermall et al. 1998). Griscelli syndrome type 3 has been ascribed to the dysfunction the *Myo5a* gene that leads to partial albinism and immunodeficiencies. Partial albinism occurs upon deficient melanosome transport. The pigment is produced, but not transported to the cell periphery and further to keratinocytes. Instead it gets stuck in the perinuclear region. These pigment clumps are visible in skin cells under microscope as well as in hair shafts of Griscelli patients (Figure 1.4)(Seabra, Mules et al. 2002).

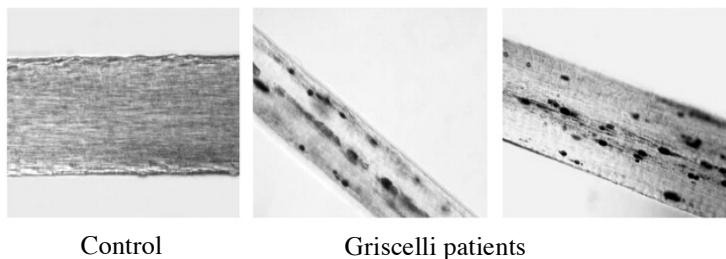


**Figure 1.4 Light microscopy of patients' hair shafts.** Left: an evenly distributed pigment of control hair shaft. Middle and right: depicted are typical large pigment clumps in Griscelli patients. These hair shafts appear to have silver color. Picture adapted from (Menasche, Ho et al. 2003).

Mice carrying null alleles of *dilute* locus that encodes *Myo5a* have lighter or so-called dilute coat color and die from neurological defects within three weeks of birth (Huang, Mermall et al. 1998; Miyata, Kishimoto et al. 2011). This mouse model of Griscelli syndrome is well described. Some of these mutations were found in the mouse *Myo5a* GD. Interestingly; three of the mutations are located within 10 amino acids of each other. They are the missense mutations Ile 1510 Asn, Met 1513 Lys, and Asp 1519 Gly (Huang, Mermall et al. 1998).

## 1.9 Melanophilin

Melanophilin (Mlph or Slac-2a) is a 590 residues long protein. It is abundant in melanocytes, where is involved in melanosome transport. There are three Mlph paralogs in human and mice, referred to as Slac-2a, Slac-2b, and Slac-2c. According to protein structure predictions Mlph shows some structured parts in particular in the N-terminus (Figure 1.5) and long intrinsically unstructured regions.

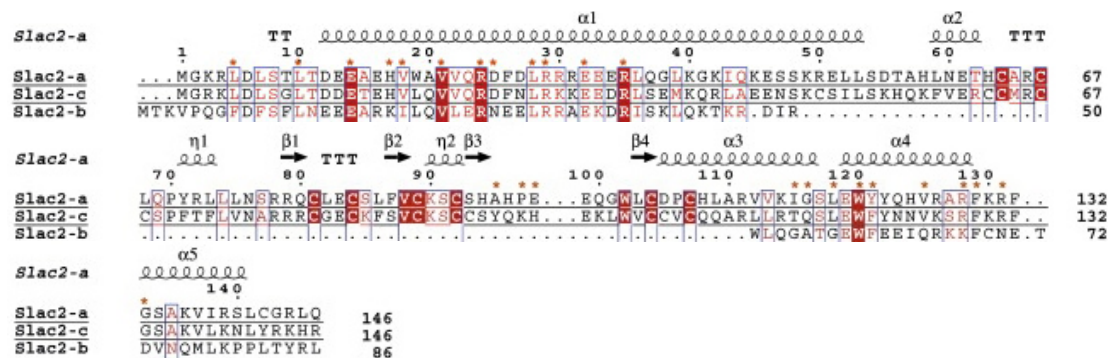


**Figure 1.5 Sequence alignment of the N-terminal Rab-binding domain of Mlph with its human paralogs.** The secondary structure is shown above the sequence. Highly conserved residues are shown with red background, less conserved residues in red. Residues important for Rab27b binding are highlighted with asterisks. Picture adapted from (Kukimoto-Niino, Sakamoto et al. 2008).

Moreover, Mlph has many sites, where Pro, Glu, Ser, and Thr are abundant. These so-called PEST sites are very sensitive to proteolysis.

Until quite recently, no high-resolution structural information for Mlph was available. In 2008, the structure of the N-terminal Mlph-Rab27b co-complex was solved and revealed this domain as a structural scaffold for Rab binding (Figure 1.6) (Kukimoto-Niino, Sakamoto et al. 2008). Interestingly, Mlph was only stable when coexpressed together with Rab27b in an *Escherichia coli* cell-free synthesis system.

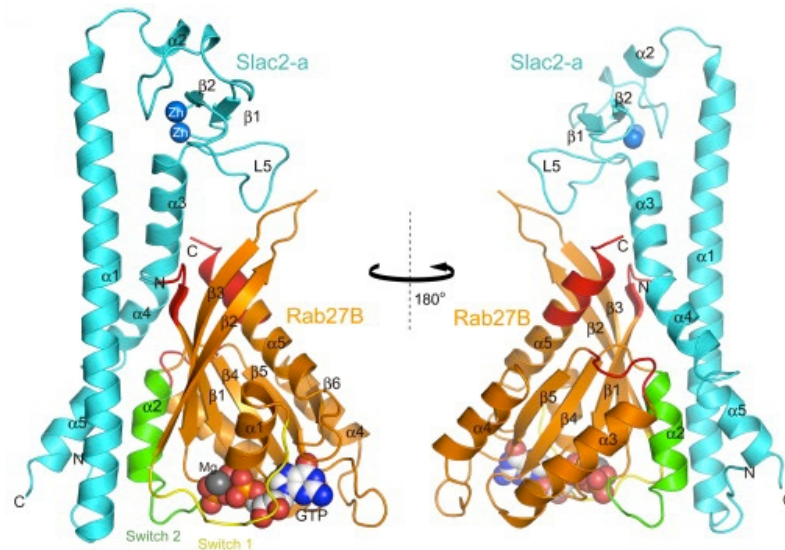


**Figure 1.6 Structure of Mlph in complex with Rab27b in ribbon representation.** Mlph is colored in cyan, Rab27b in other colors. The picture was adapted from (Kukimoto-Niino, Sakamoto et al. 2008).

The N-terminal part (residues 7-129) shares a high sequence homology to other Rab effector proteins, for example Synaptotagmin-like protein 3 (Slp-3), Granuphilin-a and -b or Rabphilin-3A. The consensus sequence contains eight cysteine residues that coordinate two  $Zn^{2+}$  ions forming a  $Zn^{2+}$  finger-binding domain and binds to the GTP-bound Rab27a or Rab27b. Instead of GTP, the structure was solved with the Rab27a Q78L mutation, which serves as a constitutive active mutant (Matesic, Yip et al. 2001). The middle region (residues 241-405 in mouse Mlph) interacts weakly with the GD of Myo5a and tightly with the exon F of this motor (residues 137-321 in mouse). Both regions bind Myo5a synergistically (Fukuda and Kuroda 2004).

A region of Mlph (373-476) is predicted to form a coil-coiled and the last 100 residues bind to microtubule-binding EB1 protein. This interaction could link myosin-dependent melanosome transport to kinesin-dependent transport, since EB1 interacts with microtubule plus ends (Wu, Tsan et al. 2005) (see paragraph 1.4 for details about EB1).

Melanophilin is both required and sufficient to link Myo5a to Rab27a (Wu, Rao et al. 2002) and thus to melanosomes or lytic granules. Lytic granules are secreted from cytotoxic T lymphocytes by exocytosis in a Rab27a-dependent manner (Stinchcombe, Barral et al. 2001).

Almost all Rab effectors have a  $\text{Ca}^{2+}$ -sensing domain at their C-terminus, targeting the proteins to the membrane. Mlph lacks this domain and instead, it binds directly to actin (Fukuda, Kuroda et al. 2002). This actin binding is somehow puzzling since in the presence of Myo5a it would compete for actin binding with the Myo5a motor domain. A strong interaction would prevent the movement of Myo5a. Strikingly, deletion of the actin-binding domain leads to impaired melanosome distribution in melanocytes (Kuroda, Ariga et al. 2003; Li, Ikebe et al. 2005).

Only mutations in mouse Mlph, but not human Mlph have been reported. Mutations in mouse Mlph showed impaired pigment transport comparable to mice with mutated Myo5a, but develop no neurological disorders. This observation is consistent with its importance in melanosome transport and its absence in neuronal cells (Matesic, Yip et al. 2001).

### **1.10 Rab GTPases**

Members of the perhaps largest class of myosin cargo adapters are small monomeric Rab GTPases. Rabs belong to the superfamily of Ras GTPases and are important for both vesicle fusion and release, decorating most of the known membrane coated particles in eukaryotic cells (Novick and Zerial 1997). Rab GTPases bind reversibly to membranes via its isoprenylated (geranyl-geranylated) C-terminus. Bound GTP switches the molecule into a biologically active state, whereas GDP inactivates the protein (Farnsworth, Kawata et al. 1991). The conformational switch upon GTP binding is large and involves an extensive hydrophobic interface between the switch I and II regions as well as stabilization of the gamma-phosphate of GTP by a hydrogen bond of a serine in the loop I region of Rab protein. The GTP core and mode of binding is highly conserved and uniform for almost all Rab GTPases (Ostermeier and Brunger 1999; Uhlig, Passlack et al. 2005). The GTPases in the switched-off state are sequestered from the cytosol by the RabGDP-dissociation inhibitor that is able to deliver them to cellular or vesicular membranes (Pfeffer, Dirac-Svejstrup et al. 1995). Some Rabs associate directly with the MyoV GDs and link the motor activity to membranes, vesicles and organelles. For instance in neuron, the GD of

Myo5a is directly bound by Rab3a (Wöllert, Patel et al. 2011). Rab3a is one of the most abundant Rab proteins in neurons and is predominantly localized to vesicles that are transported from the neuronal body to the synapse.

The crystal structure of Rab3a bound to the effector domain of Rabphilin-3a revealed the  $Mg^{2+}$  activated GTP-bound form, that is predicted to be part of an active myosin 5a complexes (Ostermeier and Brunger 1999; Wöllert, Patel et al. 2011).

In 1999, Rab3a both in GDP- or GTP-bound state was shown to interact with  $Ca^{2+}$ /CaM and mutation of R66 and R70 decreased the binding, but did not alter the ability of Rab3a to interact with RabGDI or Rabphilin (Coppola, Perret-Menoud et al. 1999). Another Rab GTPase, Rab8a was found to interact directly with Myo5a and Myo5b (Roland, Kenworthy et al. 2007) but is also involved in transferrin receptor trafficking with Myo5c (Rodriguez and Cheney 2002). Vesicle-associated Rab10 interacts with the GDs of all three type V myosins in an exon D dependent manner. Rab11a binds the GD of Myo5b and might associate also with Myo5a (Roland, Lapierre et al. 2009). As Rab11a and Rab27a are included in the experiments of my PhD thesis and are well described in literature in relation to MyoVs, a more detailed characterization is provided below.

### **1.10.1 Rab27a**

Rab27a, like other Rab GTPases, has at its C-terminus two cysteins that are posttranslationally modified by C20 geranylgeranyl groups. These hydrophobic groups insert into the lipid bilayer (Hammer and Wu 2002). Mutations of Rab27a have been linked to another type of Griscelli syndrome, called type 2. On one hand, patients exhibit pigmentary dilution and despite a normal number of T- and B-lymphocytes, the antibody production is impaired, leading to frequent infections and fever episodes. These symptoms are similar to Griscelli Syndrome type 1 (Griscelli, Durandy et al. 1978; Griscelli and Prunieras 1978). On the other hand, the patients manifest no primary neurologic features (Menasche, Pastural et al. 2000).

### 1.10.2 Rab11a

Rab11a is ubiquitously expressed but enriched in tissues with higher concentration of vesicle transport, for example insulin producing tissues (Sugawara, Shibasaki et al. 2009). Based on comparative genomics and phylogenetic trees, Rab11a is one of the ancestral Rabs, found in all eukaryotes and even *Monosiga brevicollis* that is according to the newest results in genome sequencing the closest unicellular relatives of Metazoa. The predicted last eukaryotic common ancestor is believed to already had a complex set of membrane trafficking components (Diekmann, Seixas et al. 2011). Crystal structure of monomeric Rab11a was solved with bound GDP (Griscelli and Prunieras 1978) (Figure 1.7). Two Rab11a bind to a dimeric part of Rab11-FIP2. The crystal structure of this co-complex confirmed that Rab11a binds to Rab11-FIP2 only when it is activated by GTP (Jagoe, Jackson et al. 2006; Jagoe, Lindsay et al. 2006). The Rab11a Q70L mutation serves as a constitutive active mutant (Ostermeier and Brunger 1999; Uhlig, Passlack et al. 2005).

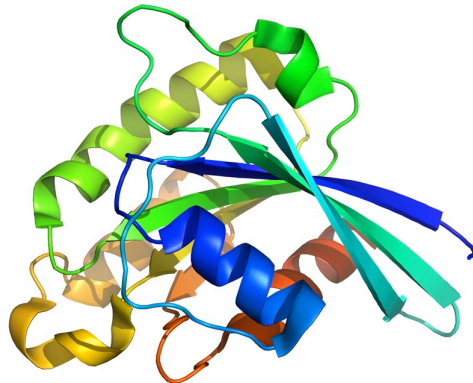


**Figure 1.7 Ribbon representation of the Rab11a monomer crystal structure.** (Griscelli and Prunieras 1978). Rab11a is depicted from N-terminus (blue) to the C-terminus (red) in rainbow colors. The picture was generated using the program Pymol, the GDP is not depicted (The PyMOL Molecular Graphics System).

### 1.11 Type V myosin in yeast and plants

The lower eukaryotes like *Saccharomyces cerevisiae* encodes only five myosin genes, two of which belong to the MyoV type motors (MYO2 and MYO4) (Berg, Powell et al. 2001).

### 1.11.1 Myo2p

The type V myosin Myo2p was first identified in 1991, in a screen for temperature-sensitive mutants involved in cell division. The motor essential for cell survival was found to be responsible for vectorial distribution of vesicles or membrane targeting in *Saccharomyces cerevisiae* (Johnston, Prendergast et al. 1991). Myo2p is involved in plethora of cellular functions and binds thus to multiple adaptor proteins and cargoes. The compact GD is solely  $\alpha$ -helical, 15 amphipathic helices are connected with one long and many short loops (Figure 1.8).

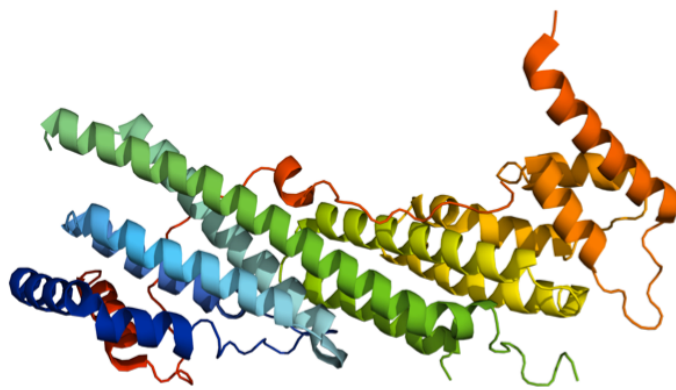


**Figure 1.8** Ribbon representation of the of Myo2p GD crystal structure from *Saccharomyces cerevisiae* (PDB ID:2F6H) (Pashkova, Jin et al. 2006). The Myo2p GD is depicted from N-terminus (blue) to the C-terminus (red) in rainbow colors. The picture was generated using the program Pymol (The PyMOL Molecular Graphics System).

When this long loop from residue 1352 to 1336 is cleaved by mild proteolysis, the two polypeptide chains of the GD was shown to stick together. However in denaturizing conditions of SDS PAGE, the GD splits into halves of about 22 kDa. This loop excision was the necessary and elegant trick of Pashkova and colleagues to obtain well diffracting crystals and solve the crystal structure (Pashkova, Jin et al. 2006). The two halves were named sub-domains I and II. Point mutations in a small region of domain I disrupt binding of Vac17p, a component of the vacuole-specific receptor complex. The second sub-domain revealed a vesicle-binding region that shares some conserved residues in the region even with distant species like *Drosophila melanogaster* and *Mus musculus*. Three known binding partners were found: Vac17p, Kar9p, and Smy1p (Pashkova, Jin et al. 2006).



### 1.11.2 Myo4p

The second member of type V myosins in yeast is Myo4p. Discovered three years later (Haarer, Petzold et al. 1994), Myo4p was found to be non-essential, but important during mitosis for mating-type switching, transport of about 40 mRNA and cortical ER to the bud tip (Estrada, Kim et al. 2003; Muller, Heuck et al. 2007). This transport is important for distribution of cellular components between mother and daughter cell (Jansen, Dowzer et al. 1996). Transported mRNAs are packed together with adaptor proteins into huge complexes that are moved by molecular motors. Particularly transport of *ASH1* mRNA into the daughter cell of a dividing cell is one of the best-studied processes. Some RNA-binding proteins important for proper *ASH1* mRNA localization and translational control during and after transport are still poorly described. However all core components for a functional RNA transport are thought to be already discovered: Myo4p is bound to adaptor proteins She2p and She3p, which are associated with *ASH1* mRNA (Muller, Heuck et al. 2007; Muller, Heym et al. 2011). This association is specific, as *ASH1* mRNA is recognized by several cis-acting RNA elements called zip codes (Muller, Richter et al. 2009). Less understood is the Myo4p driven ER-inheritance. Obviously, the transport is She2p and mRNA independent, but She3p is required and probably one or more other adaptor components (Estrada, Kim et al. 2003; Paquin and Chartrand 2008).

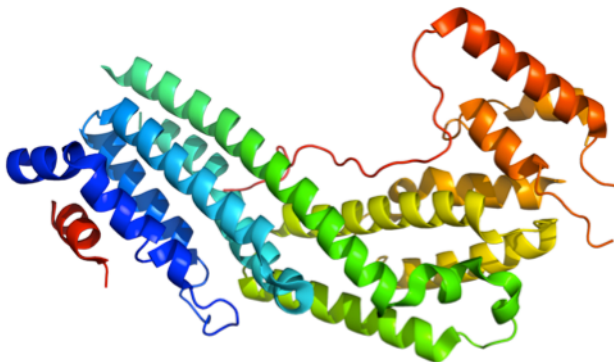


**Figure 1.9** Ribbon representation of the Myo4p GD crystal structure from *Saccharomyces cerevisiae* (PDB ID: 3MMI). Depicted from N-terminus (blue) to the C-terminus (red) in rainbow colors (Heuck, Fetka et al. 2010). The picture was generated using the program Pymol (The PyMOL Molecular Graphics System).

Determination of the Myo4p GD x-ray structure revealed 14 tightly packed helices and an unstructured loop that is wrapped around the whole molecule, similar to Myo2p (Pashkova, Jin et al. 2006; Heuck, Fetka et al. 2010). The structure also shows absence of autoinhibition-specific amino acids known from the Myo2p GD structure (Figure 1.9).

### **1.11.3 Myosins in plant**

There are only three myosin classes in plants (VII, XI and XIII) (Nunokawa, Anan et al. 2007). The plant version of type V myosin is called Myosin XI (MyoXI or *Chara*). The predicted structure of its GD seems to be similar to Myo5a GD and was observed to be associated with cellular vesicles, such as endoplasmic reticulum via direct binding to acidic phospholipids (Nunokawa, Anan et al. 2007; Reisen and Hanson 2007).

### **1.12 Myo6**

The only known myosin able to walk in reverse direction on actin filament is Myo6 (Wells, Lin et al. 1999). The dimeric molecule takes large hand-over-hand steps (30-36 nm) and move in distance up to 1-2  $\mu\text{m}$  without dissociating (Park, Ramamurthy et al. 2006), but movement of single molecules was also reported (Kellerman and Miller 1992; Wells, Lin et al. 1999). Despite the step length and processivity resembles Myo5a, Myo6 has a very short lever arm with only one IQ domain that binds CaM (Hasson and Mooseker 1994). However, another CaM binds to a unique insert next to the lever arm (Bahloul, Chevreux et al. 2004).

Myo6 is involved in a plethora of cellular functions, including directed actin-based distribution of cargoes in polarized cells, but also serves as a anchor of membranes to actin in stereocilia of hair cell in the inner ear (Seiler, Ben-David et al. 2004). This active transport on one hand and anchoring features on the other hand are striking and are related to the Myo6 ability to exist both as monomer and dimer. Such transport/anchor behavior is known only for the myosins of class VII, X, and XV (Yang, Kovacs et al. 2006; Yu, Feng et al. 2009).

Myo6 mutation leads to the *Snell's waltzer* deaf phenotype in mouse (Avraham, Hasson et al. 1995).

Recently the structure of the Myo6 cargo-binding domain (CBD) was solved (Yu, Feng et al. 2009). As the team of Zhang reports, it took them 8 years to finally solve this structure. Myo6 serves in clathrin-dependent endocytosis where Myo6 is linked to clathrin-coated vesicles via protein Disabled-2 that mediates Myo6 dimerization. Disabled-2 binds with very high affinity ( $K_D \sim 50$  nM). This finding was necessary to solve the crystal structure of part of the CBD of mouse Myo6. Formation of a co-complex with Disabled-2 locked the domain into a dimer that was stable enough to form well diffracting crystals (Yu, Feng et al. 2009). The structure of Myo6 CBD does not resemble any so far known Myosin V GD structure (Myo2p, Myo4p)(Figure 1.10). Instead of a purely  $\alpha$ -helical fold, the CBD is formed by four  $\beta$  strands ( $\beta A-\beta D$ ) to which three of six helices ( $\alpha A-\alpha F$ ) are tightly bound. The other three helices are decorating the remaining periphery of the  $\beta$  strands, leaving a bulky part of the  $\beta$  sheets exposed to the solvent. Additional 80 residues at the C-terminus were not part of the structure. This very terminus binds to lipid membranes and to an adaptor protein Optineurin and probably forms another subdomain (Yu, Feng et al. 2009). Optineurin connects Myo6 with Golgi complex during exocytosis (Sahlender, Roberts et al. 2005).

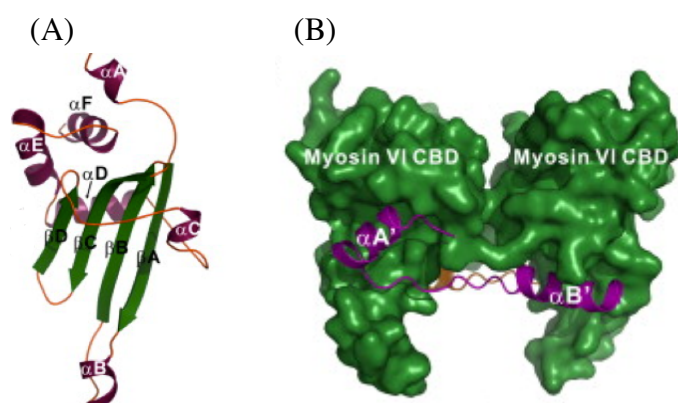


**Figure 1.10 NMR and x-ray structure of both monomeric and dimeric Myo6 CBD.** (A) Ribbon representation of monomeric Myosin VI CBD NMR structure from *Mus musculus* (PDB ID: 2KIA). The molecule is depicted from N-terminus (blue) to the C-terminus (red) in rainbow colors. (B) A surface representation of dimeric Myosin VI CBD (green) crystal structure in co-complex with a Disabled-2 peptide (magenta). Picture adapted from (Yu, Feng et al. 2009; Syamaladevi, Spudich et al. 2012).

### 1.13 Objectives

**Project 1:** My first goal was to solve the structure of **Myo5a** and **Rab27a**. These adaptor proteins connect the Myo5a motor to the transported melanosomes. The project was inspired by a publication in the journal *Cell*, where Rab3a was co-crystallized in complex with Rabphilin-3a (Ostermeier and Brunger 1999).

**Project 2:** Protein structure prediction programs suggested that the **Myo6** CBD does not fold in a way similar to CBDs of other myosins. In *Drosophila*, the Myo6 CBD was reported to directly bind to the cargo adapter Miranda, thereby supporting transport processes that are required for neuronal stem-cell differentiation. Thus my goal was to characterize this interaction and solve the structure of Myo6 CBD alone or in complex with Miranda by X-ray crystallography or NMR.

**Project 3:** The microtubule-associated EB1 links the actin-bound Myo5a complex to microtubules, which is important for certain stages of melanosome transport. The third project was to characterize the part of **Myo5a** that interacts with the C-terminal end of **EB1** and solve their co-structure.

**Project 4:** The fourth goal was to solve the crystal structures of the GDs of all three paralogs of human type V myosin. Myo5a, Myo5b, and Myo5c exhibit differential cargo preferences and recognition of the right cargo is attributed to the GD. Particular attention was paid to Myo5a, as it constitutes the most studied cargo-transporting myosin. Since it was unclear whether only Myo5a or all three human MyoV paralogs can undergo autoinhibition, I also wished to characterize the autoinhibition of Myo5a, Myo5b, and Myo5c by functional assays.

## **2. Results**

### **2.1 Structural studies on Melanophilin**

The aim was to study Mlph in more detail, because of its multifaceted functions. It serves as an indispensable link for Myo5a-dependent melanosome transport and binds directly to actin. Because it interacts with EB1, Mlph also serves as a connector between Myo5a and microtubules. Mlph is a predominantly unstructured protein of 66 kDa that is prone to degradation because of special PEST sequences (see chapter 1.9)(Wu, Tsan et al. 2005; Geething and Spudich 2007).

#### **2.1.1 Melanophilin-Rab27a complex**

The crystal structure of Rab3a-Rabphilin complex was published already in 1999 (Ostermeier and Brunger 1999). Because the Rab3a and Rabphilin adaptor proteins are homologs of Rab27a and Mlph, my first experiments were based on this publication. The similarity of experiments promised relatively fast gain of the information about binding and regulation of the two proteins. I designed thus protein fragments of Rab27a and Mlph based on the Rab3a-Rabphilin structure. Human Rab27a has 221 amino acids and 25 kDa. Because Cys 219 and Cys 220 of Rab27a are geranylgeranylated, the last three amino acids from Rab27a were removed. A Q78L mutation mimicking a GTP-activated state was introduced to ensure binding of Mlph (Table 2.1). Attempts to gain any Mlph fragment failed, because of fast degradation. Also two plasmid co-expression or co-expression of Rab27a without tag and GST or His tagged Mlph in one plasmid (pET Dual) failed due to Mlph instability (Table 2.2).

#### Rab27a Q78L protein fragments

Tag	Amino acids	Stability	kDa	Interacts with
GST	1-218	++++	25	Mlph
no tag	1-218	++++	25	Mlph

**Table 2.1 Rab27a protein fragments that were used in experiments.** Proteins are labeled from (-) to (+++), according to high or low tendency to aggregation or degradation.

Later in 2008, the crystal structure of Rab27b with N-terminal part of Mlph was published. Rab27b is a Rab27a paralog in human and shares high sequence conservation. The authors avoided degradation of proteins by co-expression Mlph with Rab27b in an *E. coli* cell-free synthesis system (Kukimoto-Niino, Sakamoto et al. 2008). My project became obsolete and was closed.

#### 2.1.2 Melanophilin-Myo5a complex

Two regions of Mlph were shown to bind to Myo5a. The more N-terminal part of Mlph (residues 147-240) interacts with the GD of Myo5a, whereas the more C-terminal part (residues 267-483) interacts with Myo5a exon F in the coil-coiled region (Fukuda and Kuroda 2004; Hume, Tarafder et al. 2006). The binding of mouse Mlph (147- 403, 147-220 and 147-201) to mouse Myo5a GD was later characterized by isothermal calorimetric titration and the  $K_d$  was measured to be about 0.5  $\mu$ M for these Mlph fragments (Geething and Spudich 2007).

For further structural or functional studies, I expressed Mlph in *E. coli*, either in presence of Myo5a or alone. Several fragments were tested in order to obtain some suitable and foremost not-degrading fragments. The protein was purified with standard chromatography techniques and with an emphasis on short purification time. Also, many of these Mlph fragments do not absorb at 280 nm and appear much larger both in SDS-PAGE and size-exclusion chromatography. This discrepancy was already observed in a previous study, in which the authors explained these abnormalities by the intrinsically unstructured nature of this molecule (Geething and Spudich 2007). Except of GST-Mlph (147 – 240) and MBP-Mlph (405 – 550) none of tested Mlph fragments had a reasonable stability from degradation (Table 2.2).

#### Melanophilin protein fragments

Tag	Amino acids	Stability	kDa	Interacts with
<b>His</b>	1-150	+	17.2	Rab27a
<b>His</b>	1-413	+	47	Rab27a
<b>MBP</b>	405 – 550	++	56	EB1
<b>GST</b>	405 – 550	-	16.5	EB1
<b>GST</b>	482 – 550	+	7.9	EB1
<b>MBP</b>	405 – 590	+	62	EB1
<b>GST</b>	405 – 590	+	21.4	EB1
<b>GST</b>	147 – 240	++	10.7	Myo5a
<b>GST</b>	147 – 404	+	28	Myo5a
<b>GST</b>	156 – 405	-	-	Myo5a
<b>GST</b>	156 – 483	-	-	Myo5a
<b>GST</b>	176-201	+	3.2	Myo5a
<b>GST</b>	267 – 405	+	46	Myo5a
<b>GST</b>	268 – 413	+	15.7	Myo5a exon F
<b>GST</b>	267– 483	-	-	Myo5a exon F

**Table 2.2 Mlph protein fragments used in experiments.** Proteins are labeled from (-) to (+++), according to high or low tendency to aggregation and degradation.

To find a Mlph fragment which is not prone to degradation and thus suitable for co-crystallization, I designed a 34 residues long fragment according to the peptide used for the ITC study mentioned above (Geething and Spudich 2007). This homologous fragment from mouse Mlph was shown to bind to mouse Myo5a GD (1446 – 1855). The corresponding human Mlph sequence is: QAQPFSGSKKKRLLSVHDFDFEGDSDQSTQPQGHs. In order to narrow down the binding region, I designed a peptide array in which this fragment was split into 15 overlapping peptides. In one peptide array each peptide was 20 residues long (20 mer) and in the other these peptides were 15 residues long (15 mer). In the peptide array each peptide is followed by a peptide whose one amino acid sequence is shifted by one residue. This way a scanning profile of the whole sequence in a peptide array is generated (Figure 2.1 A and B). These peptides were synthesized on a cellulose membrane by Dr. Georg Arnold (Laboratory for Functional Genome Analysis, Gene Center of the LMU, Germany). Briefly, I incubated the membrane with HA-tagged Myo5a GD (1446-1855) and detected the bound protein via its HA tag with an anti-HA antibody (Figure 2.1 C and D).





Later, when I solved the crystal structure of Myo5a GD (1467-1855), (see chapter 2.3.4), I repeated the co-crystallization trials but also soaking of Myo5a GD crystals. No additional density was found for Mlph peptide. However the experiments led to the identification of a crystal that diffracted to a better resolution. Interestingly, addition of peptides seemed to decrease the nucleation rate and improved crystal size (Figure 2.2 A-C), but only when the ratio between Myo5a GD and Mlph peptide was 1:1 or less. A ratio of 1:2 Myo5a GD and Mlph peptide led only to precipitation.

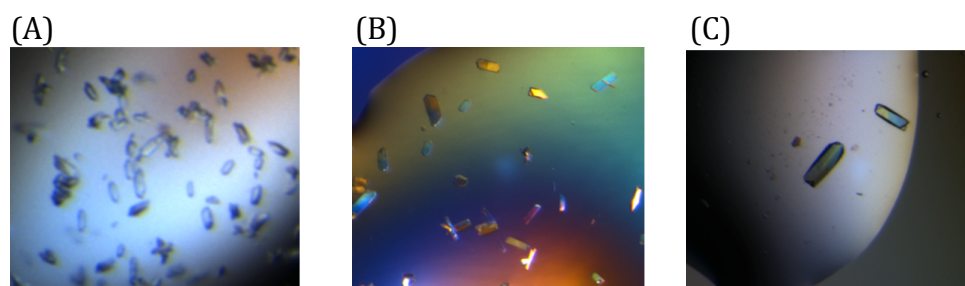


**Figure 2.2 Myo5a GD (1467 – 1855) crystals.** Pictures of crystals grown from 3 mg/ml Myo5a GD (1467-1855), 0.14 M DL-Malic acid pH 7, 35 % v/w PEG 3350. (A) Crystals of Myo5a GD. (B) Crystals of Myo5a GD with Mlph 12 mer peptide. (C) Crystals of Myo5a GD with Mlph 15 mer peptide.

### 2.1.3 Melanophilin-EB1 complex

The very C-terminal part of Mlph (491-590) binds to EB1. This interaction was identified in a GST-pull down experiment, where GST-EB1 was incubated with cell extracts. A full-length Mlph was subsequently detected (Wu, Tsan et al. 2005). Part of EB1 (185–255) was already crystallized with APC (Slep, Rogers et al. 2005) and the APC binding site reveals a high sequence homology to Mlph (405-600). The idea of this project was to use the known EB1 structure as a scaffold and crystallize the C-terminal part of Mlph in a co-complex.

I initially expressed Mlph (405-590) and EB1 (185–255) separately in *E. coli*. However for crystallization a two-plasmid co-expression was found more efficient. Whereas the GST tag of EB1 was cleaved off during purification, the Mlph (405-590) fragment was left fused to its MBP tag, which prevented degradation (Figure 2.3).

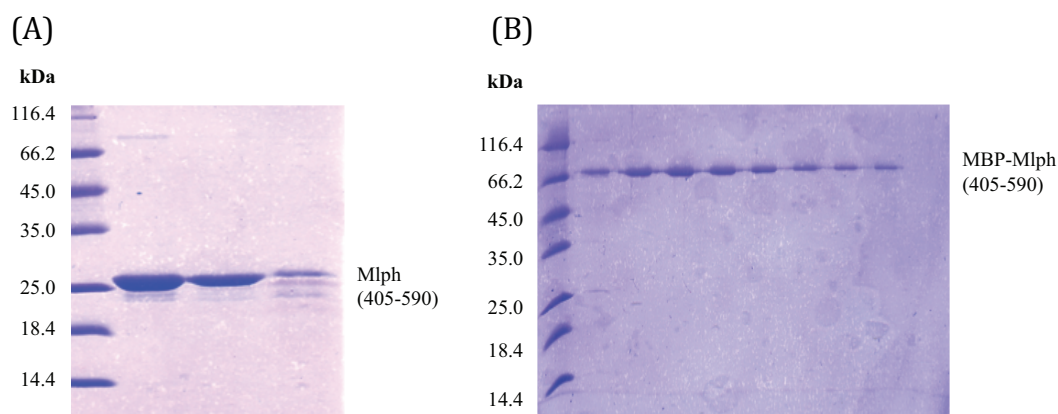


**Figure 2.3 C-terminal part of Melanophilin is prone to fast degradation unless purified as MBP-fusion protein.** Coomassie stained SDS-PAGE shows (A) Mlph (405-590). After GST tag removal, three fractions were analyzed; first fraction (left) immediately, second after two hours (in the middle), and the last after four hrs (right). (B) Coomassie stained SDS-PAGE analysis of MBP-Mlph (405-590) peak fractions from a Superdex 200 16/60 size-exclusion chromatography column.

To test, whether the reported interaction between Mlph (405-590) and EB1 (185–255) is direct, I expressed EB1 (185–255) fragment as a GST-fusion protein and Mlph (405-590) as a MBP-fusion protein. The pull down was performed both with Amylose resins and with GST beads (data not shown). A binding was detected in both experiments (Figure 2.4).

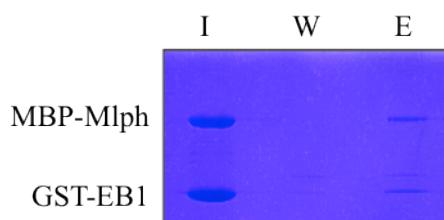


**Figure 2.4 Melanophilin forms a complex with EB1.** Coomassie stained SDS-PAGE analysis of the amylose-resin pull down assay. I (input, protein added to the reaction), W (last wash fraction), and E (elution fraction, after incubation with maltose). The analysis revealed interaction between GST-EB1 (185-255) and MBP-Mlph (405-590) protein fragments.

For crystallization experiments, proteins were purified to a high purity >95% using affinity (GST and Amylose resins) and size-exclusion chromatography. EB1 and Mlph eluted together in one peak and were subjected to initial crystallization screens. Crystals of similar shape were found in wide variety of conditions (Figure 2.5).

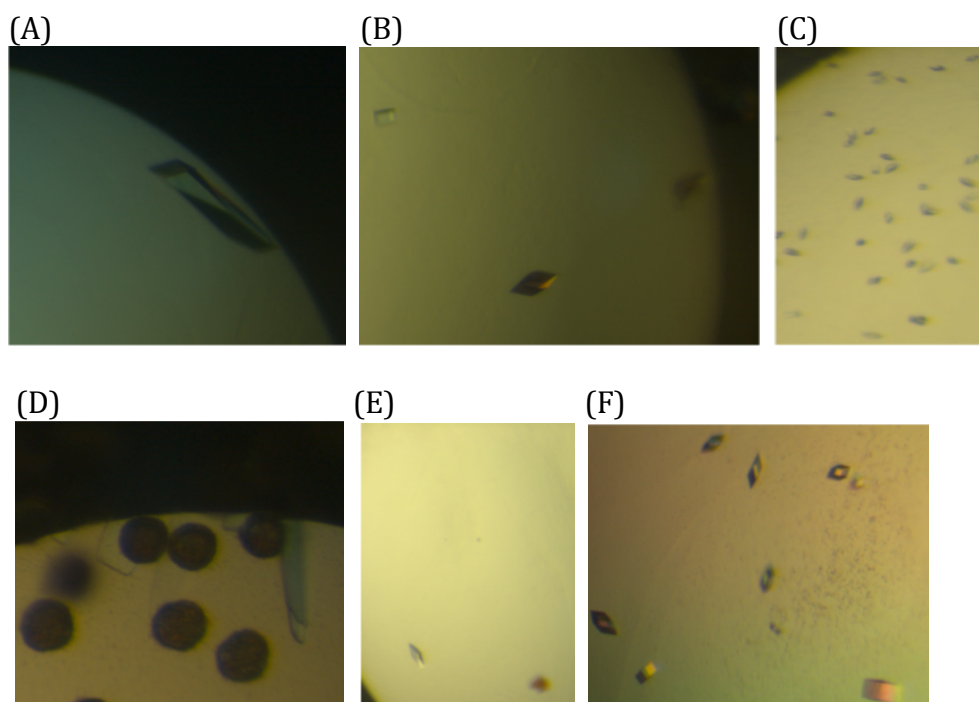


**Figure 2.5 Crystals of Mlph and EB1 complex.** Pictures of crystals grown from EB1-Mlph co-complex. Crystals were grown in following conditions: (A) 0.1 M Sodium Acetate pH 4.6, 0.2 M Ammonium Sulphate, 12 % v/w PEG 4000. (B) 0.1 M Sodium Acetate pH 4.6, 0.2 M Ammonium Sulphate, 30 % v/w PEG 2000. (C) 0.1 M Sodium Acetate pH 4.6, 40 % v/w PEG 200. (C) 20% Isopropanol, 0.1 M Sodium Acetate pH 4.6, 0.2 M  $\text{CaCl}_2$  (D) 0.1 M Sodium Acetate pH 4.6, 0.2 M  $\text{MgCl}_2$ , 25% PEG 400. (E) 0.1 M Ammonium Acetate pH 4.6, 22% PEG 400.

Unfortunately, all diffracting EB1-Mlph crystals had almost identical crystallographic parameters to the published EB1 crystal structure (Slep, Rogers et al. 2005). The space group of all crystals was C 2221 and the unit cell length ( $a = 33 \text{ \AA}$ ,  $b = 108 \text{ \AA}$ ,  $c = 37 \text{ \AA}$ ) with angles ( $90^\circ$ ,  $90^\circ$ ,  $90^\circ$ ). The electron density accommodated EB1, but no additional density was found. After several attempts to produce crystals with Mlph, the project was terminated.

## 2.2 Structural studies on Myo6 CBD

This project aimed to understand the Myo6 regulation and structural organization of the CBD (Cargo Binding Domain). At the time this project was started, little was known about this exceptional myosin that is the only known type of myosin to move its cargo in the opposite direction towards the minus end of actin filaments. Also, if Myo6 indeed undergoes autoinhibition, the structure could give an answer to the question how the inhibition is achieved. The next goal was to analyze the published interaction between Myo6 CBD and part

(residue 1-298) of the adapter protein Miranda (Petritsch, Tavosanis et al. 2003) (chapter 2.2.2). After all attempts to crystallize the CBD failed (chapter 2.2.1), I made efforts to solve the structure by Nuclear Magnetic Resonance (NMR) (chapter 2.2.3). Unfortunately, on August 7 2009 (Yu, Feng et al. 2009) the corresponding crystal and NMR structures were published. This made further work on this project obsolete.

### **2.2.1 Myo6 CBD crystallization**

In order to identify domain boundaries of the CBD, I expressed and purified several protein fragments. Basically, His or GST tagged recombinant proteins were expressed in *E. coli* and purified to a crystallographic purity >95% using affinity, anion and cation exchange, and size-exclusion chromatography. During purifications, the GST tag was usually cleaved off, His tag not.

The longest fragment contained the whole predicted domain with coil-coiled region (residue 913-1256), the shorter fragment (residue 1002-1256) the C-terminal part of the coil-coiled region. The longer fragment did not give any crystals in initial crystallization screens and the later was prone to degradation. During purification, Myo6 (913-1256) was also slightly prone to degradation, since the occurrence of the low molecular weight fragments in the SDS-PAGE (Figure 2.6) increased over time.

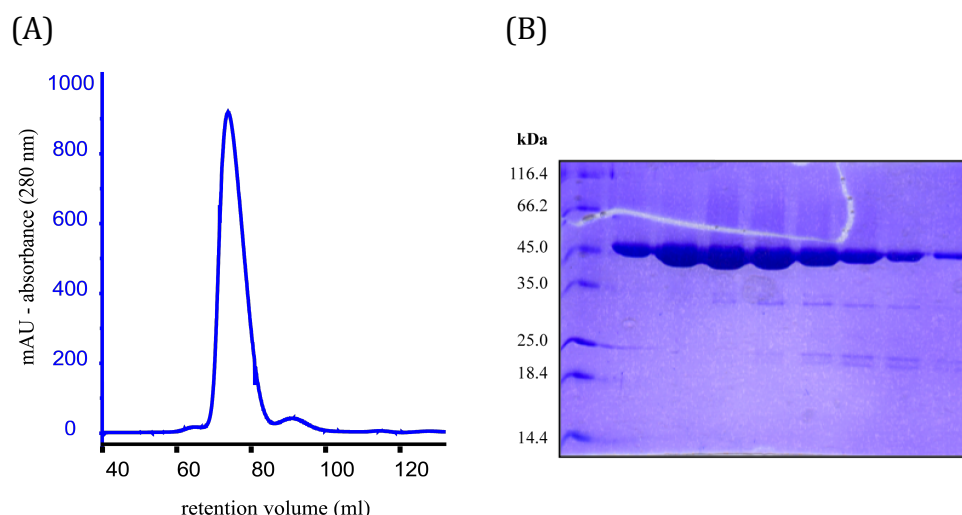


**Figure 2.6 Elution profile of His-tagged Myo6 (913-1256)** from a Superdex 200 16/60 size-exclusion chromatography column. (A) Myo6 eluted as one peak at 73 ml retention volume. Absorbance at 280 nm was measured. (B) Coomassie stained SDS-PAGE analysis of the peak fractions. The main band is His-tagged Myo6 (913-1256), the thin bands running as 35.0 and 25.0 kDa proteins are probably fragments arising from protein degradation.

Thus the Myo6 (913-1256) protein was subjected to limited proteolysis experiment at both room temperature and on ice. The stable, protease resistant fragments were cut out from SDS-PAGE, blotted and subjected to Edman sequencing. Only one N-terminus of the two fragments was identified with mass spectrometry, starting with amino acids GQVE. This corresponds to the residue 1021 (according to Uniprot database; Q01989 MYS9\_DROME). However a fragment starting with residue 1021 was prone to degradation. Two fragments less prone to degradation were found with the help of prediction programs (residue 1024-1236 and 1024-1236). I found few crystals in the initial screens in conditions: 0.2M NaF, 20% PEG 3350, 15% PEG400; 0.1 M NaAc pH 4.6, 0.1 M CaCl<sub>2</sub>; Hepes pH 7.5, 10% isopropanol, 20% PEG 4000; 0.1 M MES pH 6.5, 25% PEG 3000; but could not reproduce them. Because in some cases the ability to crystallize was increased by mutating cysteines, I mutated one cysteine in the Myo6 (913-1256 C1084S) and either one or three of them in the Myo6 (1024-1236 C1092S or C1084S, C1092S, C1203S) fragments. However, it did not change the properties and no crystals were obtained. Fragments that were tested are summarized in Table 2.3.

#### Myo6 protein fragments

Tag	Amino acids	Stability	kDa	Approach
His	913-1256	+	46	Crystallization
His	913-1256 C1084S	+	46	Crystallization
GST	1002-1256	-		
His	1021-1256	-		
His	1024-1236	++	27	Crystallization
GST	1024-1236	++	27	Crystallization
GST	1024-1236 C1092S	++	27	Crystallization
GST	1024-1236 C1084S, C1092S, C1203S	++	27	Crystallization
His	1024-1256	++	29	Crystallization
GST	1024-1256	+++	29	NMR, Crystallization

**Table 2.3 Myo6 protein fragments tested in experiments.** Protein fragments are labeled from (-) to (+++), according to high or low tendency to aggregation or degradation.

#### 2.2.2 Myo6 interaction with Miranda

The next plan was to use the co-complex of Myo6 and miranda for structural studies. Also, formation of a complex could stabilize Myo6 and such a complex could be more suitable for structural experiments. The protein-protein interaction between Myo6 CBD and miranda was analyzed by pull-down assay and co-purification. First full length His tagged miranda (1-830) was expressed and purified, but the 95 kDa protein was prone to degradation or probably not expressed at all. Later, MBP tagged miranda (residues 1-298) was incubated with His tagged Myo6 (residues 913-1256) and analyzed by pull-down assay under standard condition (Figure 2.7). Proteins were also incubated and subjected to size exclusion chromatography (data not shown), but no interaction was observed in any case.

Thus, the Myo6 CBD does not bind to miranda under conditions of these experiments and I did not continue in experiments with miranda.

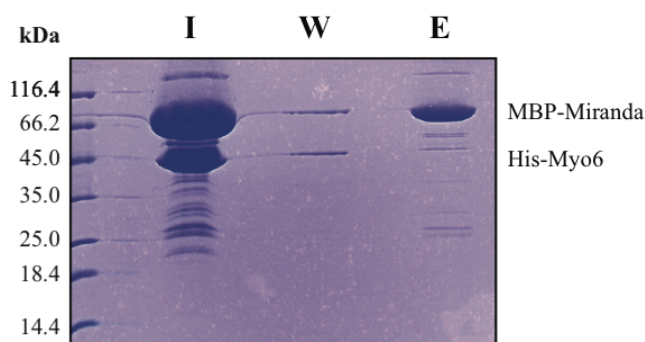


**Figure 2.7 Myo6 CBD does not form a complex with Miranda.** Coomassie stained SDS-PAGE analysis of the amylose-resin pull down assay. I (input, protein added to the reaction), W (last wash fraction), and E (elution fraction, after incubation with maltose). The analysis revealed no interaction between His-Myo6 913-1256 and Miranda 1-298 protein fragments.

### 2.2.3 Myo6 Initial NMR experiments

Since all attempt to obtain crystals suitable for x-ray analysis failed, I tried to solve the CBD structure by NMR. After several purification attempts, it was clear that all Myo6 CBD fragments tend to aggregate at high concentrations. The Myo6 (1024-1256) was chosen for NMR, because concentrations around 3 mg/ml could be achieved. It is the most stable fragment I obtained, and it was clearly monomeric during size-exclusion chromatography. However, the molecular weight of this protein fragment is 29 kDa, which is nowadays still a rather big molecule for NMR measurements. Myo6 (1024-1256) was expressed in a  $^{15}\text{N}$  labeling medium and purified with standard procedures. The protein was concentrated and subjected to measurement of two-dimensional (2D)  $^{15}\text{N}$ - $^1\text{H}$  HSQC (Heteronuclear Single-Quantum Coherence) spectrum (Figure 2.8). The NMR data were measured and validated by Dr. Tobias Madl from the laboratory of Prof. Michael Sattler (TUM Garching; Helmholtz Zentrum München, Germany). The 2D  $^{15}\text{N}$ - $^1\text{H}$ -HSQC measurement revealed a low probability of aggregation over a period of two days. Basically, the data is acquired two times before and after a period and then both results are compared. If no difference in spectrum is observed for example after two days, the protein is considered as stable. Long-term stability at room temperatures is crucial for this type of NMR measurements. Also the resulted dispersion corresponded to an about ~30 kDa protein, that shows a high degree of folding. The automatic peak search found



300 signals corresponding to amino acid composition. This number is in a good match with the composition of Myo6 (1024-1256) (Figure 2.8).

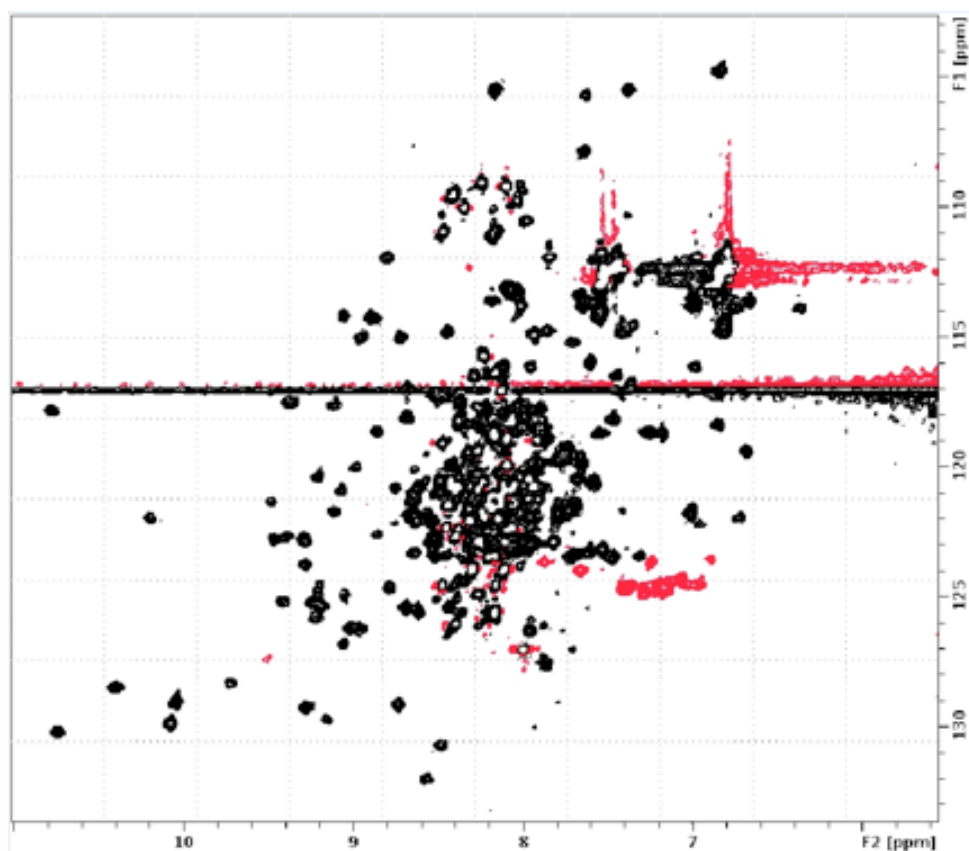


**Figure 2.8  $^{15}\text{N}$ - $^1\text{H}$ -HSQC of a Myo6 1024-1256 fragment.** Each peak in the spectrum represents a bonded N-H pair, with its two coordinates corresponding to the chemical shifts of each of the H and N atoms. Thus, the signals or peaks (depicted as black dots) correspond to amino acid number in the Myo6 1024-1256. In red circles signals referring to tryptophan (right bottom) and glycine (upper left) are highlighted. The F1 (Frequency 1,  $\omega^{15}\text{N}$ ) refers to a  $^{15}\text{N}$  chemical shift and F2 (Frequency 2,  $\omega^1\text{H}$ ) refers to a  $^1\text{H}$  chemical shift.

Thus, the initial data were very good and I could continue with the second measurement, which is 2D NOESY (Nuclear Overhauser Effect Spectroscopy). In this experiment, qualitative information about the folding is expected. Later a backbone assignment experiment was planned. The third experiment could be done with a fully deuterated protein in order to get more sharp signals. For this, I expressed the Myo6 (1024-1256) in  $\text{D}_2\text{O}$  and  $^{13}\text{C}$ -D-glucose and purified it with standard chromatographic methods. Unfortunately, during the purification, the crystal and NMR structures of Myo6 CBD were published (Yu, Feng et al. 2009).



## 2.3 Structural studies on Myo5a

### 2.3.1 Defining the limits of Myo5a GD and crystallization attempts

According to literature and secondary structure prediction, the GD of Myo5a starts with residue 1446 and ends at the very C-terminus (Fukuda, Kuroda et al. 2002). This protein fragment (Myo5a (1446-1855)) was soluble, did not degrade and gave crystals in quite many conditions of a crystallization screen. However the resolution of the diffraction pattern never exceeded 8Å even after several rounds of refinement and optimization. An example of large crystals of 50 x 50 x 250 µm that grew in condition containing 0.1 M MES pH 6.2 1.4 M MgSO<sub>4</sub> is given in Figure 2.9.

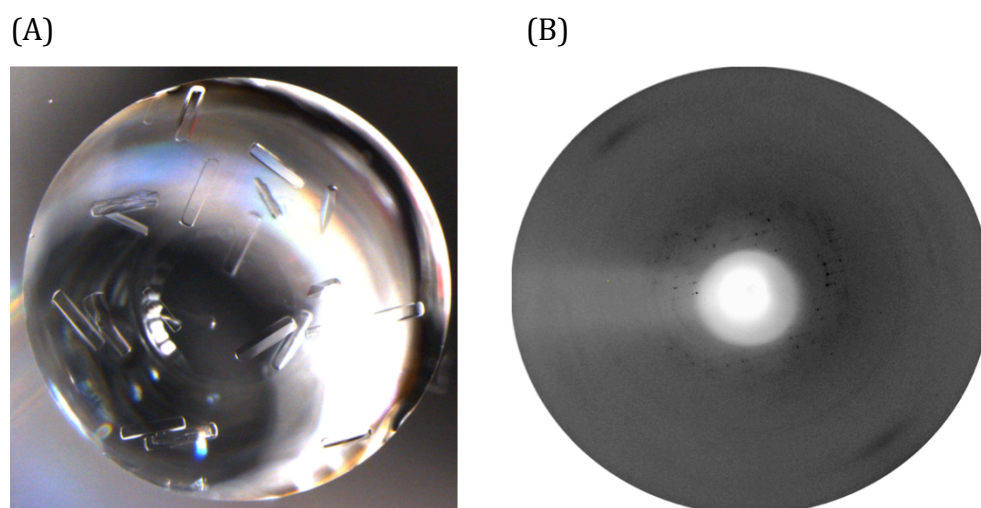


**Figure 2.9 Representative images of Myo5a (1446-1855) crystals and a representative diffraction pattern.** (A) Crystals grew in a condition containing 0.1 M MES pH 6.2, 1.4 M MgSO<sub>4</sub>. (B) Image of diffraction pattern of one of these crystals. The resolution was around 8Å.

Besides additive screens, another attempt to improve resolution was to follow the strategy used for the crystallization of Myo2p (Pashkova, Jin et al. 2006). Myo2p GD consists of 12 alpha helices connected by a long loop that is probably highly flexible. I named this region loop I in human Myo5a. Pashkova and colleagues cleaved this long loop by mild proteolysis. In denaturizing conditions, the GD splits into halves of about 22 kDa. However in native conditions, the GD was shown to stick together and only such modified protein gave high quality

crystals. I repeated the procedure with Myo5a GD and as proved by denaturizing conditions of SDS gel, the loop was cut out. But in my case the treatment did not lead to improvement of crystal quality.

In a parallel approach, I designed four fragments, where 19, 9, 6, and, 3 residues were deleted in this loop region. According to the Myo2p structure, a deletion of 19 residues was the maximum at which the helices could still be connected. I also designed a cleavage site for a sequence-specific protease, to avoid unspecific cleavage of other parts. When I expressed and purified these fragments, I realized, that deleting 19 residues leads to protein destabilization. All other fragments were behaving similar to the wild-type GD, unfortunately including the formation of low quality crystals. Also, any truncations at the C-terminus lead to decreased solubility or fast degradation.

Meanwhile, my limited proteolysis experiments and protein fragment identification by mass-spectrometric analysis suggested a fragment starting at residue 1476. This fragment was also prone to degradation. However a fragment starting at residue 1467 behaved similarly well as the Myo5a (1446-1855), in size exclusion chromatography. With the help of sequence alignment, also optimized fragments Myo5b and Myo5c were designed and expressed in both lengths corresponding to Myo5a (1446-1855) and Myo5a (1467-1855).

In order to find the domain borders of Myo5a, Myo5b, and Myo5c GD and study the difference between longer and shorter fragments, Small Angle X-ray Scattering (SAXS) measurement was performed.

### **2.3.2 Shape analysis by Small Angle X-ray Scattering**

SAXS experiments were measured at the beamline ID 14-3 at the European Synchrotron Radiation Facility (ESRF) in Grenoble, France. In brief, a solution with biological macromolecules was exposed to X-rays 10 times for 30 sec and the scattered intensity in dependence of the scattering angle was recorded. From this scattering curve overall shape information was deduced.

On one hand the resulting solution structure describes the overall shape of the molecule at the lower resolution range of about 50Å to 10Å resolution (Putnam, Hammel et al. 2007). On the other hand in contrast to crystallography the

troublesome crystallization is omitted and the proteins are measured in solution, which is more similar to physiological conditions. Also, additional information as molecular weight, oligomerization state and conformation of large flexible parts can be routinely gained (Bernado, Mylonas et al. 2007; Putnam, Hammel et al. 2007).

### 2.3.3 Shape analysis by SAXS of Myo5a, Myo5b, and Myo5c GDs

For SAXS analysis, proteins at three different concentrations in buffer solution were placed into X-rays and the respective scattered intensity was measured.

All Myo5a (1467-1855), Myo5b (1462-1849), Myo5c (1355-1742) and some of the longer fragments (Myo5a (1446-1855), Myo5b (1418-1849), Myo5c (1330-1742)) were monodisperse and monomeric in solution at 3 concentrations each (Figure 2). As the data for Myo5a (1446-1855), Myo5b (1418-1849), Myo5c (1330-1742) fragments showed aggregation, these data were not further evaluated. Thus only calculations for (1467-1855), Myo5b GD (1462-1849), Myo5c GD (1355-1742) fragments are summarized in Table 2.4; the other data are not included.

	Conc. (mg/ml)	Conc. ( $\mu$ M)	Rg (nm)	Dmax (nm)	MW by SAXS (KDa)	Theor. MW (KDa)
Myo5a GD	1.10	24.4	3.24	11.1	51	45.0
	1.3	28.9	3.08	10.8	59	
	3.0	66.7	3.12	10.9	45	
Myo5b GD	1.6	35.6	3.20	10.2	52	44.9
	2.2	48.9	3.17	11.1	44	
	2.5	55.6	3.12	10.5	39	
Myo5c GD	6.1	135.6	3.23	11.9	37	45.1
	10.0	222.2	3.29	11.6	39	
	14.1	313.3	3.17	11.0	49	

**Table 2.4 Table summarizing Small-Angle X-ray Scattering (SAXS) experimental data for Myo5a (1467-1855), Myo5b (1462-1849), Myo5c (1355-1742) fragments.** All three paralogs have similar overall dimensions and are monomeric in solution. Rg refers to radius of gyration. Dmax refers to maximum size of particle.

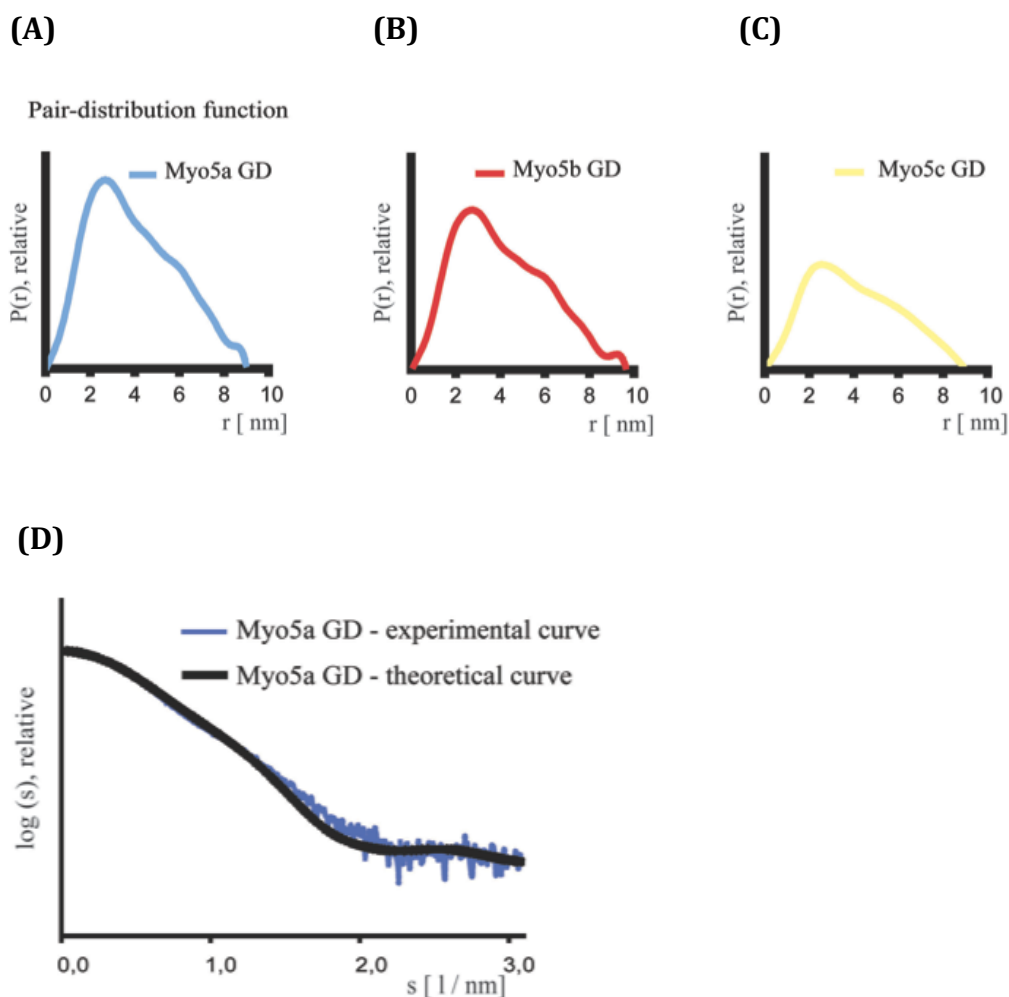


**Figure 2.10 Small-Angle X-ray Scattering (SAXS) experimental curves of Myo5a (1467-1855), Myo5b (1462-1849), Myo5c (1355-1742) fragments.** (A-C) Pair-distribution function curves for (A) Myo5a GD, (B) Myo5b GD, and (C) Myo5c GD, as were used for calculation of surface envelopes shown in Figure 2.11. (D) Overlay of the experimental scattering curve of Myo5a GD in blue with the calculated theoretical curve in black. The theoretical curve was calculated from the Myo5a crystal structure presented later in this thesis. The way in which the two curves overlay is a helpful measure of accuracy of the Myo5a surface envelope (Figure 2.11), which was very good in this case.

The surface envelopes and the experimentally determined molecular weights of the Myo5a (1467-1855), Myo5b (1462-1849), Myo5c (1355-1742) fragments were almost identical (Table 2.4; Figure 2.10 and Figure 2.11). Such shape similarity was not expected, as significant shape differences as are observed in yeast MyoVs members (Pashkova, Jin et al. 2006; Heuck, Fetka et al. 2010). However small differences in folding cannot be observed by SAXS due to limited resolution of the method (Bernado, Mylonas et al. 2007; Putnam, Hammel et al. 2007). The data also confirm that the GD consists of following fragments: Myo5a (1467-1855), Myo5b (1462-1849), and Myo5c (1355-1742). Protein fragments

Myo5a (1446-1855), Myo5b (1418-1849), Myo5c (1330-1742) consist of the GD and some additional N-terminal part, which might be flexible.

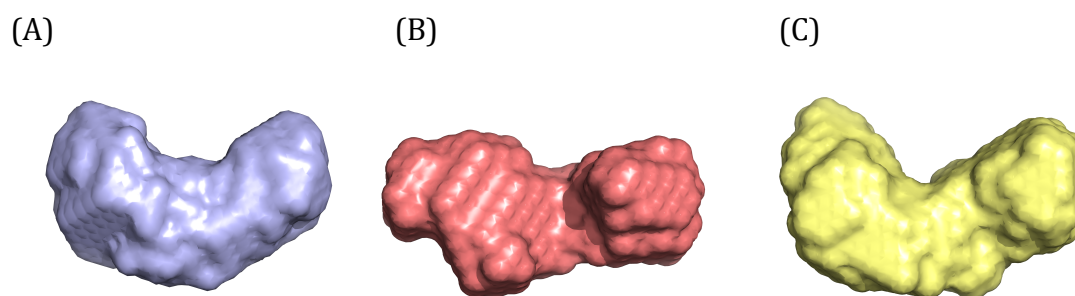


**Figure 2.11 Overall shapes of globular domains from human type V myosins obtained by Small-Angle X-ray Scattering.** (A-C) Surface envelopes calculated from SAXS data revealed that Myo5a GD (A), Myo5b GD (B), and Myo5c (C) have very similar shapes in solution.

#### 2.3.4 Crystallization of the Myo5a GD

Several truncated Myo5a GD fragments were tested in robot assisted initial 96-well format crystallization screens using common commercially available screens. 500 or 200 nl sitting drops were set up and observed under a microscope or via automatically generated images at the MPI facility. Various crystals in several conditions were found and subjected to thorough refinement trials. Crystals were cryoprotected and flash frozen prior data collection. When the freezing method was suspected to destroy the crystal, this step was omitted. Most crystals belonged to the spacegroup  $P2_12_12_1$  and were poorly diffracting. The Myo5a (1467-1855) fragment yielded crystals diffracting up to 5Å resolution. The subsequent refinement involved not only screening of modified conditions and cryoprotectants, but also alternative methods such as controlled dehydration or annealing. In one of these conditions (0.2 M Ammonium Sulfate, 0.1 M BIS-TRIS pH 6.5, and 25% w/v PEG 3350), anisotropic crystals were obtained. The crystals had reproducible diffraction patterns with high-mosaicity and good-quality data in some regions. These crystals were however useless for structure determination. Interestingly, there were also few good-diffracting crystals in the same crystallization drops. These crystals needed some improvement of cryoprotection. Unfortunately, it turned out to be extremely

impractical to find these few exceptions during cryoprotectant screening. Luckily, I noticed that the position of the crystal inside the drop was the critical parameter. Only crystals growing from the drop surface (Table 2.12 A) had a low mosaicity. These crystals grew in clusters, so the clusters were carefully split and single crystals were harvested (Figure 2.12).

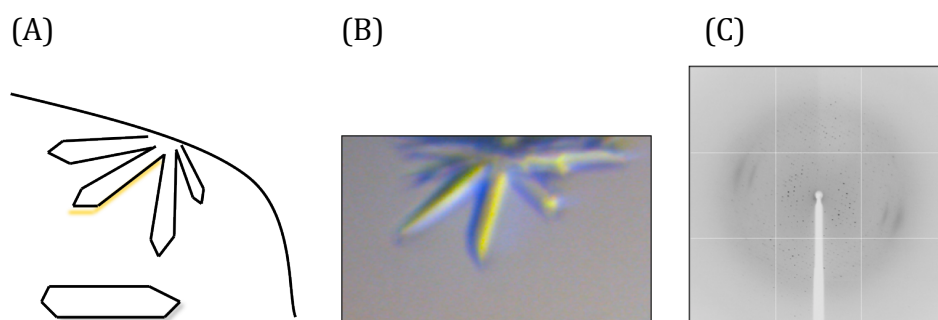


**Figure 2.12 Two kind of crystals found in one drop of Myo5a 1467-1855.** (A) Schematic drawing of crystals growing inside the drop and in clusters (yellow) from the drop surface. (B) Picture of a cluster in a drop. (C) Representative image of the respective diffraction pattern.

Attempts to solve the structure with these datasets by molecular replacement using yeast homologs (Myo2p RCSB Pdb ID: 2F6H or Myo4p RCSB Pdb ID: 3MMI) as templates failed. Thus crystals suitable for phasing were needed. Further attempts indeed gave selenomethione-derivatized protein crystals that provided enough phasing information to allow the structure determination.

I also tried to co-crystallize or soak the native crystals with two Mlph peptides of 12 and 15 residues in length (see chapter 2.1.2). Unfortunately, I found no extra electron density in the resulting structure that could be attributed to these peptides. However, the crystals resulted in better diffraction and a dataset with a better resolution dataset was obtained (Table 2.5).

### 2.3.5 Structure determination of the Myo5a GD

The structure was solved by single-wavelength anomalous dispersion (SAD) of a selenomethione-derivatized Myo5a (1467-1855) fragment (Figure 2.13).

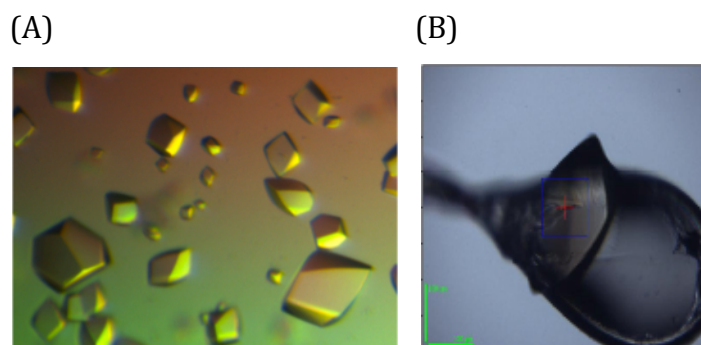


**Figure 2.13 Representative images of selenomethione-derivatized protein crystals of Myo5a (1467-1855).** (A) Diamond-shaped crystals grew in condition containing 0.1 M MES pH 6.2, 6% Dioxane, 1.45 M  $\text{MgSO}_4$ , 10 mM DTT. (B) Picture of cryoprotected and frozen crystal in a nylon loop. The picture was taken prior data collection. The green lines stand for 100  $\mu\text{m}$  lengths.

The selenomethione-derivatized protein crystals grew within 2-3 days in 100 mM MES pH 5.5, 6 % dioxane, 1.45 M  $(\text{NH}_4)_2\text{SO}_4$ , 10 mM DTT. The data was collected at the beamline ID14-4 at ESRF in Grenoble, France. The data were scaled and indexed with XDS and XSCALE (Kabsch 2010) to a space group  $\text{P3}_221$  and had 4 molecules in the asymmetric unit. The high-quality data showed a resolution up to 2.5 Å. Using the native dataset, the data were extended to the resolution of 2.5 Å. Later, a better-resolution native dataset was obtained and the final model was extended to a 2.2 Å resolution ( $R_{\text{work}}=0.21$ ;  $R_{\text{free}}=0.26$ ). Statistics are summarized in Table 2.5.

#### Data collection statistics<sup>a</sup> for Myo5a GD

Data collection	Native	Selenomethionine	
Space group	P 2 <sub>1</sub> 2 <sub>1</sub> 2 <sub>1</sub>	P 3 <sub>2</sub> 2 1	
Cell dimensions: <i>a</i> , <i>b</i> , <i>c</i> (Å)	74.06, 87.11, 130.94	146.92, 146.92, 200.00	
Cell dimensions: α, β, γ (deg)	90, 90, 90	90, 90, 120	
		Peak	Inflection
No. of crystals	1	1	
Total rotation range (deg)	180	185	185
X-ray source	ID 14-1 (ESRF)	ID 14-4 (ESRF)	
Wavelength (Å)	0.9334	0.9785	0.9790
Resolution (Å)	43.5-2.2 (2.3-2.2)	49.3-2.5 (2.6-2.5)	49.3-2.5 (2.6-2.5)
<i>R</i> <sub>sym</sub> or <i>R</i> <sub>merge</sub>	11.6 (23.7)	9.4 (25.6)	10.5 (31.3)
Mosaicity (deg)	0.3	0.092 (XDS)	0.091 (XDS)
Average redundancy	7.25 (7.4)	11.4	11.4
Observations (unique)	428125 (43514)	975152 (30352)	990059 (62038)
<i>I</i> /σ ( <i>I</i> )	14.6 (6.3)	16.3 (7.5)	15.3 (6.4)
Completeness (%)	99.5 (99.5)	100 (99.3)	100 (94.9)

#### Refinement statistics

Resolution (Å)	43.5-2.2
Reflections	43,514
Test set (%)	5
<i>R</i> <sub>work</sub> / <i>R</i> <sub>free</sub>	20.9 / 25.9
Protein mol./res.	2 / 375
Protein atoms No.	6493
Water atoms No.	427
Mean B-factors (Å <sup>2</sup> ) Protein / Water	29.4 / 12.4
Res. in favored / allowed / disallowed regions (%)	98.53% / 1.34% / 0.13%
RMS deviations: bond length (Å) / bond angle (deg)	0.0136 / 1.04

**Table 2.5 X-ray data collection, phasing and refinement statistics for Myo5a GD crystal structure.** Selenomethionine refers to the Selenomethionine-derivatized crystal (single wavelength anomalous dispersion). <sup>a</sup>values for the highest-resolution shell are in parentheses. *R*<sub>sym</sub> refers to the un-weighted R-value on *I* (Intensity) between symmetry mates. RMS Deviation refers to Root Mean Square Deviation. *R*<sub>work</sub> refers to a measure of the agreement between the crystallographic model and the experimental X-ray diffraction data

$$R = \frac{\sum ||F_{obs}| - |F_{calc}||}{\sum |F_{obs}|}$$

*R*<sub>free</sub> 5% of reflections, that was not used in the model refinement, but was used as cross validation R-factor.

The asymmetric unit contains two identical Myo5a molecules (Table 2.5), includes residues 1467-1855 and lacks electron density for loop I (residues 1640 to 1658). This loop region could therefore not be modeled (Figure 2.14 A and B). The structural core is hook-like shaped, consisting of 11 tightly packed α-helices. A long chain without any remarkable secondary structure wraps around this



compact body, followed by 3 last C-terminal residues that are folded into a small  $\beta$  sheet. The two-stranded  $\beta$  sheet folds together with the very N-terminal residues and thus brings both ends of the GD together. This  $\beta$  sheet is not found in yeast homologs and the function is so far unknown (Figure 2.14 C).

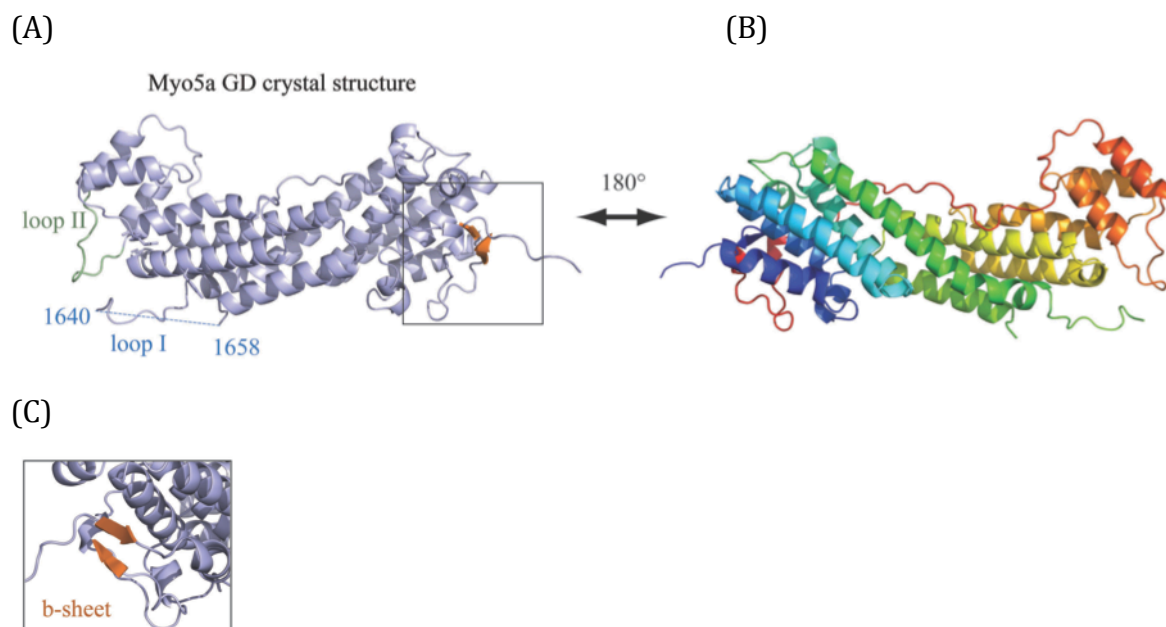


**Figure 2.14 X-ray structure of the human Myo5a GD.** (A) Ribbon representation of the Myo5a GD at 2.2 Å. Loop I, that was not modeled into the structure due to missing electron density is depicted by a blue dotted line. The loop II is highlighted in green.  $\beta$  sheet connecting the N-terminus and the very C-terminus is highlighted in orange. (B) The same structure as in (A), but rotated 180° around the vertical axis is depicted in rainbow color-coding. It follows the peptide chain from its N-terminus in blue to its C-terminus in red. (C) Close-up of  $\beta$  sheet in rectangle in (A) slightly rotated to better show the position of the small beta-sheet (orange).

### 2.3.6 Structure determination of the Myo5b GD

After solving the crystal structure of Myo5a GD, a new speculation arose, namely, that Myo5a could be a structural paralog of Myo2p and that Myo5b or Myo5c would be a paralog of Myo4p. A crystal structure of the Myo5b GD would give an answer to this question.

Myo5a and Myo5b GDs share 70.5% identical residues and additional 18.7% conservative exchanges. Therefore, based on Myo5a structure and alignment with Myo5b, I created Myo5b GD truncated at residue corresponding to Myo5a GD structure and crystallized Myo5b (1462-1849).

The crystals were grown in hanging drop format at 18 °C. The structure of Myo5b GD was solved by molecular replacement using Myo5a GD as template. The asymmetric unit ordered in space group P21212 contains one molecule and the native dataset has a resolution of 3.1 Å and ( $R_{\text{work}}=0.25$ ;  $R_{\text{free}}=0.30$ ). Statistics are summarized in Table 2.6.

**Data collection statistics<sup>a</sup> for Myo5b**

Data collection	Native
No. of crystals	1
Total rotation range (deg)	145
X-ray source	ID 23-1 (ESRF)
Wavelength (Å)	0.9778
Resolution (Å)	49.7-3.11 (3.3-3.11)
Mosaicity (deg)	0.3 (XDS)
Average redundancy	7.94 (8.0)
Observations (unique)	64207 (7677)
$I/\sigma(I)$	13.7 (2.4)
Completeness (%)	96.8 (93.6)
Rsym or Rmerge	11.3 (68.3)
Space group	P 21212
Cell dimensions: a, b, c (Å)	60.61, 78.33, 86.67
Cell dimensions: $\alpha$ , $\beta$ , $\gamma$ (deg)	90, 90, 90

**Refinement statistics**

Resolution (Å)	49.7 - 3.1
Reflections	7647
Test set (%)	5
Rwork / Rfree (%)	24.7/30.1
Protein mol./res.	1 / 351
Protein atoms	2823
Water atoms	0
B-factors (Å <sup>2</sup> ) Protein / Water	58.0 / -
Res. in preferred/ allowed/ gener/ disallowed regions (%)	81.1/ 15.5/ 1.9/ 1.5
RMS Deviations: bond length (Å)/ bond angle (deg)	0.011 / 1.428

**Table 2.6 X-ray data collection and refinement statistics for Myo5b GD crystal structure solved by molecular replacement.** <sup>a</sup>values for the highest-resolution shell are in parentheses.

$R_{\text{sym}}$  refers to the un-weighted R-value on I (Intensity) between symmetry mates. RMS Deviation refers to Root Mean Square Deviation.  $R_{\text{work}}$  refers to a measure of the agreement between the crystallographic model and the experimental X-ray diffraction data.  $R_{\text{free}}$  5% of reflections, that was not used in the model refinement, but was used as cross validation R-factor

The Myo5b (1462-1849) crystal structure revealed pronounced similarity to Myo5a GD. The overall domain organization of 11 helices, the long chain around the molecule, and the C-terminal anti-parallel  $\beta$  sheet was also found in Myo5b structure. Electron density was missing for N-terminal 4 amino acids, a loop I

region spanning from amino acids 1625 to 1651, and also a small loop II region (residues 1781 to 1789) (Figure 2.15).

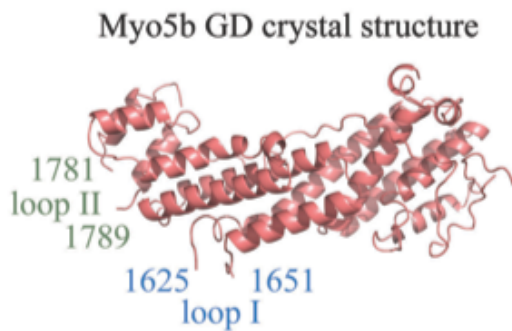


**Figure 2.15 X-ray structure of the human Myo5b GD.** (A) Ribbon representation of the Myo5b GD at at 3.1 Å resolution. The loops I and II missing in the structure due to lacking electron density are depicted as blue and green lines, respectively.

### 2.3.7 Model of Myo5c GD

Between Myo5a and Myo5c are 62.7% amino acids identical and 21.6% have conservative exchanges. I performed an automatic alignment of the protein sequences of the GDs from Myo5a, Myo5b, and Myo5c and corrected the alignment manually according to the two crystal structures (Figure 2.16).

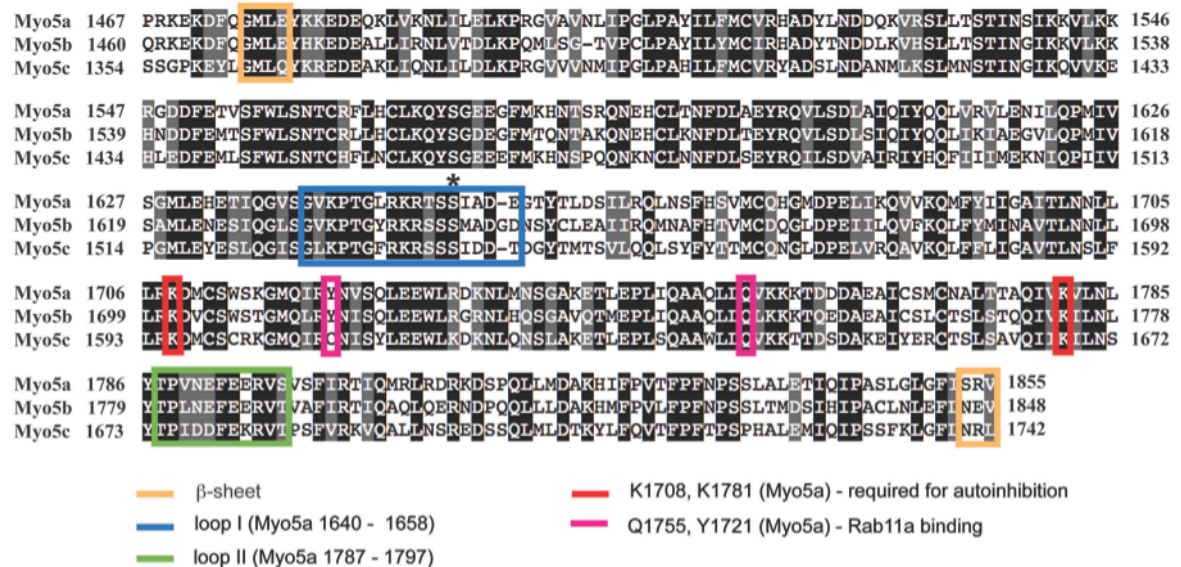
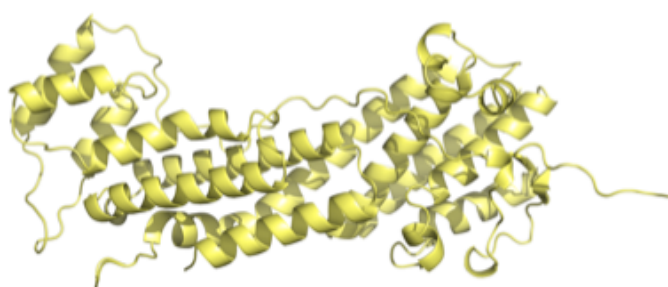


**Figure 2.16 Alignment of protein sequences of all human MyoV GDs.** Identical residues in all three paralogs are depicted with black background. Moderate conservation is depicted with grey and not conserved residues have white background. Colored rectangles mean structural or functional regions discussed in the text. Alignment was generated with the program ClustalW (Thompson, Gibson et al. 2002).

Based on this alignment, I calculated an atomic model of Myo5c (1355-1742) (Figure 2.17 A) using the program Modeller 9v7 (Sali and Blundell 1993). The atomic model not only fits surprisingly well into the SAXS envelope (Figure 2.11), it also shows no stereochemical abnormalities, as revealed by a Ramachandran plot (Figure 2.17 B).

(A)



(B)

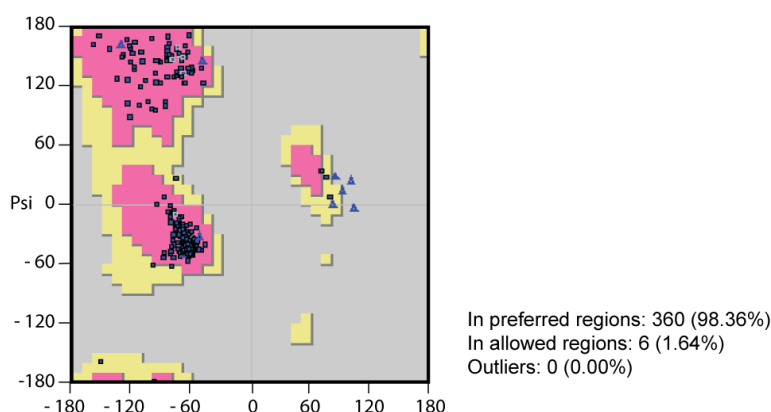


**Figure 2.17 Homology model of Myo5c GD** (A) Ribbon representation of Myo5c GD model obtained with the program Modeller 9v7 (Sali and Blundell 1993). The Myo5a and Myo5b X-tal structures (Figure 2.14 and Figure 2.15) were used as templates. (B) Ramachandran plot for the computed model of the Myo5c GD.

### 2.3.8 Myo5a GD-mutations found to cause Griscelli-syndrome

With our detailed knowledge of the structure of Myo5a GD, we could estimate the functional basis of Myo5a mutations found in Griscelli patients or the respective mouse model.

Griscelli patients or mice that were shown to have mutations in Myo5a GD often show both neurological and skin abnormalities. In one patient, a 47 bp insertion at position 4634 was shown to encode a premature stop codon. Figure 2.18 A shows in blue the normal Myo5a GD and in red color the small fragment ending with the amino acid 1545 that is produced in Griscelli patients. This small fragment folds into a three-helical bundle suggesting that it might be able to establish a stable fold (Figure 2.18 B; in red). To answer this question, I expressed a GST-fusion protein with this GD fragment. Because this fusion protein was soluble, it is likely that also the truncated Myo5a of the Griscelli patient is stable and not undergoing degradation. This finding further suggests that while the structural integrity is maintained, the severe physiological defects must be due to the deletion of regions important for its function.

In mice, particular Myo5a GD point mutations resulted in altered coat color and neurological impairment (Huang, Mermall et al. 1998). This example led to speculations that these three single mutations (Ile1512, Met1515, and Asp1521) abolish binding of the adaptor protein Mlph. This hypothesis was indeed experimentally confirmed (Fukuda and Kuroda 2004). However, when these amino acids are highlighted on the Myo5a crystal structure surface, I found only one residue (D 1521) close to the surface (Figure 2.18 C; red dot). All other residues are completely buried (Figure 2.18 D). More over, these residues are involved in intramolecular interactions. Thus, all three mutations are likely to destabilize the domain and as a consequence abolish the Mlph binding.

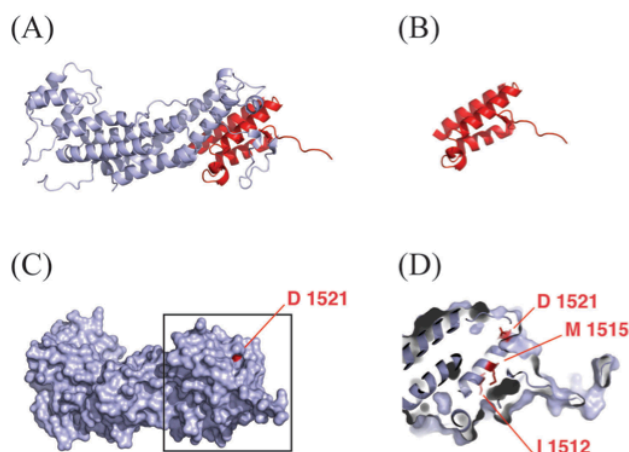


**Figure 2.18 Some Myo5a mutations found in Griscelli patients are located in the Myo5a GD.** (A) An amino acid mutation at position 1545 leads to insertion of a stop codon. Highlighted in red is the part of Myo5a GD (blue; ribbon representation) that is predicted to be expressed. (B) The same part in ribbon representation without the context of the whole domain. (C) Three residues (Ile1512, Met1515, and Asp1521) and their mutations that were found to abolish Mlph binding to Myo5a GD in mice and thus may also cause Griscelli syndrome in humans. Since only one residue (Asp 1521) is close to the surface (red dot) and others are buried, it is unlikely that the mutations directly interact with Mlph binding, but rather have impact on the molecular stability. (D) The three residues in a close-up (boxed in C) depicted both as ribbon and partial surface representation. I1512, M1515, and D1521 are highlighted in red.

### 2.3.9 Comparison of the human MyoV GD with the yeast type V Myosins

The Root Mean Square Deviation (RMSD) for Myo5a with Myo2p is 2.36 Å and for Myo5a with Myo4p is 3.17 Å (Figure 2.19 B and C). This data is not surprising, as the sequence of Myo5a is more similar to Myo2p, than of Myo5b and Myo5c. Also, the overlay of Myo5a and Myo5b GD structures gives an RMSD value of 1.11 Å (Figure 2.19 A), and the overlay of the Myo5c GD model and Myo5a yields a RMSD value of only 1.10 Å (Figure 2.19 D). The shape similarities between the atomic models of Myo5a, Myo5b, and Myo5c model confirm the SAXS data where the GDs of Myo5a and Myo5b and Myo5c revealed almost indistinguishable shapes.

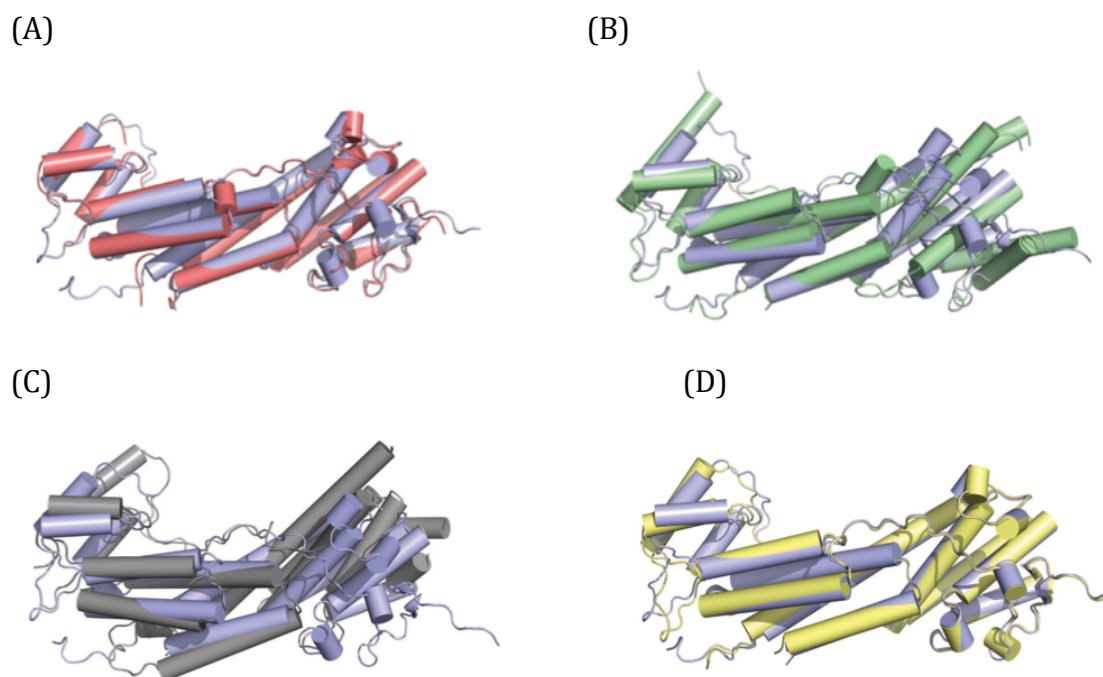


**Figure 2.19 Superpositioning of type V Myosins GDs.** (A) Overlay of Myo5a GD (blue) and Myo5b GD (red) x-tal structures (RMSD = 1.1 Å). (B) Overlay of Myo5a GD (blue) and yeast Myo2p GD (green) x-tal structures (RMSD = 2.4 Å) (C) Overlay of Myo5a GD (blue) and yeast Myo4p GD (grey) x-tal structures (RMSD = 3.2 Å) (D) Overlay of Myo5a GD (blue) x-tal structure and the homology model of Myo5c GD (yellow) (RMSD = 1.1 Å). Superpositioning was generated using COOT and SS-Superimpose.

### 2.3.10 Comparison of surface properties of the Myo5a, Myo5b, and Myo5c GD

Sequence alignments of the three MyoV GDs (Figure 2.16) followed by a surface plot show a high degree of amino acid conservation at their surfaces (Figure 2.20 A). Such conservation is more visible when I highlighted surface-exposed residues that are unique to each Myo5 paralog on the same rendering (Figure 2.20 B-D).



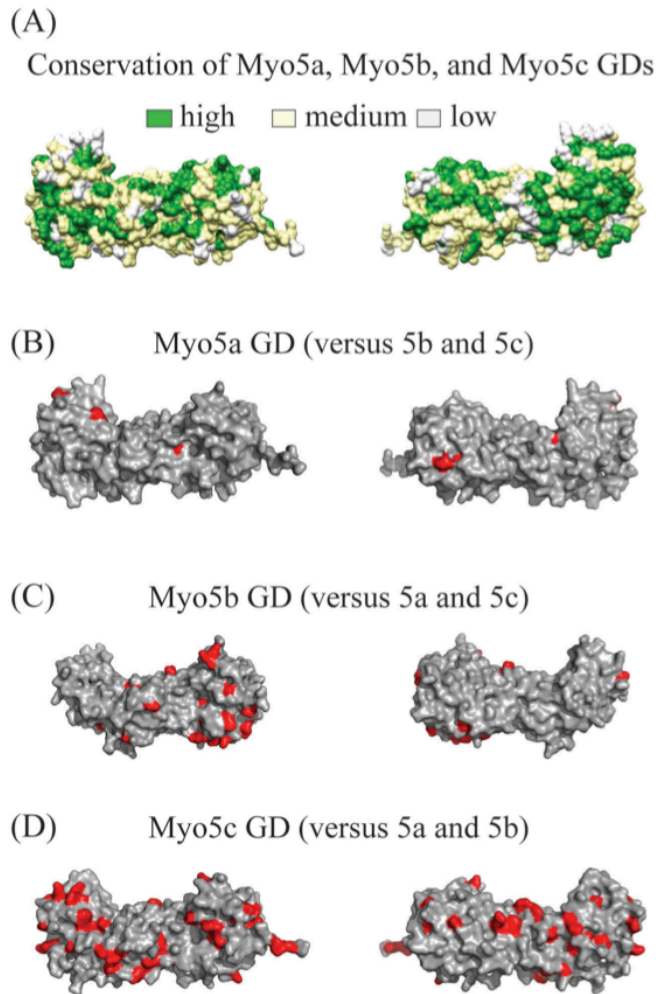


**Figure 2.20 Surface plot of amino acid conservation on Myo5a GD, Myo5b GD, and Myo5c GD.** (A) Orientation is as shown in Figure 2.14 A and rotated by 180° around the vertical axis (same as in Figure 2.14 B). (A) Amino acid conservation between human Myo5a, Myo5b, and Myo5c is plotted on the Myo5a structure. The conservation was obtained by alignment as shown in Figure 2.16. The highest sequence conservation is colored as green areas, the partial conservation as yellow areas, and white areas are lacking any conservation. (B-D) Residues unique to (B) Myo5a, (C) Myo5b, and (D) Myo5c are highlighted red on their surface, when compared to its respective human paralogs.

Whereas on the Myo5a surface only few unique patches could be identified (Figure 2.20 B; red areas), a higher degree of deviation was observed for Myo5b (Figure 2.20 C; red areas). The most distinct surface is presented by Myo5c (Figure 2.20 D; red areas), suggesting that Myo5c could bind cargoes that are not shared with the two other Myosins.

The diversity among the paralogs is also obvious when the electrostatic potentials are plotted onto their respective surfaces.



For most of the surface of all paralogs, the plot of electrostatic potentials shares no similar patches (Figure 2.21 A-C). This is even more visible, when the electrostatic potentials are calculated with the program Swiss PDB viewer (Figure 2.22). However one region of the surface has indeed almost identical charge properties in all three paralogs (dotted red circle, Figure 2.21 A).

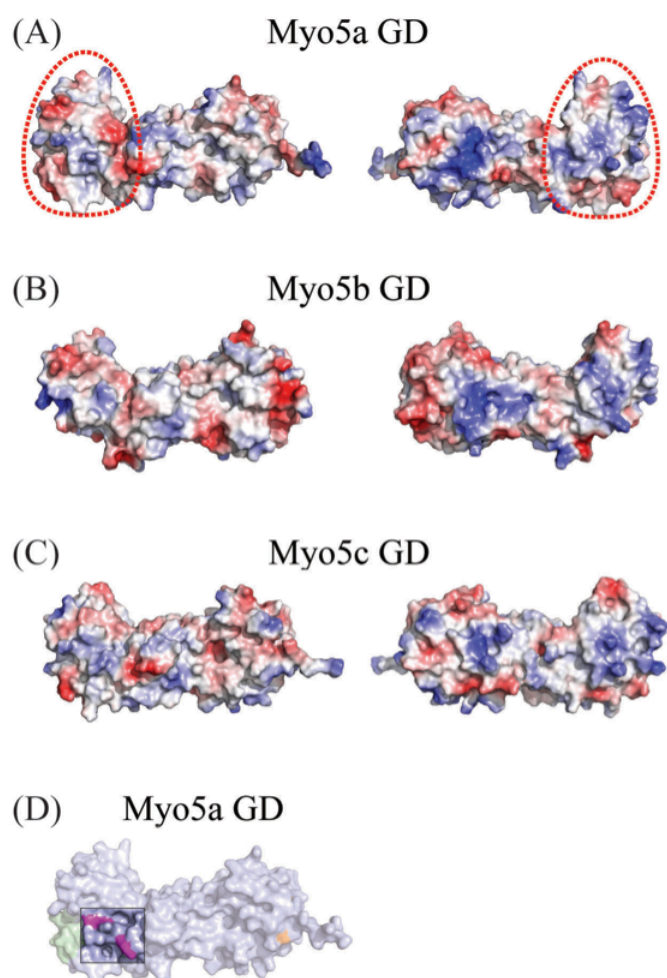


**Figure 2.21 Representation of surface potentials of Myo5a GD, Myo5b GD, and Myo5c GD.** (A-C). Orientation is as shown in Figure 2.14 A. Red areas indicate negative, whereas blue areas indicate positive surface charges. White areas indicate hydrophobic regions. (A) Part of the surface surrounded by a red dotted circle is an area where similar surface charges were found in all paralogs. Such almost identical surface charges might hint at a function common to all three paralogs. (D) Residues important for Rab11a binding are highlighted in magenta on the Myo5a GD structure. All pictures were generated in program Pymol (The PyMOL Molecular Graphics System).

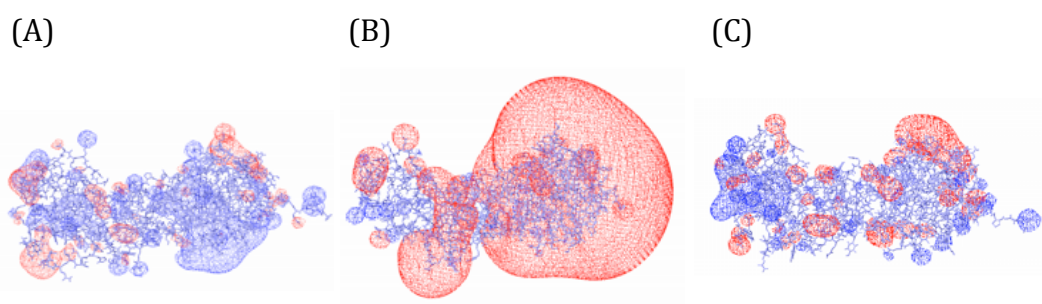


**Figure 2.22 Representation of electrostatic potentials of Myo5a, Myo5b, and Myo5c GDs calculated with the program Swiss PDB viewer.** The larger the cloud appears around a certain region, the greater its electrostatic potential is. Positive charges are depicted in blue, negative charges in red. For each image identical parameters for plotting were used.

Thus, on one hand the previously reported Rab11a-binding region of Myo5b reflects no extreme electrostatic potential (region highlighted in Figure 2.21 D), but on the other hand a region covering almost one-third of the domain shows very similar surface charge distributions amongst all three paralogs (Figure 2.21 A, circled in red). It is tempting to speculate that the latter region could mediate binding of an adaptor common to all three myosins or be required for some other general function. Nevertheless, the two amino acids previously shown to be important for autoinhibition are indeed placed in this region.

### 2.3.11 Investigation of structurally similar proteins

The DALI server (DaliLite v. 3) (Holm, Kaariainen et al. 2008) is a network service for comparing protein structures in 3D. When a structure is submitted to the server, the server compares this template with protein structures deposited in the Protein Data Bank (PDB) database for similar protein fold or domain organization. A search performed with Myo5a yielded similarities to the yeast MyV homologs as well as to some proteins of the membrane-tethering exocyst complexes. These structures were further analyzed by superimposition. Since the similarities between some members of the exocyst complexes and type V myosins had been described before (Heuck, Fetka et al. 2010), this observation was expected. Although no novel fold was found, none of these structures have a  $\beta$  sheet connecting N- and C-terminal end of the molecule (Table 2.7).

List of homology structures found by DALI server	RMSD (Å)	Description
Myo2p	3.4	Myosin type V, yeast homolog
Myo4p	4.1	Myosin type V, yeast homolog
Exocyst complex component SEC6 (The C-terminal domain)	6.5	Involved in active exocytosis
Transport protein TIP20	4.8	Required for protein transport between the Golgi and the endoplasmic reticulum
DSL1	4.7	Part of a multisubunit tethering complexes (vesicle tethering)
Protein Unc-13 homolog A (Munc13-1)	5.6	Involved in vesicle maturation during exocytosis
Exocyst complex component SEC15	5.1	Involved in active exocytosis

**Table 2.7 Proteins similar to Myo5a GD crystal structure based on their 3D Homology.**

A DALI search (Holm, Kaariainen et al. 2008) performed with Myo5a GD crystal structure as template revealed list of molecules similar in fold and domain organization. Seven of the most similar hits are listed. RMSD values could differ from other superpositionings in this thesis, because these values were generated by COOT and SS-Superimpose, which uses different algorithms.

### **2.3.12 Residues required for Myo5a autoinhibition are conserved in Myo5b and Myo5c**

Despite the limitation that autoinhibition experiments were performed with mouse Myo5a (Li, Jung et al. 2008), these data are considered as valid for all mammals. A major reason for this interpretation is that Myo5a possesses a high degree of protein sequence conservation. For instance, there are only three conservative exchanges between mouse and human Myo5a GD. Amino acids required for autoinhibition of human Myo5a correspond to K1708 and K1781. A sequence alignment with Myo5b and Myo5c shows that K1708 and K1781 are also fully conserved in these paralogs (Figure 2.16; red-boxed amino acids). When the amino acids are labeled on the structural models, they lie on the surface at similar positions (Figure 2.23 A; amino acids highlighted in red). In agreement with this, the surface plot of electrostatic potentials in all three paralogs indicates similar surface charge patches (Figure 2.23 B; red circles). However for Myo5b and Myo5c no autoinhibition has been reported.

### **2.3.13 Not only Myo5a, but also Myo5b and Myo5c GD mediates autoinhibition**

To find out if also Myo5b and Myo5c mediate autoinhibition, I performed regenerative ATPase assays under saturating ATP and F-actin conditions (Li, Jung et al. 2006; Thirumurugan, Sakamoto et al. 2006). Myo5a GD added in trans to the motor domain (Myo5a HMM) is capable to induce the autoinhibition. First, I repeated the experiment with and without the GD, but also with the Myo5a K1708A mutation as a control. The addition of GD reproducibly reduced the motor-dependent ATP hydrolysis to 60-70% (Figure 2.27). This inhibited state was defined as 100% inhibition. As 0% inhibition was defined the activity in absence of GD. A Myo5a GD with the K1708A mutation was incompetent to mediate autoinhibition and was always included as a control in all experiments (Figure 2.23 C; Figure 2.27 A). This also confirmed, that the relatively low ATPase activity in presence of the GD is indeed a result of autoinhibition and not co-purification of another factor with the GD.

The same experiment was repeated with Myo5b and Myo5c GDs. Although the assay was performed with the Myo5a motor domain (HMM); the GDs of the other paralogs inhibited the motor activity with similar strength as Myo5a GD. This result that not only suggests that Myo5b and Myo5c are regulated by autoinhibition, but also that the molecular interaction for autoinhibition is likely conserved even between all paralogs.

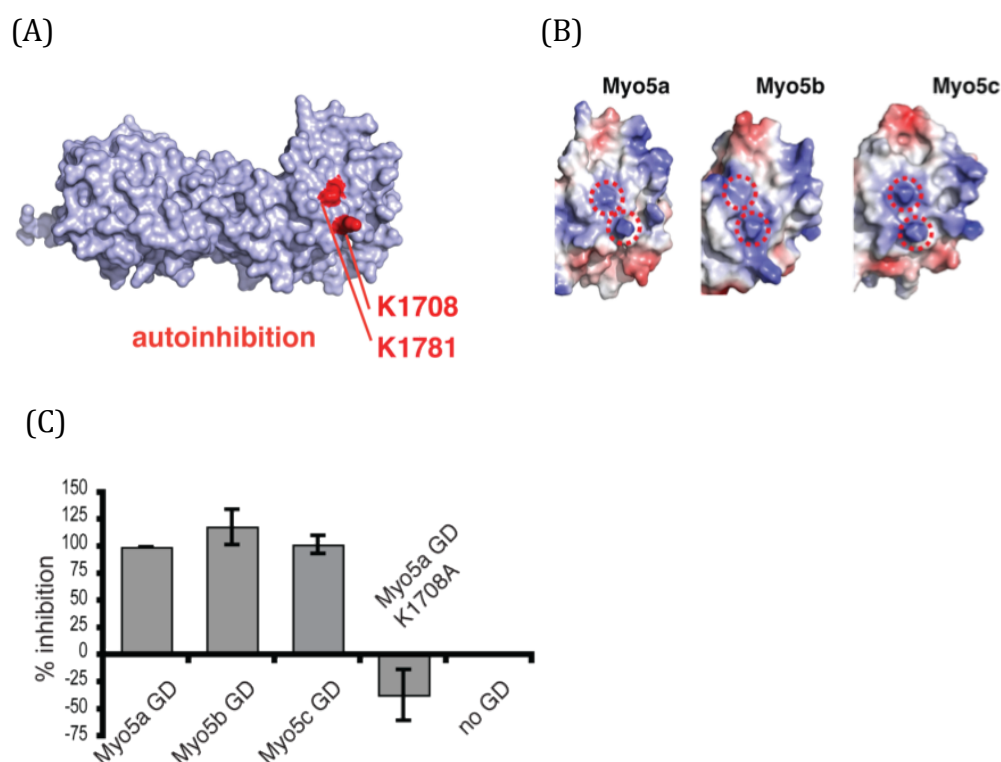


**Figure 2.23 Not only Myo5a, but also Myo5b and Myo5c GD mediate autoinhibition.** (A) Surface representation of Myo5a GD with residues K1708 and K1781 required for autoinhibition (Li, Jung et al. 2008) highlighted in red. (B) Electrostatic potentials of GDs from Myo5a, Myo5b, and Myo5c show that these residues are conserved and are located in the same position (red circles). This observation might suggest that autoinhibition is not limited to Myo5a, but is common to all human type V myosin members. (C) Autoinhibition of Myo5a HMM by the GDs of Myo5a, Myo5b, Myo5c. Inhibition by Myo5a GD alone was set to 100% for all experiments and values measured in absence of GD was set to 0% inhibition. The Myo5a GD K1708A mutant served as a control. Error bars represent standard deviations of the mean from at least three independent experiments. Each experiment was performed at least in triplets for each fragment.

### 2.3.14 Binding of Rab11a does not relieve the autoinhibition

It was reported, that addition of Mlph reduces Myo5a autoinhibition (Li, Ikebe et al. 2005). Based on this observation, it was hypothesized, that cargo binding might relieve the motor inhibition.

Rab11a was shown to directly bind Myo5b and this binding was reduced by Y1714E and Q1748R point mutations (Roland, Bryant et al. 2011)(Figure 2.24 A). First, I confirmed this binding in a pull down assay. Here I realized that His-Rab11a interacts not only with Myo5b, but also with Myo5a and not with Myo5c (Figure 2.24 B). This was in agreement with alignment, where Y1714 and Q1748 in Myo5b correspond to amino acids Y1721 and Q1755 in Myo5a. On the other hand in Myo5c only the glutamine (Q) is conserved. The tyrosine (Y) is

substituted by a cysteine (C). More surprising was an even stronger binding to Myo5a than to Myo5b. This suggests a physiologically relevant function.

In ATPase assays, addition of Rab11a had no effect on autoinhibition, even if I increased the Rab11a concentrations up to 30  $\mu$ M (Figure 2.24 C; Figure 2.27A).

I concluded that in contrast to Mlph, Rab11a is not relieving autoinhibition.

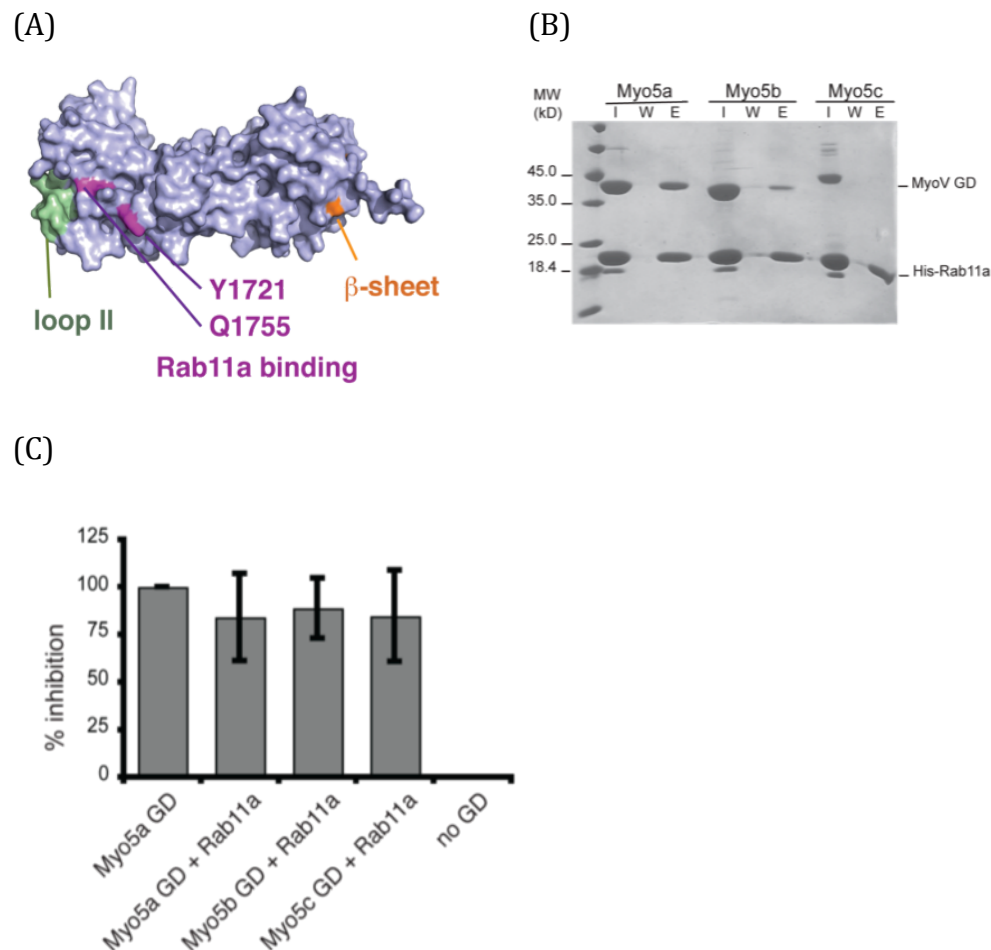


**Figure 2.24 Rab11a does not prevent autoinhibition.** (A) Surface representation of Myo5a crystal structure. Orientation is as shown in Figure 2.14 A but rotated by 180° around the vertical axis. Residues Y1721 and Q1755 required for Rab11a binding are highlighted in magenta. These residues are conserved in Myo5b (Y1714, Q1748), but not in Myo5c GDs (alignment Figure 2.16). Loop II (green) and  $\beta$  sheet (orange) are also highlighted. (B) Ni-NTA pull down experiments to confirm the Rab11a binding to Myo5b and to inspect the binding with Myo5a and Myo5c GDs. The PAGE was stained with Coomassie brilliant blue and shows I = Input, W = last wash step, E = elution fractions. The Rab11a was His-tagged GDs were not tagged. (C) Autoinhibition experiments in the presence of the GDs of Myo5a, Myo5b, and Myo5c as well as Rab11a or in absence of any GD. The Myo5a K1708A control is not shown. The presence of Rab11a had no impact on the repression.

### **2.3.15 Docking of Myo5a GD crystal structure into EM density of autoinhibited Myo5a**

In order to get more details about the interaction between the Myo5a motor domain and GD, I inspected an electron density of autoinhibited full-length Myo5a published in 2006. This low-resolution electron density (European Bioinformatics Institute (EBI) – accession code: EMD-1201) was obtained by electron microscopy (EM) and the authors modeled all published domain structures into the electron density (Liu, Taylor et al. 2006). Because at that time, no high-resolution structure of any type V myosin GD was available, interpretation of the corresponding interaction site was difficult. The authors suggested that in the flower-like structural arrangement of their structure (Figure 1.2) each Myo5a motor domain binds to a GD of its neighboring molecule. Binding to the motor was assigned to the so-called loop 1 of the motor domain (Liu, Taylor et al. 2006). Later, a x-tal structure of a yeast homolog Myo2p became available (Pashkova, Jin et al. 2006). A reassessment of the structural interpretation with the Myo2p structure suggested that the previously described interaction between the motor and the GD is rather intramolecular (Sellers, Thirumurugan et al. 2008). However the docking of yeast GD was accompanied with a great uncertainty.

I therefore placed the Myo5a motor (PDB-ID: 2DFS or 1W7I) and my GD crystal structure into this electron density (EBI – accession code: EMD-1201) and fitted the molecule by performing Molecular Dynamics Flexible Fitting (MDFF) (Trabuco, Villa et al. 2008). Of the two previously suggested orientations, I found only one possible. In this orientation the interaction is intramolecular, with each motor domain binding to the GD of the same Myo5a peptide chain (Figure 2.25 A). Since the residues K1708, and K1781 of the GD and D136 of the motor domain are located in close vicinity (Figure 2.25 B and C).

Detailed inspection of the fitting revealed that not only these three amino acids are close enough to make a molecular contact, but other parts of the molecule might be important as well. Particularly loops I and II of Myo5a GD are located close to the motor domain (Figure 2.25 B). Loop II is well coordinated and probably not flexible according to the crystal structure. The loop II is a protrusion of three short helices, which are as well highly conserved among

species. Indeed when these helices are submitted to a structure-homology search using the DALI server, the closest found homologs are EF-hands and other calcium sensing domains. However no coordinated calcium was discovered in the crystal structure or by the wavelength screen used for Selenomethione detection in crystals prior data collection (data not shown).

The crystal structure lacks electron density for loop I, and secondary structure prediction programs revealed no significant conformations for any part of the loop. Therefore I modeled the whole region (residues 1640 – 1658) as unstructured loop using COOT program (Emsley, Lohkamp et al. 2010). The most probable conformations were picked and analyzed in the context of autoinhibition. Surprisingly, when I replaced the GD with the GD with modeled loops I, both the modeled loops I and loop II could contact the lever arm or even CaM (Figure 2.25 D). To confirm my hypothesis that the interaction interface needed for autoinhibition is more complex than solely these three previously described amino acids, I performed ATPase assays with mutated loops I and II.



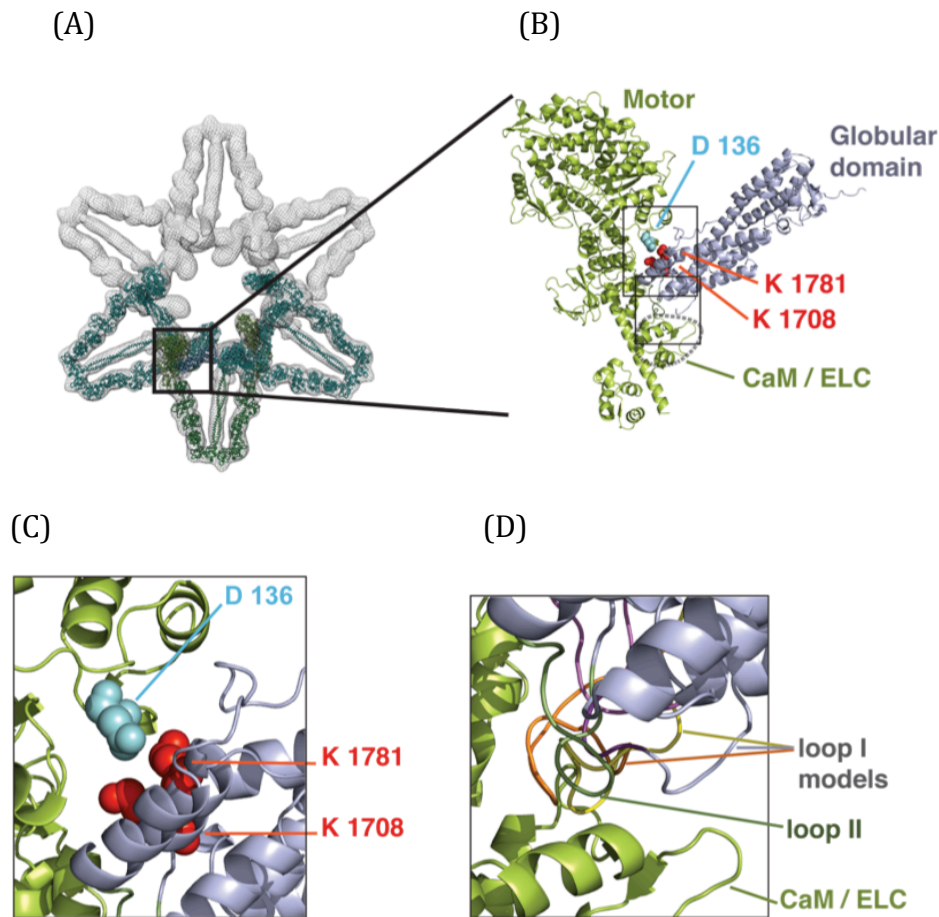


**Figure 2.25 Docking of high resolution Myo5a GD structure into EM density of autoinhibited Myo5a** (A) Previously published electron density map of autoinhibited Myo5a molecules arranged in a flower-like motif (PDB-ID of published model lacking the globular domain: 2DFS; (Liu, Taylor et al. 2006)). I modeled three (blue and green) out of six myosin dimers into the EM density (meshed surface rendering) and the high-resolution structure of Myo5a GD. All molecules are depicted in ribbon representation. The color scheme is as follows: blue, Myo5a GD; green, motor domain, lever arm, light chains, coiled coil domain; turquoise, neighboring dimers. (B) Close-up of the motor bound to GD in (A) shows the Myo5a motor (green) and the fitted GD (blue). Residues previously reported to be important for autoinhibition (D136 in motor domain and K1708, K1781) (Li, Jung et al. 2008) are shown as colored spheres. (C) Close-up of the upper rectangle in (B), in the same color code. (D) Close-up of the lower rectangle in (B) shows in yellow, orange, magenta, and grey possible spatial conformation of modeled loop I. According to this model, the loop I and thus the GD contacts not only the motor domain, but also calmodulin.

### 2.3.16 The loop I and II of the GD are required for autoinhibition

Because the loop II is well coordinated in the crystal structure, I mutated ten amino acids of the loop into an oligo-glycine chain (Myo5a GD (loop II gly), residues 1787-1797, Figure 2.26 A and B). In contrast, loop I is highly flexible and I tested deletion of 3-19 residues already in crystallization trials with Myo5a 1446-1855 (see chapter 2.3.1). Thus for ATPase assays, either 6 or 9 amino acids

in loop I (Myo5a GD (loop I  $\Delta 6/9$  aa) were deleted. All mutants were purified by size-exclusion chromatography in the last purification step. The mutants behaved in a manner indistinguishable from wild-type Myo5a GD.

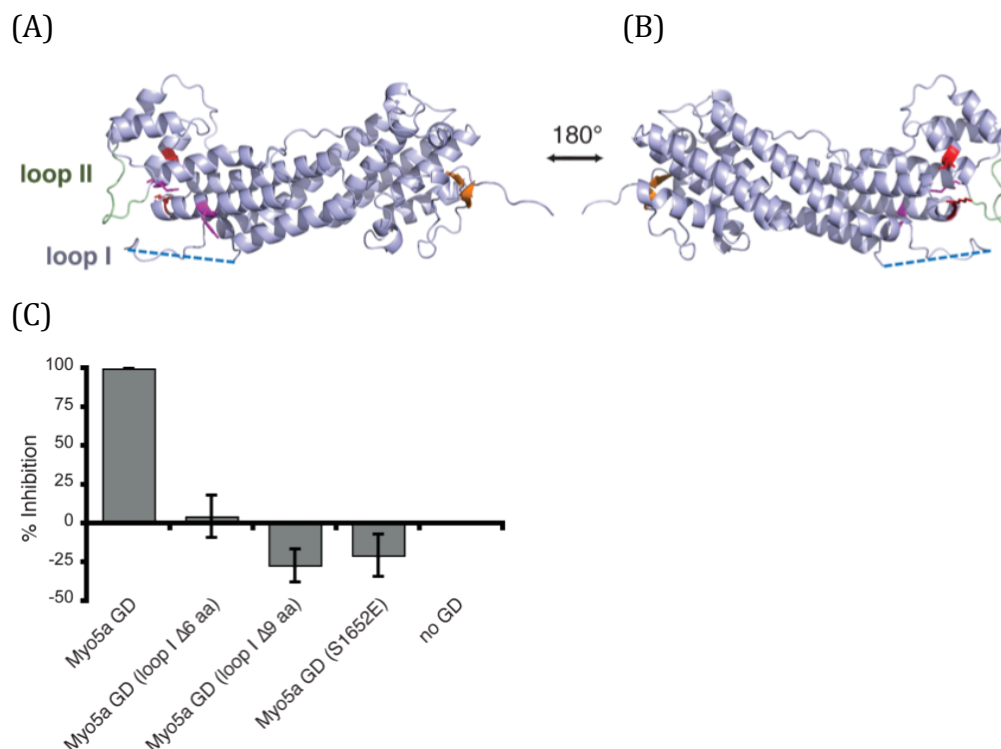


**Figure 2.26 Regions of Myo5a GD important for autoinhibition.** (A) Ribbon representation of Myo5a GD with highlighted residues required for autoinhibition: (loop I 1640-1658) in blue, (loop II: 1787-1797) in green, K1708 and K1781 in red. Also highlighted are residues required for Rab11a binding Y1721 and Q1755 in magenta and the  $\beta$ -sheet in orange. (C) ATPase assay with Myo5a GD (loop I  $\Delta 6$  aa and loop I  $\Delta 9$  aa) mutants and S1652 point mutation.

In ATPase assay experiments, both the Myo5a GD (loop I  $\Delta 6$  aa and loop I  $\Delta 9$  aa) mutants showed decreased inhibition by 50 - 70 % in comparison with the wild-type Myo5a GD (Figure 2.26 C). The loop II oligo-glycine mutant (loop II gly) led to a complete loss of inhibition (Figure 2.27 A and B).

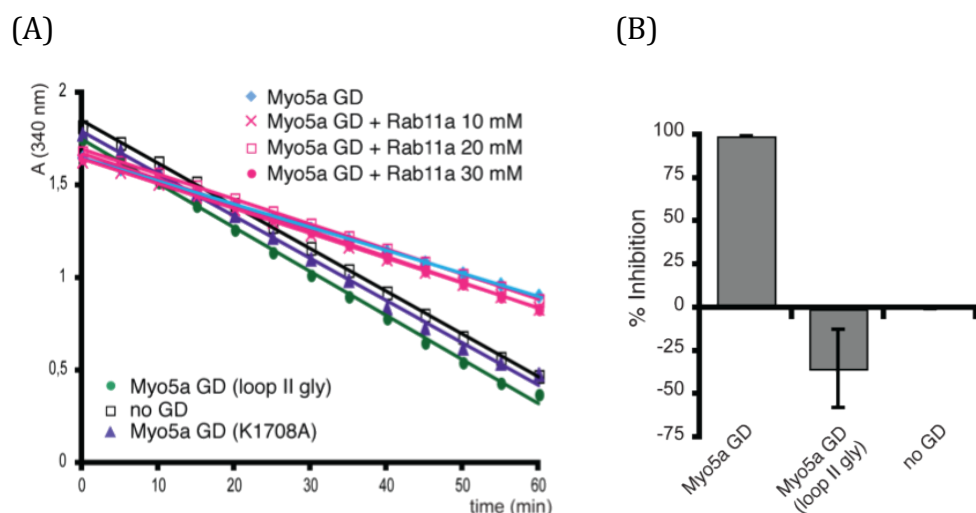


**Figure 2.27 Regenerative ATPase assays.** (A) Raw data obtained from one experiment are shown. Different human Myo5a GD fragments or the Myo5a GD with different Rab11a concentrations were added in trans to a Myo5a motor domain (HMM5). (B) ATPase assay with Myo5a GD (loop II gly).

### 2.3.17A phospho-mimicking mutation in Myo5a loop I abolishes autoinhibition

It was previously shown that phosphorylation of serine 1652 of Myo5a GD is important for Myo5a dissociation from melanosomes (Karcher, Roland et al. 2001). The residue S1652 is positioned in loop I of Myo5a GD, which is missing in the crystal structure (Figure 2.14 A and B). Glutamic acid is routinely introduced at serine position to mimic constitutively phosphorylated serine. I tested this phospho-mimicking mutant (Myo5a GD S1652E) in ATPase assays. Indeed, in ATPase assays, the motor inhibition in presence of (Myo5a GD S1652E) was almost completely lost (Figure 2.26 C). Even addition of Rab11a did not rescue the autoinhibition (data not shown). Thus phosphorylation of S1652 might be important in autoinhibition release.

### 3. Discussion

The establishment of active transport in eukaryotic cells required the invention of mechanisms that regulate cargo recognition, transport and unloading at the site of destination. Myo5a, Myo5b, and Myo5c are such indispensable ATP-dependent transport machines in vertebrates, responsible for short distance intracellular transport, as well as anchoring organelles (Hammer and Sellers 2012). The recent attention was particularly paid to the mechanisms of activation or inhibition of the motor, which correlates with ATP turnover (Akhmanova and Hammer 2010). The Myo5a GD mediates both the inhibition of motor domain as well as cargo binding and plays thus a pivotal role in Myo5a regulation. A high-resolution structure of MyoV GD of higher eukaryotes is however not available and it is unknown whether Myo5b and Myo5c are regulated by autoinhibition.

In yeast, Myo2p and Myo4p are the only known representatives of type V myosin family. Myo2p and Myo4p GDs differ in shape and cargo-binding preferences while found in the same yeast species. It has been speculated that the shape of the cargo-binding domain is responsible for cargo recognition (Heuck, Fetka et al. 2010). Because such shape variety was also expected between Myo5a, Myo5b, and Myo5c GDs, my aim was to obtain a high-resolution structure at least of one of these human myoV GDs and to generate a homology model of the other ones. The Myo5a GD was previously suggested to consist of residues 1446-1855 (Fukuda, Kuroda et al. 2002), but my attempts to crystallize this or corresponding Myo5b or Myo5c fragments failed. Further search for fragments resistant to degradation yielded the Myo5a (1467-1855) fragment.

I performed SAXS analysis with this recombinant protein fragment and its human paralogs. The SAXS analysis revealed that these fragments are monomeric and globular, which is consistent with the predicted compact shape of known cargo-binding domains. Myo5a and Myo5b GDs share 70.5% identical amino acids and the homology between Myo5a and Myo5c GDs is slightly lower with 62.7%. Surprisingly, the calculated surface envelopes showed very small shape alternations of not only between Myo5a and Myo5b, but also with Myo5c

GDs (Figure 2.10). The cargo preferences are thus not directed by the shape but rather by the surface properties.

### **3.1 Myo5 regulation by autoinhibition**

One of the milestones in Myo5a autoinhibition research was a low-resolution electron density of inhibited full-length mouse Myo5a obtained by electron microscopy. Available crystal structures of motor, lever arm, and coiled-coil were placed into the density (Liu, Taylor et al. 2006). Later, when the Myo2p GD crystal structure was published, the yeast GD served as a substitute for the lacking structure of a GD from higher eukaryotes. Two speculative models of the GD placement and binding to motor domain within the EM were discussed (Trybus, Gushchin et al. 2007; Sellers, Thirumurugan et al. 2008; Trybus 2008).

After I found by SAXS analysis that the GD is smaller, I also obtained diffracting crystals with this fragment (Myo5a 1467-1855) and finally solved the structure of the Myo5a GD. When I performed fitting of the Myo5a GD into the existing low-resolution electron density, I found only one orientation possible. This fitting not only confirmed three residues (D136, K1708, and K1781) already found to be important for autoinhibition, but revealed two additional surface patches close enough to interact with the head. Interestingly, both patches consisted of highly conserved loops. Loop I is about 18 residues long and unstructured, but well conserved among species. Because of lacking electron density, the loop I could not be modeled unambiguously and is missing in the Myo5a crystal structure. I modeled therefore few most probable conformations of loop I. When I placed these models into the autoinhibited EM density, I observed that the loop could reach not only the lever arm and CaM but also perhaps even an IQ motif, in case CaM would not be present.

As confirmed by ATPase assays, mutation or deletion of the loops I and II turns the molecule into its active state. A triangle-shaped pocket, where the loops I and II fit nicely, is probably composed of motor domain, lever arm and CaM. Such a pocket with large interaction surface could lock the head in a conformation unfavorable for the rotational movement required for active motility or even ADP release.

There are only two myosin type V structures from yeast published to date, Myo2p and Myo4p (Pashkova, Jin et al. 2006; Heuck, Fetka et al. 2010). A comparison of these type V myosin structures with Myo5a GD revealed some pronounced similarities like domain composition and folding, but they differ in the overall shape. However the Myo5a GD shape is more similar to Myo2p than to Myo4p (Figure 2.19).

Finally, I also solved crystal structure of the Myo5b GD. This domain was similar to Myo5a GD in the overall shape and fold. It also contains a beta-sheet located at the very C-terminus. Both structures were used for computational structure-homology prediction of the Myo5c GD. The Myo5c model revealed high similarity to Myo5a. My results show that all human paralogs have this small beta-sheet, the function is however unknown. Also a structural homology search with the DALI server revealed a beta-sheet in structurally most related proteins such as the exocyst complex.

In addition, when I repeated the ATPase assay with Myo5b and Myo5c GD, the Myo5a motor was inhibited equally well as with Myo5a GD. This is consistent with a high conservation of the surface amino acids on the GD of all three human paralogs required for autoinhibition and suggests a conserved mechanism of autoinhibition. Lifting of autoinhibition should be theoretically possible only in the presence of cargo. Indeed, a partial release of autoinhibition was shown for Mlph. In contrast to Mlph, Rab11a in the presence of Myo5a or Myo5b GD does not show any release of autoinhibition.

### **3.2 Myo5 regulation by cargo binding and phosphorylation**

It is not known how large cargo complexes with many components are and how is it ensured, that the myosin does not starts moving along actin filaments before all components are loaded. One could imagine that a pre-assembled complex requires an additional signal to lift the inhibition and activates the complex for movement. Such trigger could ensure that no part of the cargo is missing. A protein long enough to span around all cargo would be suitable. Such long unstructured protein is Mlph, which together with Myo5a and Rab27a forms a transport complex in melanocytes. Here, Rab27a is bound to melanin-containing

vesicles called melanosomes. The exact order, in which Myo5a, Mlph, and Rab27a are recruited, is however not known. Also Rab11-FIP2 that is part of the Myo5b-Rab11a-Rab11-FIP2 complexes has similar features. Mlph and Rab11-FIP2 bind to the myosin rod or to loops in the rod region and to the GD. Moreover, both proteins bind to a Rab adaptor protein. The Rabs bind directly to the cargo. Interestingly, both have coiled-coil domains that dimerizes (Hales, Griner et al. 2001; Wu, Rao et al. 2002; Heuck, Fetka et al. 2010). Another example is the mainly unstructured adaptor protein She3p. When the N-terminal part of She3p was dimerized with a GST or GCN4 tag, the stability of binding to Myo4p was enhanced (Heuck, Du et al. 2007). Thus dimerization of an adaptor protein could stabilize the dimeric and active state of all type V myosins. This is consistent with experiments in this thesis, where Rab11a binding itself does not lift the autoinhibition, possibly because it does not stabilize the dimeric state of Myo5a. Moreover Mlph was already shown to partial restore the Myo5a actin activated ATPase activity *in vitro* (Li, Ikebe et al. 2005). Another possibility for Myo5a regulation is a posttranslational modification. Rogers and colleagues found that phosphorylation of Myo5a on serine 1650 drives its dissociation from melanosomes in mitotic *Xenopus* egg extracts. Dissociation from melanosomes is likely achieved by the Myo5a complex disassembly. Not only the responsible calmodulin dependent protein kinase II was identified, but also it was shown that the kinase interacts with the Myo5a tail (Costa, Mani et al. 1999; Karcher, Roland et al. 2001). This serine 1650 phosphorylation might be also involved in localization, as the modified Myo5a was found in nuclear speckles (Pranchevicius, Baqui et al. 2008). Thus, phosphorylation might alter the affinity or selectivity between myosin and the cargo.

Whether posttranslational modification are also involved in regulation of autoinhibition is a subject of discussion. The only example was conducted in an *in vitro* experiment with the corresponding mouse Myo5a S1650E mutation. In this assay, melanophilin-induced ATPase activity of Myo5a was tested and introduction of S1650E mutation abolished the activation (Hume, Tarafder et al. 2006). However the presence of relatively high salt concentration (200m mM KCl) in this experiment might alter the ATPase activity regulation and is almost

2-fold higher than the salt concentration used in experiments of other authors (Li, Jung et al. 2006; Thirumurugan, Sakamoto et al. 2006).

This phosphorylation site is not found in yeast, but a reversible *in vivo* phosphorylation of the N-terminal three amino acids of the Myo2p GD was demonstrated. However no effect on the motor activity or motility of this phosphorylation was described (Legesse-Miller, Zhang et al. 2006).

In my experiments, a phosphorylation-mimicking mutation S1652E at the human Myo5a GD restored motor activity in ATPase assays. Interestingly, this phosphorylation site is placed in the loop I region and is highly conserved in higher eukaryotes. Since several labs are dealing with many types of results showing both activation and inactivation, no convincing conclusion can be made about the role of GD phosphorylation. Probably some experimental conditions or cofactors are playing a decisive role.

### **3.3 Regulation by $\text{Ca}^{2+}$ concentration**

Another suggested mode of regulation of autoinhibition is via different calcium concentrations. Experimental data for full-length Myo5a shows folded and unfolded form. The unfolded or elongated form is achieved by increasing the  $\text{Ca}^{2+}$  concentration. At micromolar  $\text{Ca}^{2+}$  levels the full-length Myo5a unfolds and is active and moves along actin. At millimolar  $\text{Ca}^{2+}$  range or salt concentration at 600 mM KCl, the bound calmodulins are believed to dissociate and the motor is inactive, but the molecule is elongated. The folded form corresponds the inactive or autoinhibited state and it forms in absence of  $\text{Ca}^{2+}$  or presence of low  $\text{Ca}^{2+}$  (in EGTA conditions). The conformational change was revealed by analytical ultracentrifugation, single molecule TIRF microscopy as well as with electron microscopy (Li, Mabuchi et al. 2004; Lu, Kremmentsova et al. 2006). Experiments with dimeric truncated Myo5a where the GD is missing (Myo5a HMM), showed that calcium levels do not regulate its actin-activated ATPase activity. In contrast to the full-length molecule, the Myo5a HMM might be only regulated by dissociation of calmodulins.

The reason why calcium regulation differs for full-length and truncated molecules is unknown. Some molecules that bind Myo5a like Rab GTPase, dynein



light chain or regulatory light chain have about the same size as CaM or ELC. One could imagine that they have been copurified and left unrecognized. Indeed, one report describes tissue-isolated Myo5a that was copurified with dynein light chain (Espindola, Banzi et al. 2008). However, this possibility remains speculative and requires further investigation. Another possibility is that the GD senses calcium and changes its conformation. Automatic search programs found several calcium binding motifs in the GD. The DALI structural homology search found three short helices that structurally resembles the EF-hand, positioned next to the loop I, in close proximity of the motor-binding region.

I inspected many processed data files from soaking and co-crystallization experiments, but did not find additional electron density for bound calcium in the solved structures. Nor did a wide spectrum wavelength scan of crystals at synchrotron beam lines reveal a strong peak of bound calcium cations.

### **3.4 The Myo5a autoinhibition model**

A previous publication suggested that solely one amino acid of the motor domain (D136) and two amino acids of the GD (K1708 and K1781) are responsible for autoinhibition. Based on the studies summarized in this thesis, it has become clear that binding of Myo5a motor to GD is regulated by a more complex mechanism. I confirmed that indeed mutation of K1708A does impair the autoinhibition, but I also found that deletion of loop I or mutation of loop II has nearly the same effect.

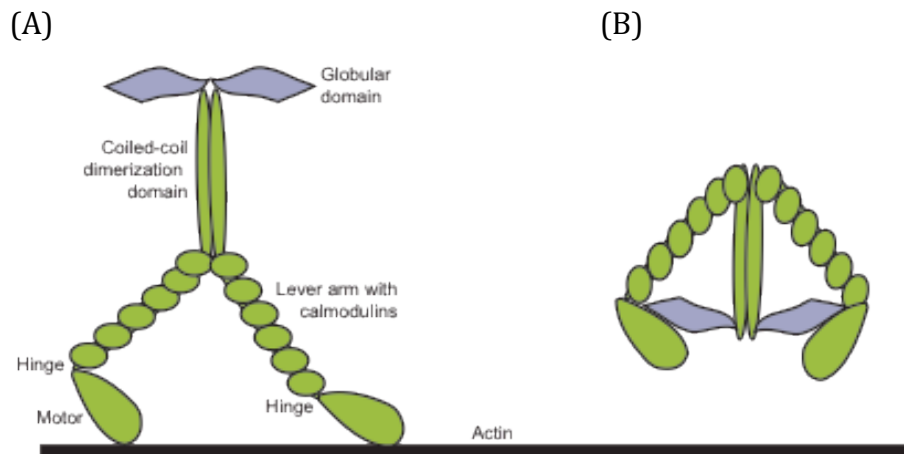


**Figure 3.1 Model of Myo5a autoinhibition.** Schematic drawing of an autoinhibition model of full length Myo5a. (A) Active state. The molecule is in its dimeric state; the hinge between motor domain and lever arm is flexible and enables movement. The hinge angle is changing during a step (see Figure 3.2 A). ATP is hydrolyzed. (B) Autoinhibited state.

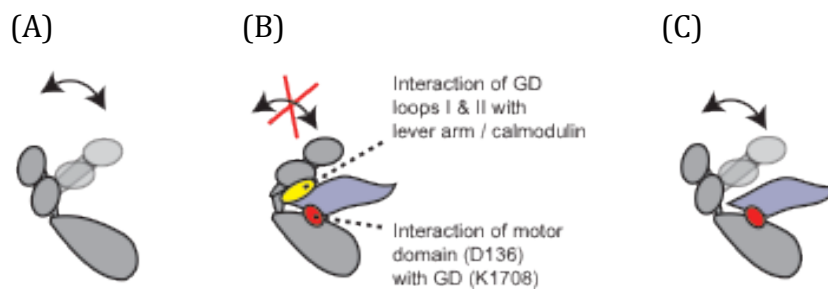


**Figure 3.2 Model of Myo5a autoinhibition-hinge angle changing during a step.** Schematic drawing of Myo5a motor domain and part of the lever arm and two CaMs (as depicted in Figure 3.1 A). (A) Absence of GD enables full movement of the hinge or the angle depends on nucleotide binding state during ATP hydrolysis (B). The same molecule as in (A), but the GD binds to the motor domain or perhaps to the lever arm and CaM. The hinge is in a fixed position, the molecule is unable to move along actin and ATP is not hydrolyzed. (C) The same molecule as in (A), the GD binds to the motor domain, but the movement of the hinge is not fixed.

Thus rather than a three-residues interaction, a large and highly conserved patch on the GD is involved in the interaction. Moreover not only the motor domain, but also the lever arm and perhaps even the CaM or IQ motif, when CaM is not present are likely to play a role in autoinhibition.

In human, multiple myosins are expressed with distinct but perhaps overlapping subcellular localizations and potentially overlapping functions. This thesis investigates the myosin-dependent transport and describes in detail the myosin type V regulation at the molecular level. However, a major challenge in the future will be to assess how the myosin cargo is recognized, bound to the motor protein and how the cargo is eventually unloaded. Another question is of course how these three important steps are regulated. This work contributes to further

research and understanding of myosin transport and thus unraveling the physiological functions at the molecular level particular in human.

## 4. Materials and methods

### 4.1 Chemicals

All used chemicals and other standard laboratory consumables with appropriate purity were purchased from Gibco BRL Life Technologies (Karlsruhe, Germany), Merck (Darmstadt, Germany), Roche Diagnostics (Mannheim, Germany), Roth (Karlsruhe, Germany), and Sigma-Aldrich (Hamburg, Germany) unless stated otherwise. Enzymes and reagents for molecular biology and gel electrophoresis were purchased from Fermentas (St. Leon-Rot, Germany), Invitrogen (Karlsruhe, Germany), New England Biolabs (Frankfurth am Main, Germany) or Qiagen (Hilden, Germany). Oligonucleotides were ordered from Thermo Fisher (Schwerte, Germany), Antibodies from Abcam (Cambridge, USA). Insect cell and bacterial cultivation media and chemicals were purchased from Becton Dickinson (Heidelberg, Germany), Invitrogen (Karlsruhe, Germany) and Thermo Fisher scientific (Schwerte, Germany). Pre-packed chromatographic column were purchased from GE Healthcare (Munich, Germany). Crystallization screens and other consumables were purchased from Hampton Research (Aliso Viejo, CA, USA), Jena Bioscience (Jena, Germany) or Qiagen (Hilden, Germany).

### 4.2 DNA Oligonucleotides for cloning

No.	Name	sequence (5' to 3')
hv002	hMyo5a 1446 For	aaa gga tcc atg gag aac ata tct cca gga
hv005	hMyo5a 6loop For	gta tct ggg gtg aag ccc aca tcc agt atc gca gat gag ggc
hv006	hMyo5a 6loop Rev	gcc ctc atc tgc gat act gga tgt ggg ctt cac ccc aga tac
hv007	hMyo5a 9loop For	gta tct ggg gtg aag ccc aca gca gat gag ggc acc tac aca
hv008	hMyo5a 9loop Rev	tgt gta ggt gcc ctc atc tgc tgt ggg ctt cac ccc aga tac
hv009	hMyo5a 19loop For	ggt atg cta gag cat gaa aca gca gat gag ggc acc tac aca
hv010	hMyo5a 19loop Rev	tgt gta ggt gcc ctc atc tgc tgt ttc atg ctc tag cat acc
hv011	hMyo5a 1654 NdeI For	aa aaa cat atg gca gat gag ggc acc tac aca gac
hv012	hMyo5a 1645 stop EcoRI	aaa gaa ttc tca ccc tgt ggg ctt cac ccc aga tac
hv013	hMyo5a 1855 Stop XhoI Rev	aaa ctc gag tca gac ccg tga aat gaa gcc cag
hv014	hMyo5a R1481K For	atg ctg gaa tac aag aag gag gat gag caa aaa
hv015	hMyo5a R1481K Rev	ttt ttg ctc atc ctc ctt ctt gta ttc cag cat
hv016	hMyo5a V1696 I For	cag atg ttc tac atc ata ggg gcc atc acc ctg
hv017	hMyo5a V1696 I Rev	cag ggt gat ggc ccc tat gat gta gaa cat ctg
hv018	hMyo5a 1476 BamHI For	aaa gga tcc atg ctg gag tac aag aag gag gat

hv019	hMyo5a 1463 BamHI For	aaa gga tcc atg cca gtc aac att ccc cgg aaa gaa
hv020	hMyo5a 1504 BamHI For	aaa gga tcc atg ctg att cca ggg tta cca gca tat atc
hv023	hMyo5a 1552 F->M For	aaa aga ggt gacgatatggaaactgtctcttc
hv024	hMyo5a 1552 F->M Rev	gaa gga gac agt ttc catatcgtcacctctttt
hv025	hMyo5a 1618 L->M For	ctc gtg cgg gtg atg gag aac atc ctt cag cca
hv026	hMyo5a 1618 L->M Rev	tgg ctgaaggatgttctccatcacccgcacgag
hv027	hMyo5a 1701 I->M For	tacatcatagggcccatgacccctgaacaacctt
hv028	hMyo5a 1701 I->M Rev	aag gttgttcagggtcatggccctatgatga
hv029	hMyo5a PrecPro For	ctggaagtctgttccaggggctgccgatggggcacctacaca
hv030	hMyo5a 1 For	aaagtcgactcagcgagcctcaattttgagttt
hv031	hMyo5a PrecPro Rev	aggcccttggaacagaacttcagccctgtgggcttccccaga
hv032	hMyo5a 1451 BamHI For	aaa gga tcc cgc cat gag ctc aac agg cag gtc
hv033	hMyo5a 1467 BamHI For	aaa gga tcc atg ccc cgg aaa gaa aag gat ttc caa
hv034	hMyo5a 1406 BamHI For	aaaggatccacccggctgaccaacgaaaactg
hv035	PrPro-hMyo5a 1406 For	gttctgttccaggggccacccggctgaccaacgaa
hv038	hMyo5a 1 BamHI For	aaaggatccatggctgcgtcggagctctacaca
hv039	hMyo5a 792 Sall Rev	aaagtcgactcatgccttcgcatgcgtaggta
hv040	hMyo5a 766 Sall Rev	aaagtcgactcacagtttgcagctcctaattt
hv041	hMyo5a 1855 NotI Rev	tcggccgctcagaccgtgaaatgaagccag
hv042	mMyo5a 913 Sall Rev	aaagtcgactcagcgagcctcaattttgagttt
hv043	hMyo5a K1708A For	aaccttctcctcggggtgacatgtgtctcc
hv044	hMyo5a K1708A Rev	ggagcacatgtcagcccgaggagaagggtt
hv045	hMyo5a K1781A For	gccagattgtggccgtgttgaattgtat
hv046	hMyo5a K1781A Rev	atacaaatcaacacggccacaatctgggc
hv047	hMyo5a loop1787-1797 pG	gtcaaatgttgaatctgtacggcggaggaggcggtg gaggtggaggagggtggagtttcatttatccgactata
hv048	hMyo5a loop1787-1797 pG	tatagtgcggataaatgaaactccacctctccacctcc accgctctcccggtacagattcaacactttgac
hv049	hMyo5a GCN4 FlagTag NotI	aaagcggcgcgtcacttatcgtcatcgtcttatagtaa cttcgccaactaatttctt
hv050	hMyo5a 1105 gcn4 For	accctgatgctgaatgtgatgaacaacttgaagacaag
hv051	hMyo5a 1105 gcn4 Rev	ctgtcttcaagttgttcatcacattcagcatcagggt
hv052	hMyo5a 1 BssH II For	aaagcgcgcattggcgcgtccgagctctaccaag
hv053	hMyo5a 1 BssH II FlagTag	aaagcgcgcattgactataaggacgatgacgataagg gcgcccgcgtccgagctctacacc
hv054	GCN4 FlagTag NotI Rev	aaaaagcggcgcgtcacttatcgtcatcgtcttatagtc aacttcgccaactaatttcttaattctggcaacctatttccaa
hv055	hMyo5a 1472 BamHI For	aaaggatccgatttccaaggaatgctggagtaca
hv056	hMyo5a PrPro 1467	gaagtctgttccagggggccgaaagaaaaggatttc
hv057	mMyo5a 462 seq Rev	gacatgcatgttgaattgtgttg
hv058	mMyo5a 427 seq For	gctgtcaagcagcactctttcat
hv059	mMyo5a 925 seq For	atggagaacaagattatgcagct
hv060	mMyo5a 925 seq Rev	agctgcataatctgttctccat
hv061	hMyo5a 1545 Stop XhoI	aaactcgagtcacttcaagactttttgatgct
hv062	hMyo5a 1842 Stop XhoI	aaactcgagtcactgtaggtttctagggcta
hv063	hMyo5a Huang 3aaMut For	tataactgtttaaatgtgtacgacatgctggttat
hv064	hMyo5a Huang 3aaMut Rev	ataaccagcatgtctacacatttaacaagttata
hv065	hMyo5a D1521G For	tacgacatgctggttatctgaacgatga

hv066	hMyo5a D1521G Rev	tcacgttcagataaccagcatgtcga
hv067	hMyo5a S1652E For	actagtgaatcgagatgaggg
hv068	hMyo5a S1652E Rev	gccctcatcggtatctcgaggttcgtt
hv069	hMyo5a G9loop-1642-1650	ggcgtatctgggtgggaggaggcggtggaggtggaggaggtccagt
hv070	hMyo5a G9loop-1642-1650	atctgcgatactggaacctctccacctccaccgcctctcccacccag
hv071	hMyo5a G4loop-1645-1648	gtgaagcccacagggggaggaggtcgaacctccagatcgcagat
hv072	hMyo5a G4loop-1645-1648	atctgcgatactggaggttcgacctctccccctgtgggttcac
hv073	hMyo5a E1794A For	gttaatgagtttgaagcaagggtcagtttca
hv074	hMyo5a E1794A Rev	tgaactgagacccttgctcaaaactattaac
hv075	hMyo5a E1793A For	ccggttaatgagtttcagaaagggtctcagtt
hv076	hMyo5a E1793A Rev	aactgagaccctttctgcaaaactattaaccgg
hv077	hMyo5b 1418 Bam HI For	aaa gga tcc atg agg aga cac cat gaa ctc aca a
hv078	hMyo5b 1849 XhoI Rev	aaa ctc gag tca gac ttc att gag gaa ttc cag
hv079	hMyo5b 1462 BamHI For	aaa gga tcc cgg aaa gag aag gat ttc cag ggc
hv080	hMyo5b 1457 BamHI For	aaa gga tcc agg cag gtc acg gtc cag cgg aaa
hv081	hMyo5b 1443 BamHI For	aaa gga tcc gca ttg gcc cag agt gag agg aag
hv082	hMyo5b 1469 BamHI For	aaa gga tcc ggc atg ctg gag tac cac aaa gag
hv083	hMyo5b 1517 BamHI For	aaa gga tcc aac gac gat ctc aag gtg cac tcc
hv084	hMyo5b 1464 BamHI For	aaaggatccaaggattccagggtcagtg
hv085	hMyo5b 1466 BamHI For	aaaggatcctccagggtcagtgagta
hv086	hMyo5b 1498 BamHI For	aaa gga tcc gtg ccc tgt ctc ccc gcc tac ctc
hv087	hMyo5b 1845 Stop XhoI Rev	ctcagtcagaggaattccagattgag
hv088	hMyo5b 1473 BamHI For	aaaggatccccacaaggagcagggccct
hv089	hMyo5b 1456 Stop XhoI Rev	ctcagtcactgcctgttgagctcatggcggtt
hv090	hMyo5c 1391 BamHI For	aaa gga tcc atg atc ccc ggg ctg ccg gct
hv091	hMyo5c 1368 BamHI For	aaa gga tcc aag aga gaa gac gag gcc aag ctc
hv092	hMyo5c 1355 BamHI For	aaa gga tcc tca gga ccc aag gag tac ctt gga
hv093	hMyo5c 1411 BamHI For	aaa gga tcc aat gat gcc aac atg ctg aag tcc
hv094	hMyo5c 1742 XhoI Rev	aaa ctc gag cta taa cct att cag aaa gcc tag
hv095	EB1 185Bam HI For	aaa gga tcc gtg ggc aac gga gac gag gag
hv096	EB1 255 EcoRI Rev	ttt gaa ttc tta tat cac aaa gcc ttc atc
hv097	MLph 550 Not I Rev	aaa agc ggc cgc tta ctt tct tct cag aag ata
hv098	MLph 482 Bam HI For	aaa gga tcc gag gtt tca gac att gaa tcc agg
hv109	MLph 176 EcoRI Rev	aaagaattccaggccagcccttggcagcaaa
hv110	MLph 201 PrPro Rev	gggcccctggaacagaacttcagatctgagtcctcgaagtgcga
hv111	MLph 404 PrPro Rev	gggcccctggaacagaacttcaggagcaggtctcctggtcact
hv112	MLph 404 Stop NotI Rev	ttcgccgctagggacgaggtctcctggtcact
hv113	MLph 240 PrPro Rev	gggcccctggaacagaacttcagagccttctgaggggctgc
hv114	MLph 240 Stop NotI Rev	ttcgccgctaaagcctgtgaggggctgc
hv115	MLph 147 EcoRI For	aaagaattcggtggagctgggcctgaactgata
hv116	MLph 176 EcoRI For	aaagaattccaggccagcccttggcagcaaa
hv117	MLph 201 PrPro Rev	gggcccctggaacagaacttcagatctgagtcctcgaagtgcga
hv118	MLph 201 NotI Rev	ttcgccgctaatctgagtcctcctgaagtc
hv119	hRab27a 1 NdeI For	aaa cat atg tctgatg gagattatga

hv120	hRab27a 218 NdeI Rev	aag aaa agg aga aag ggg cat gac tcg agt gc
hv121	Miranda 1 BamHI For	aaa gga tcc atg tct ttc tcc aag gcc aag
hv122	Miranda 1 NdeI For	aaa cat atg tct ttc tcc aag gcc aag ttg aag
hv123	Miranda 298 Rev	gca ctc gag tta cag gct gca gtg ctc gcg ggc
hv124	Miranda 830 Rev	aaa ctc gag cta gat gtt gcg cgc ctt ga
hv125	Myo6 913 For	aaa cat atg aac acc aag ctt aag gag cag caa
hv126	Myo6 1024 For	aaa gga tcc ggc cag gtg gag gat agt cca cca
hv127	Myo6 1030 For	aaa cat atg cca cca gtt ata cgc aat ggt gtc
hv128	Myo6 1256 Rev	gca ctc gag cta ctg ttg ttt ctg cat tgc tgc
hv129	Myo6 1236 XhoI Rev	aaa ctc gag cta agc ctt gcc ccc gtt gcg
hv130	Myo6 1002 BamHI For	aaa gga tcc cgg cag cag ctc gaa cag gaa cgt
hv131	Myo6 1084&1092 C->S For	acgtccagcgatattgagctgctggaggccagccgtcag
hv132	Myo6 1084&1092 C->S Rev	ctgacggctggcctccagcagctcaatcgtggacgt
hv133	Myo6 1203 C->S For	gacgacatgcagatgagcgaactgagcctggag
hv134	Myo6 1203 C->S Rev	ctccaggctcagttcgtcatctgcatgtcgtc
hv135	Myo6 1051 BamHI For	aaaggatccgaaaatgttcgagcccaacaacag
hv136	Rab11a 6 NheI For	aaa gga tcc gactgactacctctttaa
hv137	Rab11a 173 EcoRI Rev	aaagaattctcagtaaatctctgttaaaattgt
hv138	hRab11a Q70L For	gacacagcagggttagagcgatatcga
hv139	hRab11a Q70L Rev	tcgatatcgctctaaccctgctgtgtc
hv140	mCaM 1 SmaI For	aaacccgggaatggcagatcaactgacagaa
hv141	mCaM 147 NheI Rev	aaagctagctcacttcgctgtcatcatctgta

### 4.3 Plasmids

#### Purchased plasmid DNA

Name	Tag	Source
pET28a	N-terminal 6xHis	Merck
pGEX-6P-1	N-terminal GST	GE Healthcare
pETM40	N-terminal MBP	EMBL Heidelberg, modified by A. Heuck
pET Duet-1	N-terminal 6xHis	Merck
pFastBac Dual		Invitrogen
pFastBac 1		Invitrogen

#### Plasmids for protein expression in *E. coli* or insect cells

No.	Name	Mutation / deletion	Vector
phv001	mMyo5a 1446-1855		pGEX-6P
phv002	mMyo5a 1446-Rmut-1855	R->K mutation	pGEX-6P
phv003	mMyo5a 1446-Vmut-1855	V->I mutation	pGEX-6P
phv005	HA-Tag hMyo5a 1446-1855		pGEX-6P
phv006	hMyo5a 1476-1855 My6 #3		pGEX-6P
phv007	hMyo5a 1446-loop19-1855		pGEX-6P
phv008	hMyo5a 1446-loop9-1855		pGEX-6P
phv009	hMyo5a 1446-loop6-1855 #6		pGEX-6P
phv010	hMyo5a 1504-1855 My4		pGEX-6P
phv011	hMyo5a 1463-1855 My3 #2		pGEX-6P
phv012	hMyo5a 1467-1855 MyP #4		pGEX-6P
phv013	hMyo5a 1654-1855		pDUET-1

phv014	hMyo5a 1446-1645 and 1654-1855	coexpression	pDUET-1
phv015	Myo5a 747 (= 156-405 aa)	Myo5a	pGEX-6P
phv016	Myo5a 981 (= 156-483 aa)	Myo5a	pGEX-6P
phv017	Myo5a 414 (= 267-405 aa)	Myo5a	pGEX-6P
phv018	Myo5a 648 (= 267-483 aa)	Myo5a	pGEX-6P
phv019	Myo5a 747 (= 156-405 aa)	Myo5a	pFastbac 1
phv020	Myo5a 981 (= 156-483 aa)	Myo5a	pFastbac 1
phv021	Myo5a 414 (= 267-405 aa)	Myo5a	pFastbac 1
phv022	Myo5a 648 (= 267-483 aa)	Myo5a	pFastbac 1
phv023	Myo5a 405-600	Myo5a	pGEX-6P
phv024	Myo5a 1-150 #3	Myo5a	pGEX-6P
phv025	Myo5a 1-150 Rab 1-218 #1	Myo5a + Rab27a	pET Duet
phv026	Myo5a 1-600 #1	Myo5a	pGEX-6P
phv027	Myo5a 1-150 Rab 1-221 #8	Myo5a + Rab27a	pET Duet
phv028	Rab27a 1-Q78L-221	Rab27a	pGEX-6P
phv029	MBP-Myo5a 405-600 #1	Myo5a	pETM40
phv030	MBP-Myo5a 405-550 #2	Myo5a	pETM40
phv031	MBP-Myo5a 482-550 #7	Myo5a	pETM40
phv032	GST-Myo5a 405-550 #1	Myo5a	pGEX-6P
phv033	GST-Myo5a 482-550 #1	Myo5a	pGEX-6P
phv034	GST-Myo5a 405-550 #3	Myo5a	pGEX-6P
phv035	hEB1 Vale #A	EB1	pGEX-6P
phv037	Mir 1-298 #3	Miranda	MBP vector
phv038	Mir 1-298 #3	Miranda	pGEX-6P
phv039	Mir 1-830 #5	Miranda	pET28a
phv041	Myo6 1024-1236 (1203 C->S #1)	Myo6	pGEX-6P
phv042	Myo6 913 5 (913-1256)	Myo6	pET28a
phv043	Myo6 1030 2 (1030-1256)	Myo6	pGEX-6P
phv044	Myo6 1024-1256 #F	Myo6	pGEX-6P
phv045	Myo6 1002-1256 #1	Myo6	pGEX-6P
phv046	Myo6 1024-1236 #2	Myo6	pGEX-6P
phv047	Myo6 913-1236 #4	Myo6	pET28a
phv048	Myo6 1051-1236 #1	Myo6	pGEX-6P
phv049	Myo6 1024-1236 (CCC->SSS #4)	Myo6	pGEX-6P
phv050	Myo6 1024-1256 #D	Myo6	pGEX-6P
phv052	ELC fl	ELC	pFastBac 1
phv053	Myo5a 1-1105 GCN4-Flag	Myo5a (HMM)	pFBac Dual
phv054	Myo5b (1462-1849)	Myo5b	pGEX-6P
phv055	Myo5b (1418-1849)	Myo5b	pGEX-6P
phv056	Myo5c (1355-1742)	Myo5c	pGEX-6P
phv057	Myo5c (1330-1742)	Myo5c	pGEX-6P
phv058	Myo5a 1467-K1708A-1855	K1708A mutation	pGEX-6P
phv059	Myo5a 1467-K1781A-1855	K1781A mutation	pGEX-6P
phv060	Myo5a 1467-(I1512, M1515, D1521)-1855	I1512, M1515, D1521 mutations	pGEX-6P
phv061	Myo5a 1467-1545	Myo5a	pGEX-6P
phv062	Myo5a 1467-S1552E-1855	S1552E mutations	pGEX-6P
phv063	Myo5a GD (loop II gly)	deletion	pGEX-6P
phv064	Myo5a GD (loop I Δ6 aa)	deletion	pGEX-6P
phv065	Rab11a 6-Q70L-173	Q70L mutation	pGEX-6P
phv066	CaM 1-147	calmodulin	pET28a



## Purchased cDNAs

Name	Species	Vector	Source
Myo5a neuronal	rat	EGFP – BRMV	Gift from Dr. Hüttelmeier, Marcel Osten Uni Halle (originally from Takumi)
Myo5a	mouse	pBACe3.6	RIKEN, MGI:3536088
Myo5b	human	pSlo1.0A	ImaGenes-RPCIB731A221138Q
Myo5c	human	pSlo1.1A	ImaGenes-IOH39998
Myo6	Drosophila Melanogaster	pBlueScript	Gift from C. Petritsch
Miranda	Drosophila Melanogaster	pBlueScript SW	Gift from C. Petritsch

## 4.4 Competent bacterial strains

Strain	Essential genotype	Source
XL1 Blue	<i>recA1 endA1 gyrA96 thi-1 hsdR17 supE44 relA1 lac</i> [F' <i>proAB lacIqZΔM15 Tn10</i> (Tetr)].	Invitrogen
BL21 Star (DE3)	F- <i>ompT hsdSB(rB-, mB-) gal dcm rne131</i> (DE3)	Invitrogen
B834 (DE3)	F- <i>ompT gal met r<sub>BM8</sub></i>	Novagen
DH10 Bac	F- <i>mcrA Δ(mrr-hsdRMS-mcrBC) φ80lacZΔM15 ΔlacX74 recA1 endA1 araD139 Δ(ara, leu)7697 galU galK λ-rpsL</i> nupG/bMON14272/pMON7124	Invitrogen

## 4.5 Insect cells lines

Strain	Essential genotype	Source
Sf21	Originated from ovaries of the Fall Army worm, <i>Spodoptera frugiperda</i> (used for baculovirus isolation and propagation)	Invitrogen
Sf9	Originated from ovaries of the Fall Army worm, <i>Spodoptera frugiperda</i> (used temporarily for baculovirus propagation)	Invitrogen
High Five™ Cells (BTI-TN-5B1-4)	Originated from the ovarian cells of the Cabbage Looper, <i>Trichoplusia ni</i> (used for protein expression)	Invitrogen

## 4.6 Antibodies

Name	Species	Dilution	Source
anti-HA (3F10)	rat	1:1000 / Western blot	Roche
anti-rat-IgG-HRPO	rabbit	1: 10 000 / Western blot	Abcam

## 4.7 Solutions and buffers

Medium	Composition
lysogeny broth (LB)	10g/l Bacto tryptone, 5g/l Bacto yeast extract, 5g/l NaCl, (pH 7.0 set with NaOH)
LB Agar plates	10g/l Bacto tryptone, 5g/l Bacto yeast extract, 5g/l NaCl, (pH 7.0 set with NaOH), 15g/l agar
SOC	20g/l Bacto tryptone, 5g/l Bacto yeast extract, 0.5g/l NaCl, 2.5 mM KCl, 10 mM MgCl <sub>2</sub> , 20 mM Glucose (pH 7.0 set with NaOH)
DH10 Bac	1 % (w/v) bacto tryptone, 0.5 % (w/v) bacto yeast extract, 0.5 % (w/v) NaCl, 1 M IPTG, 100 mg/l X-Gal (bromo-chloro-galactopyranoside), 7 g/l gentamycin, 10 g/l tetracycline, 50 g/l kanamycin
DH10 Bac Agar plates	1 % (w/v) bacto tryptone, 0.5 % (w/v) bacto yeast extract, 0.5 % (w/v) NaCl, 1 M IPTG, 100 mg/l X-Gal (bromo-chloro-galactopyranoside), 7 g/l gentamycin, 10 g/l tetracycline, 50 g/l kanamycin, 15g/l agar
Selenomethionine minimal	7.5 mM (NH <sub>4</sub> ) <sub>2</sub> SO <sub>4</sub> , 8.5 mM NaCl, 55 mM KH <sub>2</sub> PO <sub>4</sub> , 100 mM K <sub>2</sub> HPO <sub>4</sub> , 1 mM MgSO <sub>4</sub> , 20 mM glucose, 1 mg/l CaCl <sub>2</sub> , 1 mg/l FeCl <sub>2</sub> , 1 mg/l Thiamine, 1 mg/l Biotin, 1 μg/l trace elements as follows: Cu <sup>2+</sup> , Mn <sup>2+</sup> , Zn <sup>2+</sup> , MoO <sub>4</sub> <sup>2-</sup> , 100 mg/l amino acids: L-alanine, L-arginine, L-aspartic acid, L-cysteine, L-glutamate, L-glycine, L-histidine, L-isoleucine, L-leucine, L-lysine, L-phenylalanine, L-proline, L-serine, L-threonine, L-tyrosine, L-valine, L-selenomethionine

<sup>15</sup> N labeling – for NMR (per liter)	100 ml M9 medium (10x), 10 ml trace elements solution (100x), 20 ml 20% (w/v) glucose, 1 ml 1M MgSO <sub>4</sub> , 0.3 ml 1M CaCl <sub>2</sub> , 1 ml Thiamine (1mg/ml), 1 ml Biotin (1mg/ml)
Sf-900 III SFM (Invitrogen)	Medium for inset cell culture
HyClone (Thermo)	Medium for inset cell culture

## Supplements

Supplement	Composition	Purpose
Trace elements solution (100x), (per liter)	5g EDTA, 0.83g FeCl <sub>3</sub> x 6 H <sub>2</sub> O, 84 mg ZnCl <sub>2</sub> , 13 mg CuCl <sub>2</sub> x 2 H <sub>2</sub> O, 10 mg CoCl <sub>2</sub> x 6 H <sub>2</sub> O, 10 mg H <sub>3</sub> BO <sub>3</sub> , 1.6 mg MnCl <sub>2</sub> x 6 H <sub>2</sub> O (pH 7.5 set with HCl)	<sup>15</sup> N labeling – for NMR
M9 medium (10x), (per liter)	60 g Na <sub>2</sub> HPO <sub>4</sub> , 30 g KH <sub>2</sub> PO <sub>4</sub> , 5g NaCl, 5g <sup>15</sup> NH <sub>4</sub> Cl	<sup>15</sup> N labeling – for NMR

Antibiotics and stock solutions	Stock solution	Final concentration
Ampicilin	100 mg/ml	100 µg/ml
Gentamycin (for DH10Bac plates)	7 mg/ml	7 µg/ml
Gentamycin (for cell culture)	50 mg/ml	10 µg/ml
Kanamycin	50 mg/ml	50 µg/ml
Tetracyclin	10 mg/ml	10 µg/ml
IPTG (for cell culture induction/ DH10Bac plates)	1 M	0.25-0.3 mM/0.5 mM
X-Gal (bromo-chloro galactopyranoside)	100 mg/ml	100 µg/ml

## 4.8 Peptides used for co-crystallization

Name	Species	Sequence
12mer	human	RLLSVHDFDFEG
15mer	human	KKRLLSVHDFDFEGD

## 4.9 Software

DNA sequences comparison and alignment was performed with the NCBI database (<http://www.ncbi.nlm.nih.gov>) with the BLAST (The Basic Local Alignment Search Tool) server (Altschul, Madden et al. 1997) (<http://blast.ncbi.nlm.nih.gov/Blast.cgi>). The physical and chemical parameters of recombinant proteins as theoretical pI, molecular weight and extinction coefficients were calculated with ProtParam (Gasteiger, Hoogland et al. 2005) part of the ExPASy proteomics Server tools (<http://www.expasy.ch>). Protein sequence alignment was performed with ClustalW (Thompson, Gibson et al. 2002), Superposition with COOT (Emsley, Lohkamp et al. 2010), calculation and representation of the electrostatic surface, images of the crystal structures were done with Chimera (Pettersen, Goddard et al. 2004), and Swiss PDB Viewer (Guex and Peitsch 1997) and Pymol (The PyMOL Molecular Graphics System), structure superpositions with SSM (Krissinel and Henrick 2004).

### **Electron microscopy density fitting**

Initial docking of Myo5a GD crystal structure into the EM density was done with Chimera. Dr. Thomas Becker (Gene Center, Germany) performed molecular dynamics flexible fitting (MDFF) (Trabuco, Villa et al. 2008).

## **4.10 Molecular biology**

### **Standard molecular cloning methods**

Cloning techniques were performed according to standard protocols of Sambrook and Russel, 2000 (Sambrook and Russell 2000). Polymerase chain reaction (PCR) was used for DNA fragments amplification. Point mutations or mutations and deletions of gene fragments were generated with PCR. DNA fragments and vectors were analyzed by agarose gel electrophoresis, digest by DNA restriction enzymes and ligated. All restriction enzymes were used with supplied buffers according to manufacturer's protocol.

The agarose gels were stained with ethidium bromide, later only with GelRed (Biotium). The plasmid DNA was transformed into chemically competent *E. coli* cells (XL1 Blue) and selected on LB agar plates with the respective antibiotic. Single colony was used to inoculate a 5 ml LB medium with antibiotics and cultivated over night at 37°C. The plasmid or fragment DNA isolation and purification was performed with purchased kits (NucleoSpin-Plasmid / Nucleospin-Extract II, both from Macherey-Nagel, Düren, Germany). DNA sequence was validated by sequencing at Eurofins MWG Operon (Ebersberg, Germany). The plasmid DNA and DNA fragments were stored at -20°C.

For baculovirus expression, the Bac-to-Bac system protocol was followed (Invitrogen). Cloning techniques used for bacmid DNA from *E. coli* DH10 Bac cells are the same as described for plasmid DNA from XL1 Blue *E. coli* cells.

In brief, the DH10 Bac cells were transformed and selected according to the Bac-to-Bac protocol. The DNA plasmids were isolated with isopropanol precipitation and stored at 4°C, freezing was avoided.

## **4.11 Protein Expression**

### **4.11.1 Recombinant protein expression in *E.coli***

Gene of interest was cloned into pGEX-6P-1, pET28a, or pETM40 vector and expressed in *E. coli* BL21 (DE3) Star. Typically, single colony was used to inoculate a 30 ml LB medium and cultivated at 37°C. All used medium was supplemented with appropriate antibiotics (and addition of 2g/l glucose for expression of MBP-tagged proteins). After 4-6 hours the 30 ml of LB medium was transferred to a 3 L LB media. The cell culture was grown at 37 °C to an OD<sub>600</sub> of 0.3-0.4 and cooled down to 18 °C. At OD<sub>600</sub> of 0.5-0.6, the protein expression was induced by addition of 0.25 mM Isopropyl-β-D-thiogalactopyranosid (IPTG). The cells were grown at 140 rpm over night and harvested by centrifugation (15 min, 3500 g) at 4 °C. The pellets were resuspended in the appropriate buffer, flash frozen in liquid nitrogen and stored at -80°C.

### **4.11.2 Recombinant protein expression in insect cells (Myo5a HMM)**

Initially, sf9 cells were used, but later sf21 proved to be more efficient and easier to propagate. These cells were transfected with 1-2 µg bacmid DNA (Myo5a HMM 1-1105-GCN4, with calmodulin in pFastBac Dual or essential light chains in pFastBac 1) at the density of 0.4 x 10<sup>6</sup> cells/ml. For transfection, 2 x 2 ml of sf21 cells were incubated with FuGENE HD transfection reagent (Roche) and the bacmid DNA for four or five days at 27.5°C without shaking. After four days, the cells mostly displayed signs of infection. The supernatant (P0, 4 ml) was removed and cultivated with 10 ml sf21 cells at the density of 1.4 x 10<sup>6</sup> cells/ml. The cells were incubated at 27.5°C with shaking 95 rpm. After four days, the supernatant (P1) was harvested at 2000 g, sterile filtered and 2 ml were used for a large-scale infection of 500 ml sf 21 cells at the density of 0.4 x 10<sup>6</sup> cells/ml. After another four days, the supernatant (P2) was harvested at 2000 g and sterile filtered. The virus stocks were stored at 4°C. For expression, 500 ml *Spodoptera frugiperda* High Five (Hi5) cells at the density of 1.0 x 10<sup>6</sup> cells/ml were infected with 20-30 ml P2 virus stock of both viruses. The cells were incubated for three or four days at 27.5°C with shaking at 95 rpm.

## **4.12 Protein purification**

### **4.12.1 Protein fragments purification with 6xHis tag**

Typical purification protocol for Rab11a (6-173, with Q70L mutation), Myo6 (913-1236) and all mutations, Miranda and other protein fragments with 6xHis tag. All purification steps were carried out at 4 °C. After addition of Roche complete protease inhibitor tablet and 10 mM PMSF to the lysis buffer containing 200 mM NaCl, 50 mM Tris pH 7.5, and 0.1%  $\beta$ -ME the cells were disrupted by sonication and centrifuged for 45 min, 27000 g at 4°C. The supernatant was loaded on a pre-equilibrated Ni-NTA FF 5 ml column (GE Healthcare). The column was washed with 20-column volume of lysis buffer. Unless stated otherwise, the fusion protein was eluted from the column with 5 column volumes of elution buffer (200 mM NaCl, 25 mM Tris pH 7.5, 200 mM imidazole). The proteins were further purified by ion exchange and prior size exclusion chromatography, the protein was concentrated using a centrifugal filter device (Amicon Ultra, Millipore, Billerica, USA), and centrifuged (30 min, 13 000 rpm, 16 000 g, 4 °C). The final buffer contained 50 mM Hepes pH 7.5, 200 mM NaCl, and 0.1%  $\beta$ -ME (Myo6 (913-1236)), 10 mM Tris pH 7.0, 0.1%  $\beta$ -ME (Mir (1-830)), 25 mM Tris pH 8, 100 mM NaCl, 15 mM imidazole, 2 mM  $MgCl_2$ , 0.1 %  $\beta$ ME ((Rab11a (6-173, with Q70L mutation))).

### **4.12.2 Purification of fragments with GST-tag**

Globular domain (GD) fragments of human Myo5a (1467-1855), Myo5b (1462-1849), Myo5c (1355-1742), the Griscelli mutant GD of Myo5a, Rab27a and other fragments with GST tag were purified as described for 6x His-tagged proteins, but with a Glutathione FF column (GE Healthcare). The lysis buffer contained 0.5 M NaCl, 50 mM Tris pH 7.5, and 2 mM DTT. On the column, the bound GST-tagged proteins were additionally washed with high-salt buffer (50 mM Tris pH 7.0 (or pH 7.5 for Myo5b GD and Myo5c GD), 1 M NaCl, and 2 mM DTT). Unless stated otherwise, GST was cleaved by 50  $\mu$ g PreScission Protease (GE healthcare, Munich, Germany) and removed, and the proteins were purified by ion exchange

and size exclusion chromatography. The final buffer contained 50 mM Tris pH 7.0 (or pH 7.5 for Myo5b GD and Myo5c GD), 140 mM NaCl and 2 mM DTT.

#### **4.12.3 Purification of fragments with MBP-tag**

The MBP-fusion proteins (Mlph fragments) were purified as described for 6xHis-tag proteins, but the clear lysate was incubated for 1 h with 1-2 ml amylose resins. The resin was washed with 150 ml wash buffer (20 mM Tris pH 7.5, 200 mM NaCl). The protein was eluted with 10 ml elution buffer (20 mM Tris pH 7.5, 200 mM NaCl, 1 mM EDTA, 10 mM maltose) into 15 ml wash buffer. The fusion protein was further purified as described for other proteins.

#### **4.12.4 Purification and crystallization of the protein complexes**

The procedure of purification and crystallization was similar for following proteins: Mlph-Rab27a complex, Mlph-EB1 complex, Myo5a-Mlph complex, Myo5a-Mlph peptide complex, Myo5a-Rab11a complex.

After co-expression and purification, the proteins were applied to a size exclusion column (Superdex S200 16/60), concentrated using a centrifugal filter device (Amicon Ultra, Millipore, Billerica, USA), and centrifuged (20 min, 13 000 rpm, 16 000 g, 4 °C). The protein complex was analyzed by SDS-PAGE. The initial screens were set up with robot (Hydra II system; Thermo Scientific) in a 96 well plate format. 500 nl of protein and 500 nl of reservoir solution was mixed in a sitting drop and incubated over 80 µl of precipitant solution in reservoir (common crystallization screens, for example Index I from Hampton Research). Promising conditions from initial screens were refined. For further refinement, 1 µl of protein and 1 µl of reservoir solution were mixed in a sitting drop and incubated over 0.5 ml of reservoir solution. For these refinements, 24 well plate format for hanging drop vapor diffusion was used. The plates were incubated at 4 or 18°C.

#### **4.12.5 Purification of Myo5a HMM**

The cells were pelleted for 10 min at 2000 g at 5°C and resuspended in 50 ml lysis buffer (20 mM Imidazol pH 7.5, 200 mM NaCl, 5 mM MgCl<sub>2</sub>, 1 mM EDTA, 1

mM EGTA, 7% sacharose, 1 mM PMSF, and 2mM DTT). The Flag-tagged murine Myo5a HMM with essential light chains and calmodulins was purified according to standard protocols. To unbind myosin from actin, ATP concentration was 3 mM during purification, the protein was kept at 5°C during the whole purification. Briefly, the cell extract was incubated for 3 hrs with agarose Flag beads, washed with (20 mM imidazol pH 7.5, 150 mM KCl, 5 mM MgCl<sub>2</sub>, 1 mM EDTA, 1 mM EGTA, 1 mM PMSF, and 2mM DTT) and eluted with 0.5 mg Flag peptide. The eluted protein was dialyzed over night (10 mM imidazol pH 7.5, 50 mM KCl, 2 mM MgCl<sub>2</sub>, 1 mM EGTA, and 2 mM DDT) and stored in 50 % glycerol at -20 °C.

#### **4.12.6 Selenomethionine-substituted Myo5a GD expression and purification**

Selenomethionine-substituted Myo5a GD was expressed in methionine auxotrophic *E. coli* strain B834 (DE3) grown in selenomethionine containing minimal medium. The recombinant fragment was purified as the native Myo5a GD, but in presence of 20 mM DTT.

#### **4.12.7 Purification of calmodulin**

Murine (amino acid sequence identical with human) calmodulin was cloned into pET28a with NcoI and NheI for expression without a tag. After expression in *E. coli*, the protein was purified with HiTrap Phenyl sepharose (GE Healthcare) and size exclusion chromatography column.

#### **4.12.8 Purification of actin**

Actin was purified from frozen rabbit muscle acetone powder (Sigma-Aldrich, M6890) using standard protocols (Lehrer and Kerwar 1972). Actin was kept at 5°C during the purification. 5g of rabbit muscle was cut into pieces with scalpel, crushed in a mortar and extracted 6 times with ca. 50 ml G-buffer (2 mM Tris pH 8, 0.2 mM CaCl<sub>2</sub>, 0.2 mM ATP, and 0.5 mM DTT) and then stirred for 20-30 min. The solution was each time filtered with Gaze Compress (Hartmann).

The first filtrate was discarded. The flow thru from other filtrates was collected up to ca. 240 ml and cleared by a ultracentrifugation: rotor Ti 45, 41 krpm, 30 min, 4°C. Supernatant was collected and 800 mM KCl, 2 mM MgCl<sub>2</sub>, 0.5 mM DTT, and 1 mM ATP was added (F-buffer - final concentrations). pH 8 was adjusted with KOH. Actin was let to polymerize over night under slow stirring at 4°C.

On next day, the polymerized actin was pelleted: Rotor 45 Ti, 41 krpm, 3h, 4°C. The pellets were washed with G-buffer and than resuspended in the G-buffer using a dounce homogenizer (Braun Melsungen AG). The actin was dialyzed for 4 hrs against 1L of G-buffer and than over night in another 1L. On next day, the solution was ultracentrifuged: Rotor Ti 70.1, 44 krpm, 2h, 4°C and the supernatant with pure F-actin was collected. Polymerized F-actin was stabilized with phalloidin and in aliquots shock frozen in liquid nitrogen and stored at -80°C.

#### **4.12.9 Protein analysis**

Protein samples were analyzed by 8-17% SDS-PAGE as described by Laemmli (Laemmli 1970) in a Mini-Protean 3 System (Bio-Rad, München, Germany). After separation, gels were stained with Coomassie solution (0.2% Coomassie Brilliant blue R-250, 50% (v/v) ethanol, 7% (v/v) acetic acid).

Peptide array membrane was incubated over night (4°C, BSA-MySp buffer: 5% BSA, 20 mM Hepes pH 7.5, 125 mM NaCl, 1 mM DTT). The membrane was washed with MySp buffer: 20 mM Hepes pH 7.5, 125 mM NaCl, 1 mM DTT and incubated for 2 hr at 4°C with protein (50 µM HA-Myo5a GD), washed three times (MySp buffer) and incubated with the primary antibody (1 hr, 4°C, diluted in BSA-MySp). After washing (three times with MySp buffer), the membrane was incubated 1 hr at RT with the secondary antibody (BSA-MySp buffer). After washing (three times with MySp buffer), the bound secondary antibody was visualized with an ECL kit (Pierce, Thermo Scientific). The exposed film (GE Healthcare) was developed in a Kodak M35 developing machine.



## **4.13 Biochemistry**

### **4.13.1 Pull down assay Myo6 and Miranda**

His-Myo6 (913 -1256) and MBP-Miranda (1-298), 50 µg each were preincubated for 10 min and then for another 10 min with 50 µl amylose resins. The buffer was: 25 mM Tris pH 7.5, 200 mM NaCl, and 1 mM DTT. The reaction was washed 5 times with 200 µl of this buffer, except of the last wash step, which was 50 µl buffer. For visualization 1/10 of the input, 1/5 of the last wash step, and 1/10 of the eluted fraction were analyzed with SDS-PAGE and Coomassie staining.

### **4.13.2 Pull down assay Myo5a, Myo5b, Myo5c, and Rab11a**

Myosin fragments with no tag: Myo5a (1467-1855), Myo5b (1462-1849), and Myo5c (1355-1742) GD (50 µg) and 5-fold excess of 6 x His-tagged Rab11a were used in this assay. The proteins were incubated with 50 µl of Ni-Sepharose for 1 h in wash buffer (20 mM Tris pH 7.4, 140 mM NaCl, 2 mM MgCl<sub>2</sub>, 20 mM imidazole, and 0.1 % β-ME). Sepharose was washed five times with 200 µl of wash buffer followed by a wash step with 50 µl. Proteins were eluted with 50 µl wash buffer containing 750 mM imidazole. For visualization, 1/10 of the input, 1/5 of the final wash, and 1/5 of the eluted fraction was analyzed by SDS-PAGE and Coomassie staining.

### **4.13.3 Crystallization of Myo5a GD**

Crystals of Myo5a GD (1467-1855) were grown at 18°C by hanging-drop vapor-diffusion using 1:1 mixture of protein (1 mg/ml) and crystallization solution containing 0.112-0.125 M succinic acid pH 7.0, 16-18 % PEG 3350 for native crystals and 100 mM MES pH 5.5, 6 % dioxane, 1.45 M (NH<sub>4</sub>)<sub>2</sub>SO<sub>4</sub>, 10 mM DTT for selenomethionine (SeMet) substituted crystals. After several rounds of optimization and refinement, crystals appeared within 2-3 days. Native crystals were cryoprotected in 10% ethylene glycol, SeMet crystals in 20% glycerol. The datasets were recorded from a single crystal at the following beamlines: Myo5a Native at ID14-1 and Myo5a SeMet-substituted at ID14-4, both at the European

Synchrotron Radiation Facility. Wavelengths of data collection for Myo5a are shown in Table 2.5.

#### **4.13.4 Crystallization of Myo5b GD**

Crystals of Myo5b were grown at 18°C by hanging-drop vapor-diffusion using 1:1 mixture of protein (0.8 mg/ml) and crystallization solution containing 50 mM Tris pH 7.0, 200 mM succinic acid and cryoprotected with 25 % glycerol. Dataset was recorded from a single crystal at the beamline ID23-1 at the European Synchrotron Radiation Facility. The dataset was collected at the wavelengths of 0.9778Å.

#### **4.13.5 Myo5a GD structure determination**

Datasets were integrated and scaled using XDS (Kabsch 2010) and Scala (1994). Since attempts to solve the crystal structure of Myo5a GD by molecular replacement with yeast homologs (Myo2p, PDB-ID: 2F6H or Myo4p PDB-ID: 3MMI) as templates failed, the structure was solved by single-wavelength anomalous dispersion (SAD). 84 selenium atoms were located using hkl2map/SHELXD program (Sheldrick et al. 2010), phases to 2.5 Å obtained with SHARP (Bricogne, Vonrhein et al. 2003). After partial automatic model building with Arp/wARP (Langer, Cohen et al. 2008), further manual model building was carried out with COOT (Emsley, Lohkamp et al. 2010). The model was later extended to 2.2 Å resolution with Phaser molecular replacement (Mc Coy et al. 2007). Refinement was performed using Phenix (Adams, Afonine et al. 2011). The final model was analyzed using SFCHECK (1994).

#### **4.13.6 Myo5b GD structure determination**

The structure of Myo5b GD was solved by Phaser molecular replacement (Mc Coy et al. 2007) with the Myo5a GD structure as template and a native dataset with a resolution of 3.1 Å. The manual model building was carried out with COOT (Emsley, Lohkamp et al. 2010). Refinement was performed using Phenix (Adams, Afonine et al. 2011). The final model was analyzed using SFCHECK (1994).

#### **4.13.7 Homology model of Myo5c GD**

Amino acid sequence alignment with ClustalW (Thompson, Gibson et al. 2002) was performed with globular tail of human myosin 5a (1467-1855) and 5b (1462-1849), and Myo5c (1355-1742). The alignment was modified manually according to the solved crystal structures. The atomic model of Myo5c GD (1355-1742) (Figure 2.17 A) was calculated using the program Modeller 9v7 (Sali and Blundell 1993).

#### **4.13.8 ATPase assay**

Actin-activated MgATPase assays were measured according to (Li, Jung et al. 2008) with 20 mM MOPS-KOH pH 7.0, 100 mM NaCl, 10 U/ml lactate dehydrogenase, 7.2 U/ml pyruvate kinase, 1.2 mM NADH, 2 mM PEP, 2 mM  $MgCl_2$ , 40-100 nM Myo5a HMM, 10  $\mu$ M GST-Myo5a GD/ GST-Myo5b GD/ GST-Myo5c GD, 10  $\mu$ M GST-Myo5a GD (loop I  $\Delta$ 6 aa), 10  $\mu$ M GST-Myo5a GD (loop I  $\Delta$ 9 aa), 10  $\mu$ M GST-Myo5a GD (loop II gly), 10  $\mu$ M GST-Myo5a GD (K1708A), 10-30  $\mu$ M Rab11a, 10  $\mu$ M actin, 1 mM ATP at 25°C. The system of enzymes (lactate dehydrogenase / pyruvate kinase) regenerates hydrolyzed ATP under nicotinamide adenine dinucleotide (NADH) consumption. The NADH decomposition is proportional to the decrease of absorbance (340 nm) and thus the ATP consumption.

#### **4.13.9 Small-angle X-ray scattering (SAXS)**

SAXS measurements were carried out at beamline ID 14-3 (European Synchrotron Radiation Facility, France), at a wavelength of 0.931 Å. Various concentrations of protein samples (from 1.1 to 14 mg/ml) in 50 mM Tris pH 7.0 (or pH 7.5 for Myo5b and Myo5c GD), 140 mM NaCl and 2 mM DTT were exposed 10 times for 30 s at 293 K. Each data trace was subjected to a linear fit in the Guinier region ( $Q^2 < 0.013 \text{ Å}^{-2}$ ) to determine the values of the slope ( $-R_g^2/3$ ) and the y intersection  $\{\ln[I(0)]\}$ . Intrinsic values of  $I(0)/\text{concentration}$  and  $R_g$  were estimated by linear extrapolation to zero concentration. Using a reference of bovine serum albumin, the scattering intensities were extrapolated to zero angle

$I(0)$ . SAXS data were analyzed with the software package ATSAS 2.1 (Konarev, Petoukhov et al. 2006). The pair correlation function  $P(r)$  was calculated using the GNOM program package. Bead *ab initio* models were calculated with GASPORp (Svergun, Petoukhov et al. 2001) and averaged with DAMAVER (Volkov and Svergun 2003). The  $P(r)$  functions of the model were obtained from the crystal structures were calculated using CRY SOL and GNOM (Svergun, Barberato et al. 1995).

## 5. ABBREVIATIONS

%	per cent
°C	degree Celsius
β-ME	β-mercaptoethanol
μ	micro
σ	sigma
A (Ala)	alanine
Å	Ångström
A <sub>280</sub> , A <sub>260</sub>	absorption at wavelength 260 nm/ 280 nm
aa	amino acid
ADP	adenosine diphosphate
ATP	adenosine triphosphate
BSA	bovine serum albumin
C (Cys)	cysteine
C-terminal	carboxy-terminal
CaM	calmodulin
CBD	cargo binding domain
D (Asp)	aspartic acid
Da	Dalton
deg	degree
dm, <i>D. melanogaster</i>	<i>Drosophila melanogaster</i>
DNA	deoxyribonucleic acid
E (Glu)	glutamic acid
<i>E. coli</i>	<i>Escherichia coli</i>
EM	electron microscopy
EDTA	ethylenediaminetetraacetic acid
F (Phe)	phenylalanine
F-actin	filamentous actin
for	forward
g	gram / standard acceleration
G (Gly)	glycine
G-actin	globular actin
GD	globular domain
GFP	Green Fluorescence Protein
GST	glutathione S-transferase
h	hour / human
H / H (His)	helix / histidine
HEPES	hydroxyethyl piperazineethanesulfonic acid
HMM	Myo5a fragment (without GD)
I (Ile)	isoleucine
K (Lys)	lysine
k	kilo
Kan	kanamycin
K <sub>d</sub>	equilibrium-dissociation constants
KHC	kinesin heavy chain
KIF	kinesin, member of superfamily protein
l	litre
L (Leu)	leucine
LB	lysogeny broth
m	milli / meter
M / M (Met)	molar / methionine
MBP	maltose-binding protein
MES	2-(N-morpholino)ethanesulfonic acid
min	minutes
Mlph	melanophilin / Slac2-a
Myo5a	myosin 5a
Myo5b	myosin 5b
Myo5c	myosin 5c
n	nano

N (Asn)	asparagine
N-terminal	amino-terminal
NaCl	sodium chloride
NADH	nicotineamid adenine dinucleotide
Ni-NTA	nickel-nitrilotriacetic acid
NMR	nuclear magnetic resonance
NOESY	Nuclear Overhauser Effect Spectroscopy
OD <sub>600</sub>	Optical density at 600 nm
P (Pro)	proline
PAGE	polyacrylamide gel electrophoresis
PCR	polymerase chain reaction
PEG	polyethylene glycol
pH	potentia hydrogenii
PMSF	phenylmethanesulphonylfluoride
Q (Gln)	glutamine
R (Arg)	arginine
Rab11a-FIP2	Rab11 family-interacting protein 2
rev	reverse
RMSD	root mean square deviation
RNA	ribonucleic acid
rpm	revolutions per minute
RT	room temperature
s	second
S (Ser)	serine / Svedberg
<i>S. cerevisiae</i>	<i>Sacharomyces cerevisiae</i>
SAD	single anomalous diffraction
SAXS	small angle X-ray scattering
SDS	sodium dodecyl sulfate
SeMet	selenomethionine
T (Thr)	threonine
TIRF	total internal reflection fluorescence
TRIS	tris-(hydroxymethyl)-aminomethane
V (Val)	valine
W (Trp)	tryptophan
wt	wild type
w/v	weight per volume
x-gal	5-bromo-4-chloro-indolyl galactopyranoside
Y (Tyr)	tyrosine

## 6. REFERENCES

- Adams, P. D., P. V. Afonine, et al. (2011). "The Phenix software for automated determination of macromolecular structures." *Methods* 55(1): 94-106.
- Akhmanova, A. and J. A. Hammer, 3rd (2010). "Linking molecular motors to membrane cargo." *Curr Opin Cell Biol* 22(4): 479-487.
- Altschul, S. F., T. L. Madden, et al. (1997). "Gapped BLAST and PSI-BLAST: a new generation of protein database search programs." *Nucleic Acids Res* 25(17): 3389-3402.
- Avraham, K. B., T. Hasson, et al. (1995). "The mouse Snell's waltzer deafness gene encodes an unconventional myosin required for structural integrity of inner ear hair cells." *Nat Genet* 11(4): 369-375.
- Bahloul, A., G. Chevreux, et al. (2004). "The unique insert in myosin VI is a structural calcium-calmodulin binding site." *Proc Natl Acad Sci U S A* 101(14): 4787-4792.
- Berg, J. S., B. C. Powell, et al. (2001). "A millennial myosin census." *Mol Biol Cell* 12(4): 780-794.
- Bernado, P., E. Mylonas, et al. (2007). "Structural characterization of flexible proteins using small-angle X-ray scattering." *J Am Chem Soc* 129(17): 5656-5664.
- Bienz, M. (2001). "Spindles cotton on to junctions, APC and EB1." *Nat Cell Biol* 3(3): E67-68.
- Bricogne, G., C. Vonrhein, et al. (2003). "Generation, representation and flow of phase information in structure determination: recent developments in and around SHARP 2.0." *Acta Crystallogr D Biol Crystallogr* 59(Pt 11): 2023-2030.
- Bu, W. and L. K. Su (2001). "Regulation of microtubule assembly by human EB1 family proteins." *Oncogene* 20(25): 3185-3192.
- CCP4 (1994). "The CCP4 suite: programs for protein crystallography." *Acta Crystallogr D Biol Crystallogr* 50(Pt 5): 760-763.
- Chen, X., A. K. Walker, et al. (2006). "Organellar proteomics: analysis of pancreatic zymogen granule membranes." *Mol Cell Proteomics* 5(2): 306-312.
- Cheney, R. E., M. K. O'Shea, et al. (1993). "Brain myosin-V is a two-headed unconventional myosin with motor activity." *Cell* 75(1): 13-23.
- Coppola, T., V. Perret-Menoud, et al. (1999). "Disruption of Rab3-calmodulin interaction, but not other effector interactions, prevents Rab3 inhibition of exocytosis." *EMBO J* 18(21): 5885-5891.
- Costa, M. C., F. Mani, et al. (1999). "Brain myosin-V, a calmodulin-carrying myosin, binds to calmodulin-dependent protein kinase II and activates its kinase activity." *J Biol Chem* 274(22): 15811-15819.
- Desnos, C., S. Huet, et al. (2007). "'Should I stay or should I go?': myosin V function in organelle trafficking." *Biol Cell* 99(8): 411-423.
- Diekmann, Y., E. Seixas, et al. (2011). "Thousands of rab GTPases for the cell biologist." *PLoS Comput Biol* 7(10): e1002217.

- Dzijak, R., S. Yildirim, et al. (2012). "Specific nuclear localizing sequence directs two myosin isoforms to the cell nucleus in calmodulin-sensitive manner." *PLoS One* 7(1): e30529.
- Emsley, P., B. Lohkamp, et al. (2010). "Features and development of Coot." *Acta Crystallogr D Biol Crystallogr* 66(Pt 4): 486-501.
- Espindola, F. S., S. R. Banzi, et al. (2008). "Localization of myosin-Va in subpopulations of cells in rat endocrine organs." *Cell Tissue Res* 333(2): 263-279.
- Espreafico, E. M., D. E. Coling, et al. (1998). "Localization of myosin-V in the centrosome." *Proc Natl Acad Sci U S A* 95(15): 8636-8641.
- Estrada, P., J. Kim, et al. (2003). "Myo4p and She3p are required for cortical ER inheritance in *Saccharomyces cerevisiae*." *J Cell Biol* 163(6): 1255-1266.
- Fan, G. H., L. A. Lapierre, et al. (2004). "Rab11-family interacting protein 2 and myosin Vb are required for CXCR2 recycling and receptor-mediated chemotaxis." *Mol Biol Cell* 15(5): 2456-2469.
- Farnsworth, C. C., M. Kawata, et al. (1991). "C terminus of the small GTP-binding protein smg p25A contains two geranylgeranylated cysteine residues and a methyl ester." *Proc Natl Acad Sci U S A* 88(14): 6196-6200.
- Fujiwara, T., S. Suzuki, et al. (2006). "Mapping a nucleolar targeting sequence of an RNA binding nucleolar protein, Nop25." *Exp Cell Res* 312(10): 1703-1712.
- Fukuda, M. and T. S. Kuroda (2004). "Missense mutations in the globular tail of myosin-Va in dilute mice partially impair binding of Slac2-a/melanophilin." *J Cell Sci* 117(Pt 4): 583-591.
- Fukuda, M., T. S. Kuroda, et al. (2002). "Slac2-a/melanophilin, the missing link between Rab27 and myosin Va: implications of a tripartite protein complex for melanosome transport." *J Biol Chem* 277(14): 12432-12436.
- Gasteiger, E., C. Hoogland, et al. (2005). "Protein Identification and Analysis Tools on the ExPASy Server;" *The Proteomics Protocols Handbook*, Humana Press (2005): 571-607.
- Geething, N. C. and J. A. Spudich (2007). "Identification of a minimal myosin Va binding site within an intrinsically unstructured domain of melanophilin." *J Biol Chem* 282(29): 21518-21528.
- Griscelli, C., A. Durandy, et al. (1978). "A syndrome associating partial albinism and immunodeficiency." *Am J Med* 65(4): 691-702.
- Griscelli, C. and M. Prunieras (1978). "Pigment dilution and immunodeficiency: a new syndrome." *Int J Dermatol* 17(10): 788-791.
- Guex, N. and M. C. Peitsch (1997). "SWISS-MODEL and the Swiss-PdbViewer: an environment for comparative protein modeling." *Electrophoresis* 18(15): 2714-2723.
- Haarer, B. K., A. Petzold, et al. (1994). "Identification of MYO4, a second class V myosin gene in yeast." *J Cell Sci* 107 ( Pt 4): 1055-1064.
- Hales, C. M., R. Griner, et al. (2001). "Identification and characterization of a family of Rab11-interacting proteins." *J Biol Chem* 276(42): 39067-39075.
- Hales, C. M., J. P. Vaerman, et al. (2002). "Rab11 family interacting protein 2 associates with Myosin Vb and regulates plasma membrane recycling." *J Biol Chem* 277(52): 50415-50421.
- Hammer, J. A., 3rd and J. R. Sellers (2012). "Walking to work: roles for class V myosins as cargo transporters." *Nat Rev Mol Cell Biol* 13(1): 13-26.



- Hammer, J. A., 3rd and X. S. Wu (2002). "Rabs grab motors: defining the connections between Rab GTPases and motor proteins." *Curr Opin Cell Biol* 14(1): 69-75.
- Hasson, T. and M. S. Mooseker (1994). "Porcine myosin-VI: characterization of a new mammalian unconventional myosin." *J Cell Biol* 127(2): 425-440.
- Heuck, A., T. G. Du, et al. (2007). "Monomeric myosin V uses two binding regions for the assembly of stable translocation complexes." *Proc Natl Acad Sci U S A* 104(50): 19778-19783.
- Heuck, A., I. Fetka, et al. (2010). "The structure of the Myo4p globular tail and its function in ASH1 mRNA localization." *J Cell Biol* 189(3): 497-510.
- Holm, L., S. Kaariainen, et al. (2008). "Searching protein structure databases with DaliLite v.3." *Bioinformatics* 24(23): 2780-2781.
- Huang, J. D., M. J. Cope, et al. (1998). "Molecular genetic dissection of mouse unconventional myosin-VA: head region mutations." *Genetics* 148(4): 1951-1961.
- Huang, J. D., V. Mermall, et al. (1998). "Molecular genetic dissection of mouse unconventional myosin-VA: tail region mutations." *Genetics* 148(4): 1963-1972.
- Huls, D., Z. Storchova, et al. (2012). "Post-translational modifications regulate assembly of early spindle orientation complex in yeast." *J Biol Chem* 287(20): 16238-16245.
- Hume, A. N., A. K. Tarafder, et al. (2006). "A coiled-coil domain of melanophilin is essential for Myosin Va recruitment and melanosome transport in melanocytes." *Mol Biol Cell* 17(11): 4720-4735.
- Ikebe, M., S. Hinkins, et al. (1983). "Correlation of enzymatic properties and conformation of smooth muscle myosin." *Biochemistry* 22(19): 4580-4587.
- Ikebe, M., X. D. Li, et al. (2005). "Conformational change and regulation of myosin molecules." *Adv Exp Med Biol* 565: 61-72; discussion 72, 359-369.
- Ishikawa, T. (2012). "Structural biology of cytoplasmic and axonemal dyneins." *J Struct Biol*.
- Jacobs, D. T., R. Weigert, et al. (2009). "Myosin Vc is a molecular motor that functions in secretory granule trafficking." *Mol Biol Cell* 20(21): 4471-4488.
- Jagoe, W. N., S. R. Jackson, et al. (2006). "Purification, crystallization and preliminary X-ray diffraction studies of Rab11 in complex with Rab11-FIP2." *Acta Crystallogr Sect F Struct Biol Cryst Commun* 62(Pt 7): 692-694.
- Jagoe, W. N., A. J. Lindsay, et al. (2006). "Crystal structure of rab11 in complex with rab11 family interacting protein 2." *Structure* 14(8): 1273-1283.
- Jansen, R. P., C. Dowzer, et al. (1996). "Mother cell-specific HO expression in budding yeast depends on the unconventional myosin myo4p and other cytoplasmic proteins." *Cell* 84(5): 687-697.
- Johnston, G. C., J. A. Prendergast, et al. (1991). "The *Saccharomyces cerevisiae* MYO2 gene encodes an essential myosin for vectorial transport of vesicles." *J Cell Biol* 113(3): 539-551.
- Kaan, H. Y., D. D. Hackney, et al. (2011). "The structure of the kinesin-1 motor-tail complex reveals the mechanism of autoinhibition." *Science* 333(6044): 883-885.
- Kabsch, W. (2010). "Xds." *Acta Crystallogr D Biol Crystallogr* 66(Pt 2): 125-132.

- Kabsch, W., H. G. Mannherz, et al. (1990). "Atomic structure of the actin:DNase I complex." *Nature* 347(6288): 37-44.
- Karcher, R. L., J. T. Roland, et al. (2001). "Cell cycle regulation of myosin-V by calcium/calmodulin-dependent protein kinase II." *Science* 293(5533): 1317-1320.
- Kellerman, K. A. and K. G. Miller (1992). "An unconventional myosin heavy chain gene from *Drosophila melanogaster*." *J Cell Biol* 119(4): 823-834.
- Konarev, P. V., M. V. Petouhkov, et al. (2006). "ATSAS2.1, a program package for small-angle scattering data analysis." *J Appl Cryst* 39: 277-286.
- Korinek, W. S., M. J. Copeland, et al. (2000). "Molecular linkage underlying microtubule orientation toward cortical sites in yeast." *Science* 287(5461): 2257-2259.
- Krendel, M. and M. S. Mooseker (2005). "Myosins: tails (and heads) of functional diversity." *Physiology* (Bethesda) 20: 239-251.
- Krissinel, E. and K. Henrick (2004). "Secondary-structure matching (SSM), a new tool for fast protein structure alignment in three dimensions." *Acta Crystallogr D Biol Crystallogr* 60(Pt 12 Pt 1): 2256-2268.
- Kudryashov, D. S., M. R. Sawaya, et al. (2005). "The crystal structure of a cross-linked actin dimer suggests a detailed molecular interface in F-actin." *Proc Natl Acad Sci U S A* 102(37): 13105-13110.
- Kukimoto-Niino, M., A. Sakamoto, et al. (2008). "Structural basis for the exclusive specificity of Slac2-a/melanophilin for the Rab27 GTPases." *Structure* 16(10): 1478-1490.
- Kuroda, T. S., H. Ariga, et al. (2003). "The actin-binding domain of Slac2-a/melanophilin is required for melanosome distribution in melanocytes." *Mol Cell Biol* 23(15): 5245-5255.
- Langer, G., S. X. Cohen, et al. (2008). "Automated macromolecular model building for X-ray crystallography using ARP/wARP version 7." *Nat Protoc* 3(7): 1171-1179.
- Lansbergen, G. and A. Akhmanova (2006). "Microtubule plus end: a hub of cellular activities." *Traffic* 7(5): 499-507.
- Lapierre, L. A., R. Kumar, et al. (2001). "Myosin vb is associated with plasma membrane recycling systems." *Mol Biol Cell* 12(6): 1843-1857.
- Legesse-Miller, A., S. Zhang, et al. (2006). "Regulated phosphorylation of budding yeast's essential myosin V heavy chain, Myo2p." *Mol Biol Cell* 17(4): 1812-1821.
- Lehrer, S. S. and G. Kerwar (1972). "Intrinsic fluorescence of actin." *Biochemistry* 11(7): 1211-1217.
- Li, Q. and S. K. Sarna (2009). "Nuclear myosin II regulates the assembly of preinitiation complex for ICAM-1 gene transcription." *Gastroenterology* 137(3): 1051-1060, 1060 e1051-1053.
- Li, X. D., R. Ikebe, et al. (2005). "Activation of myosin Va function by melanophilin, a specific docking partner of myosin Va." *J Biol Chem* 280(18): 17815-17822.
- Li, X. D., H. S. Jung, et al. (2006). "The globular tail domain of myosin Va functions as an inhibitor of the myosin Va motor." *J Biol Chem* 281(31): 21789-21798.

- Li, X. D., H. S. Jung, et al. (2008). "The globular tail domain puts on the brake to stop the ATPase cycle of myosin Va." *Proc Natl Acad Sci U S A* 105(4): 1140-1145.
- Li, X. D., K. Mabuchi, et al. (2004). "Ca<sup>2+</sup>-induced activation of ATPase activity of myosin Va is accompanied with a large conformational change." *Biochem Biophys Res Commun* 315(3): 538-545.
- Lindsay, A. J. and M. W. McCaffrey (2009). "Myosin Vb localises to nucleoli and associates with the RNA polymerase I transcription complex." *Cell Motil Cytoskeleton* 66(12): 1057-1072.
- Liu, J., D. W. Taylor, et al. (2006). "Three-dimensional structure of the myosin V inhibited state by cryoelectron tomography." *Nature* 442(7099): 208-211.
- Lu, H., E. B. Kremmentsova, et al. (2006). "Regulation of myosin V processivity by calcium at the single molecule level." *J Biol Chem* 281(42): 31987-31994.
- Marchelletta, R. R., D. T. Jacobs, et al. (2008). "The class V myosin motor, myosin 5c, localizes to mature secretory vesicles and facilitates exocytosis in lacrimal acini." *Am J Physiol Cell Physiol* 295(1): C13-28.
- Matesic, L. E., R. Yip, et al. (2001). "Mutations in Mlph, encoding a member of the Rab effector family, cause the melanosome transport defects observed in leaden mice." *Proc Natl Acad Sci U S A* 98(18): 10238-10243.
- Menasche, G., C. H. Ho, et al. (2003). "Griscelli syndrome restricted to hypopigmentation results from a melanophilin defect (GS3) or a MYO5A F-exon deletion (GS1)." *J Clin Invest* 112(3): 450-456.
- Menasche, G., E. Pastural, et al. (2000). "Mutations in RAB27A cause Griscelli syndrome associated with haemophagocytic syndrome." *Nat Genet* 25(2): 173-176.
- Miller, K. E. and M. P. Sheetz (2000). "Characterization of myosin V binding to brain vesicles." *J Biol Chem* 275(4): 2598-2606.
- Miyata, M., Y. Kishimoto, et al. (2011). "A role for myosin Va in cerebellar plasticity and motor learning: a possible mechanism underlying neurological disorder in myosin Va disease." *J Neurosci* 31(16): 6067-6078.
- Mori, T., R. D. Vale, et al. (2007). "How kinesin waits between steps." *Nature* 450(7170): 750-754.
- Morris, C. A., A. L. Wells, et al. (2003). "Calcium functionally uncouples the heads of myosin VI." *J Biol Chem* 278(26): 23324-23330.
- Muller, M., A. Heuck, et al. (2007). "Directional mRNA transport in eukaryotes: lessons from yeast." *Cell Mol Life Sci* 64(2): 171-180.
- Muller, M., R. G. Heym, et al. (2011). "A cytoplasmic complex mediates specific mRNA recognition and localization in yeast." *PLoS Biol* 9(4): e1000611.
- Muller, M., K. Richter, et al. (2009). "Formation of She2p tetramers is required for mRNA binding, mRNP assembly, and localization." *RNA* 15(11): 2002-2012.
- Muller, T., M. W. Hess, et al. (2008). "MYO5B mutations cause microvillus inclusion disease and disrupt epithelial cell polarity." *Nat Genet* 40(10): 1163-1165.
- Nascimento, A. A., R. G. Amaral, et al. (1997). "Subcellular localization of myosin-V in the B16 melanoma cells, a wild-type cell line for the dilute gene." *Mol Biol Cell* 8(10): 1971-1988.

- Novick, P. and M. Zerial (1997). "The diversity of Rab proteins in vesicle transport." *Curr Opin Cell Biol* 9(4): 496-504.
- Nunokawa, S. Y., H. Anan, et al. (2007). "Binding of chara Myosin globular tail domain to phospholipid vesicles." *Plant Cell Physiol* 48(11): 1558-1566.
- Oda, T., M. Iwasa, et al. (2009). "The nature of the globular- to fibrous-actin transition." *Nature* 457(7228): 441-445.
- Ostermeier, C. and A. T. Brunger (1999). "Structural basis of Rab effector specificity: crystal structure of the small G protein Rab3A complexed with the effector domain of rabphilin-3A." *Cell* 96(3): 363-374.
- Otwinowski, W. M. a. Z. (1997). *Processing of X-ray Diffraction Data Collected in Oscillation Mode*. New York, C. W. Carter, Jr. & R. M. Sweet, Eds., Academic Press.
- Paquin, N. and P. Chartrand (2008). "Local regulation of mRNA translation: new insights from the bud." *Trends Cell Biol* 18(3): 105-111.
- Park, H., B. Ramamurthy, et al. (2006). "Full-length myosin VI dimerizes and moves processively along actin filaments upon monomer clustering." *Mol Cell* 21(3): 331-336.
- Pashkova, N., Y. Jin, et al. (2006). "Structural basis for myosin V discrimination between distinct cargoes." *EMBO J* 25(4): 693-700.
- Pestic-Dragovich, L., L. Stojiljkovic, et al. (2000). "A myosin I isoform in the nucleus." *Science* 290(5490): 337-341.
- Petritsch, C., G. Tavosanis, et al. (2003). "The Drosophila myosin VI Jaguar is required for basal protein targeting and correct spindle orientation in mitotic neuroblasts." *Dev Cell* 4(2): 273-281.
- Pettersen, E. F., T. D. Goddard, et al. (2004). "UCSF Chimera--a visualization system for exploratory research and analysis." *J Comput Chem* 25(13): 1605-1612.
- Pfeffer, S. R., A. B. Dirac-Svejstrup, et al. (1995). "Rab GDP dissociation inhibitor: putting rab GTPases in the right place." *J Biol Chem* 270(29): 17057-17059.
- Pranchevicius, M. C., M. M. Baqui, et al. (2008). "Myosin Va phosphorylated on Ser1650 is found in nuclear speckles and redistributes to nucleoli upon inhibition of transcription." *Cell Motil Cytoskeleton* 65(6): 441-456.
- Prekeris, R. and D. M. Terrian (1997). "Brain myosin V is a synaptic vesicle-associated motor protein: evidence for a Ca<sup>2+</sup>-dependent interaction with the synaptobrevin-synaptophysin complex." *J Cell Biol* 137(7): 1589-1601.
- Purcell, T. J., C. Morris, et al. (2002). "Role of the lever arm in the processive stepping of myosin V." *Proc Natl Acad Sci U S A* 99(22): 14159-14164.
- Putnam, C. D., M. Hammel, et al. (2007). "X-ray solution scattering (SAXS) combined with crystallography and computation: defining accurate macromolecular structures, conformations and assemblies in solution." *Q Rev Biophys* 40(3): 191-285.
- Reisen, D. and M. R. Hanson (2007). "Association of six YFP-myosin XI-tail fusions with mobile plant cell organelles." *BMC Plant Biol* 7: 6.
- Richards, T. A. and T. Cavalier-Smith (2005). "Myosin domain evolution and the primary divergence of eukaryotes." *Nature* 436(7054): 1113-1118.
- Rodriguez, O. C. and R. E. Cheney (2002). "Human myosin-Vc is a novel class V myosin expressed in epithelial cells." *J Cell Sci* 115(Pt 5): 991-1004.

- Rogers, S. L., R. L. Karcher, et al. (1999). "Regulation of melanosome movement in the cell cycle by reversible association with myosin V." *J Cell Biol* 146(6): 1265-1276.
- Roland, J. T., D. M. Bryant, et al. (2011). "Rab GTPase-Myo5B complexes control membrane recycling and epithelial polarization." *Proc Natl Acad Sci U S A* 108(7): 2789-2794.
- Roland, J. T., A. K. Kenworthy, et al. (2007). "Myosin Vb interacts with Rab8a on a tubular network containing EHD1 and EHD3." *Mol Biol Cell* 18(8): 2828-2837.
- Roland, J. T., L. A. Lapierre, et al. (2009). "Alternative splicing in class V myosins determines association with Rab10." *J Biol Chem* 284(2): 1213-1223.
- Sahlender, D. A., R. C. Roberts, et al. (2005). "Optineurin links myosin VI to the Golgi complex and is involved in Golgi organization and exocytosis." *J Cell Biol* 169(2): 285-295.
- Sali, A. and T. L. Blundell (1993). "Comparative protein modelling by satisfaction of spatial restraints." *J Mol Biol* 234(3): 779-815.
- Sambrook, J. and D. W. Russell (2000). *Molecular cloning: a laboratory manual*. Cold Spring Harbour, New York, Cold Spring Harbour Laboratory Press.
- Schlamp, C. L. and D. S. Williams (1996). "Myosin V in the retina: localization in the rod photoreceptor synapse." *Exp Eye Res* 63(6): 613-619.
- Seabra, M. C., E. H. Mules, et al. (2002). "Rab GTPases, intracellular traffic and disease." *Trends Mol Med* 8(1): 23-30.
- Seiler, C., O. Ben-David, et al. (2004). "Myosin VI is required for structural integrity of the apical surface of sensory hair cells in zebrafish." *Dev Biol* 272(2): 328-338.
- Sellers, J. R., K. Thirumurugan, et al. (2008). "Calcium and cargoes as regulators of myosin 5a activity." *Biochem Biophys Res Commun* 369(1): 176-181.
- Sellers, J. R. and C. Veigel (2006). "Walking with myosin V." *Curr Opin Cell Biol* 18(1): 68-73.
- Seperack, P. K., J. A. Mercer, et al. (1995). "Retroviral sequences located within an intron of the dilute gene alter dilute expression in a tissue-specific manner." *EMBO J* 14(10): 2326-2332.
- Slep, K. C., S. L. Rogers, et al. (2005). "Structural determinants for EB1-mediated recruitment of APC and spectraplakins to the microtubule plus end." *J Cell Biol* 168(4): 587-598.
- Slep, K. C. and R. D. Vale (2007). "Structural basis of microtubule plus end tracking by XMAP215, CLIP-170, and EB1." *Mol Cell* 27(6): 976-991.
- Stinchcombe, J. C., D. C. Barral, et al. (2001). "Rab27a is required for regulated secretion in cytotoxic T lymphocytes." *J Cell Biol* 152(4): 825-834.
- Su, L. K. and Y. Qi (2001). "Characterization of human MAPRE genes and their proteins." *Genomics* 71(2): 142-149.
- Sugawara, K., T. Shibasaki, et al. (2009). "Rab11 and its effector Rip11 participate in regulation of insulin granule exocytosis." *Genes Cells* 14(4): 445-456.
- Sun, D., C. L. Leung, et al. (2001). "Characterization of the microtubule binding domain of microtubule actin crosslinking factor (MACF): identification of a novel group of microtubule associated proteins." *J Cell Sci* 114(Pt 1): 161-172.

- Svergun, D., C. Barberato, et al. (1995). "CRY SOL – a Program to Evaluate X-ray Solution Scattering of Biological Macromolecules from Atomic Coordinates." *Journal of Applied Crystallography* 28: 768-773.
- Svergun, D. I., M. V. Petoukhov, et al. (2001). "Determination of domain structure of proteins from X-ray solution scattering." *Biophys J* 80(6): 2946-2953.
- Syamaladevi, D. P., J. A. Spudich, et al. (2012). "Structural and functional insights on the Myosin superfamily." *Bioinform Biol Insights* 6: 11-21.
- Szperl, A. M., M. R. Golachowska, et al. (2011). "Functional characterization of mutations in the myosin Vb gene associated with microvillus inclusion disease." *J Pediatr Gastroenterol Nutr* 52(3): 307-313.
- The PyMOL Molecular Graphics System, V. S., LLC. Pymol. L. Schrödinger.
- Thirumurugan, K., T. Sakamoto, et al. (2006). "The cargo-binding domain regulates structure and activity of myosin 5." *Nature* 442(7099): 212-215.
- Thompson, J. D., T. J. Gibson, et al. (2002). "Multiple sequence alignment using ClustalW and ClustalX." *Curr Protoc Bioinformatics* Chapter 2: Unit 2 3.
- Trabuco, L. G., E. Villa, et al. (2008). "Flexible fitting of atomic structures into electron microscopy maps using molecular dynamics." *Structure* 16(5): 673-683.
- Trybus, K. M. (2008). "Myosin V from head to tail." *Cell Mol Life Sci* 65(9): 1378-1389.
- Trybus, K. M., M. I. Gushchin, et al. (2007). "Effect of calcium on calmodulin bound to the IQ motifs of myosin V." *J Biol Chem* 282(32): 23316-23325.
- Trybus, K. M., T. W. Huiatt, et al. (1982). "A bent monomeric conformation of myosin from smooth muscle." *Proc Natl Acad Sci U S A* 79(20): 6151-6155.
- Uhlig, M., W. Passlack, et al. (2005). "Functional role of Rab11 in GLUT4 trafficking in cardiomyocytes." *Mol Cell Endocrinol* 235(1-2): 1-9.
- Vale, R. D. (2003). "The molecular motor toolbox for intracellular transport." *Cell* 112(4): 467-480.
- Veigel, C. and C. F. Schmidt (2011). "Moving into the cell: single-molecule studies of molecular motors in complex environments." *Nat Rev Mol Cell Biol* 12(3): 163-176.
- Verhey, K. J. and T. A. Rapoport (2001). "Kinesin carries the signal." *Trends Biochem Sci* 26(9): 545-550.
- Volkov, V. V. and D. I. Svergun (2003). "Uniqueness of ab initio shape determination in small-angle scattering." *J Appl Cryst* 36: 860-864.
- Volpicelli, L. A., J. J. Lah, et al. (2002). "Rab11a and myosin Vb regulate recycling of the M4 muscarinic acetylcholine receptor." *J Neurosci* 22(22): 9776-9784.
- Vreugde, S., C. Ferrai, et al. (2006). "Nuclear myosin VI enhances RNA polymerase II-dependent transcription." *Mol Cell* 23(5): 749-755.
- Wagner, W., S. D. Brenowitz, et al. (2011). "Myosin-Va transports the endoplasmic reticulum into the dendritic spines of Purkinje neurons." *Nat Cell Biol* 13(1): 40-48.
- Wang, F., K. Thirumurugan, et al. (2004). "Regulated conformation of myosin V." *J Biol Chem* 279(4): 2333-2336.
- Wang, Z., J. G. Edwards, et al. (2008). "Myosin Vb mobilizes recycling endosomes and AMPA receptors for postsynaptic plasticity." *Cell* 135(3): 535-548.
- Wells, A. L., A. W. Lin, et al. (1999). "Myosin VI is an actin-based motor that moves backwards." *Nature* 401(6752): 505-508.

- Wendt, T., D. Taylor, et al. (2001). "Three-dimensional image reconstruction of dephosphorylated smooth muscle heavy meromyosin reveals asymmetry in the interaction between myosin heads and placement of subfragment 2." *Proc Natl Acad Sci U S A* 98(8): 4361-4366.
- Wöllert, T., A. Patel, et al. (2011). "Myosin5a tail associates directly with Rab3A-containing compartments in neurons." *J Biol Chem* 286(16): 14352-14361.
- Wong, Y. L., K. A. Dietrich, et al. (2009). "The Kinesin-1 tail conformationally restricts the nucleotide pocket." *Biophys J* 96(7): 2799-2807.
- Wu, X., T. Sakamoto, et al. (2006). "In vitro reconstitution of a transport complex containing Rab27a, melanophilin and myosin Va." *FEBS Lett* 580(25): 5863-5868.
- Wu, X. S., K. Rao, et al. (2002). "Identification of an organelle receptor for myosin-Va." *Nat Cell Biol* 4(4): 271-278.
- Wu, X. S., G. L. Tsan, et al. (2005). "Melanophilin and myosin Va track the microtubule plus end on EB1." *J Cell Biol* 171(2): 201-207.
- Yang, Y., M. Kovacs, et al. (2006). "Dimerized *Drosophila* myosin VIIa: a processive motor." *Proc Natl Acad Sci U S A* 103(15): 5746-5751.
- Yu, C., W. Feng, et al. (2009). "Myosin VI undergoes cargo-mediated dimerization." *Cell* 138(3): 537-548.

# CURRICULUM VITAE

Name	<b>HANA VELVARSKÁ</b>
Date, place of birth	11.10.1980, Brandeis an der Elbe (Brandys n.L.), Czech Republic
Nationality	Czech
Current address	Platanenstr. 10, 81377, München, Germany
08/06 – 10/12	<b>Gene Center</b> of the Ludwig –Maximilian–University of Munich & Helmholtz Zentrum München, Germany PhD in the group of Dr. Dierk Niessing “Structural and functional studies on Myosin type V – dependent transport in vertebrates”
09/02 – 07/06	<b>Charles-University</b> , Prague, Czech Republic Master of Science: “Enzymatic transformation of some vasorelaxing substances to nitric oxide”
04/05 – 10/05	<b>Ruprecht-Karls-University</b> , Heidelberg, Germany
09/00 – 09/02	<b>Masaryk-University</b> , Brno, Czech Republic General chemistry
09/96 – 08/00	<b>Evropska High School</b> , Prague, Cech Republic Abitur

Date: 21.09.2012

Signature .....



## AKNOWLEDGMENT

I would like to thank my supervisor Dierk Niessing for his ideas, creative criticism, and particularly for continuous supply of interesting projects. And later on, when the projects had to be terminated one after another, for a continuous supply of encouragement and patience.

I am also very grateful to Klaus Förstemann and Daniel Wilson for being the members of my thesis advisory committee and Mario Halic and Klaus Förstemann for being the first and second examiners of my thesis.

Throughout my work at the Gene Center, I very appreciate the enjoyable atmosphere, interesting discussions and help from other past or present colleagues. I am grateful to Dirk Kostrewa and Sabine Schneider for suggestions in X-ray data processing, Gregor Witte for introducing me into the SAXS data evaluation, and Thomas Becker for performing MDFF.

Thanks to all members of Niessing lab, especially Marisa, Alex, and Roland for a nice atmosphere. And a very special thanks to Sigrun for keeping the lab running smoothly, transforming the lab into La Scala, and for her excellent help with cloning.

I want to thank Thomas and Achim for having a great time and sports coaching.

I would like to thank Pavel & Duratec and especially express my gratitude to my family for their everlasting support and understanding.